THE GEOLOGY AND GEOCHEMISTRY OF THE BANDED IRON FORMATION IN CHAGO-WEREKALU, WELLEGA PROVINCE

A Thesis

Presented to

The Faculty of Science

Addis Ababa University

In Partial Fulfillment

of the Requirements for the Degree

Master of Science in Geology

by

Abera Getahun

October, 1985.

ADDIS ABABA UNIVERSITY

School of Graduate Studies

The Geology and Geochemistry of the Banded Iron Formation in Chago-Werekalu, Wellega Province

by

Aberra Getahun

Faculty of Science

Approved by: _____

Prof. Roberto Valera
Advisor

Dr. Bekele Megersa
Examiner

Dr. Albert Yama Nkounga
Examiner

Dr. Peccerillo Angelo
Examiner

Prof. Mottana Annibale
Examiner

Mr. A,K. Wahi
Examiner

ABSTRACT

The rocks of the studied area form part of the Wollega Birbir group of the upper complex and consist of a series of metasedimentary and plutonic proterozoic rocks. The minieralogical assemblage indicate that the metamorphism is of the greenshist facies.

The variation diagram constructed for the various plutonic rocks strongly suggest comagmatic origin by crystal fractionation.

Major and trace element analyses of representative samples of the Chago iron formation, the plutonic and younger effusive rocks are presented. The Chago iron formation can be classified as precambrian banded iron formation and is in many respects similar to the oxide facies iron formation of Lake Superior type. The Chago iron formation consists only of iron oxides and minor amount of silica with total absence of iron silicate, sulfide and carbonate minerals.

Trace element geochemistry suggests that the iron formation was chemically precipitated as oxidate sediments in which the principal iron mineral, magnetite, was formed at low temperature in a shallow near shore environment.

LIST OF FIGURES

TABLES

ACKNOWLEDGMENTS

I would like to express my deep appreciation for the constant supervision and encouragement I received from my advisor, Professor R. Valera in the preparation of this thesis, Dr. A. Peccerillo for commenting on the description of the thin sections and geochemistry of the plutonic and effusive rocks, and Dr. G. Calderoni for critically reviewing the geochemistry of the iron bearing metasedimentary units.

Speciall thanks are due to Dr. Shibru Tedla, Dean of Graduate studies for his help in arranging and providing vehicle and financial support through the Swedish Agency for Research Cooperation (SAREC).

The author is also indebted to Ato Getahun Demissie, Head of the Ethiopian Institute of Geological Surveys (EIGS), and all at the Chemical Laboratory of the Ministry of Mines and Energy, who were helpful and cooperative during the time of chemical analysis.

I am indebted to Yisalemush Teffera for the preparation of all the drawings. Gratitude is expressed to Semen Zewdie and Menkir Girma, who were real encouragements throughout the preparation of this dissertation.

The writer further extends his appreciation to Ato Beraki W. Haimanot, who bore the pain of typing the manuscript.

INTRODUCTION

1.1 Purpose of Investigation

Although a considerable work has been carried out by different workers only a little attempt was made in evaluating the origin of the iron formation and in classifying it in one of the types known as Precambrian iron formations.

The purpose of this study is to provide new data on the geology and origin of the iron formation based on surface geological mapping on a scale of 1:50,000 of an area about 231 sq. km., trench mapping, laboratory studies on petrographic and micrographic analysis and geochemical analysis of trench and surface samples for major and trace elements.

1.2 Location and Accessibility

Gulliso-Chago is located in Western Ethiopia about 65 km. west of Ghimbi, in Wollega Administrative Region and is bound by latitudes $9^{o}00'$ and $9^{o}12'$ N and longitudes $35^{o}24'$ and $35^{o}30$ E.

The town of Gulliso is about 505 km. from Addis Ababa and is accessible by an all weather road which passes through the middle of the studied area via Aira to Dembidolo.

As the area is highly dissected by rivers and streams with dense vegetation cover along their route, accessibility is restricted along the main Ghimbi-Dembidolo road and other feeder roads which lead to the various mineral prospects of the region like Chago, Worekalu, and to various missionary stations that are

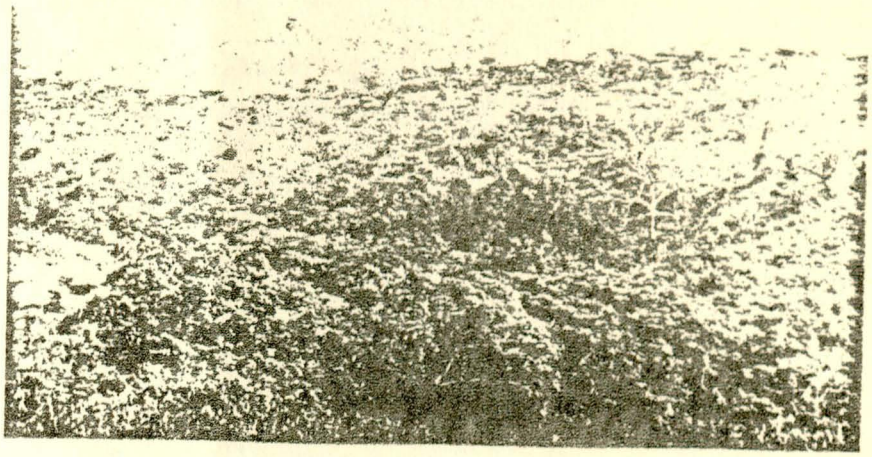

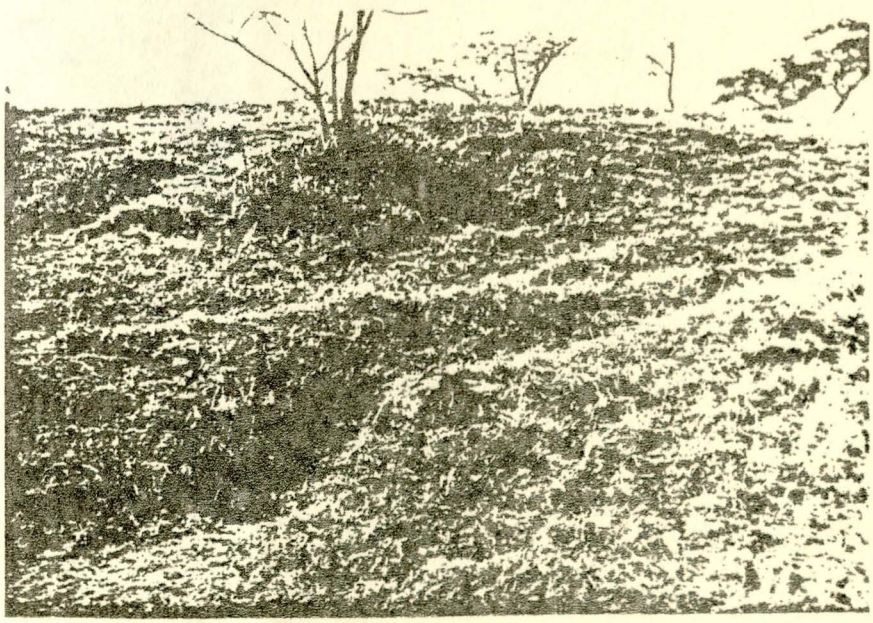

Fig. *1* : General view of the studied area.

present within the studied area. Other than the main roads which are accessible by four-wheel drive, there exists many foot trails which enable one to move from one place to the other.

1.3 Geographical Setting

1.3.1 Regional

Ethiopia is divided into five major physiographic units which reflect, to a great extent the geological history and the structure of the region (Fig. 2).

1. The Ethiopian Rift System which divides the territory into two major plateaus and their associated lowlands.
2. The North-Western plateau and associated lowlands, which represent more than half of the country, and where the lowlands are situated towards the Sudan border and along the coastal regions of the Red Sea.
3. The South-Eastern plateau and associated lowlands, most of which is constituted by extensive flat plains starting from the Ogaden basin to the east and the Wabi-Shebelle and the Genale plains in the West.
4. The other units are the localized steep areas of the rift escarpment and,
5. The Afar depression which has with its limits the lowest point 125 m. below sea level and is very active and tectonically disturbed with a basaltic lava lake.

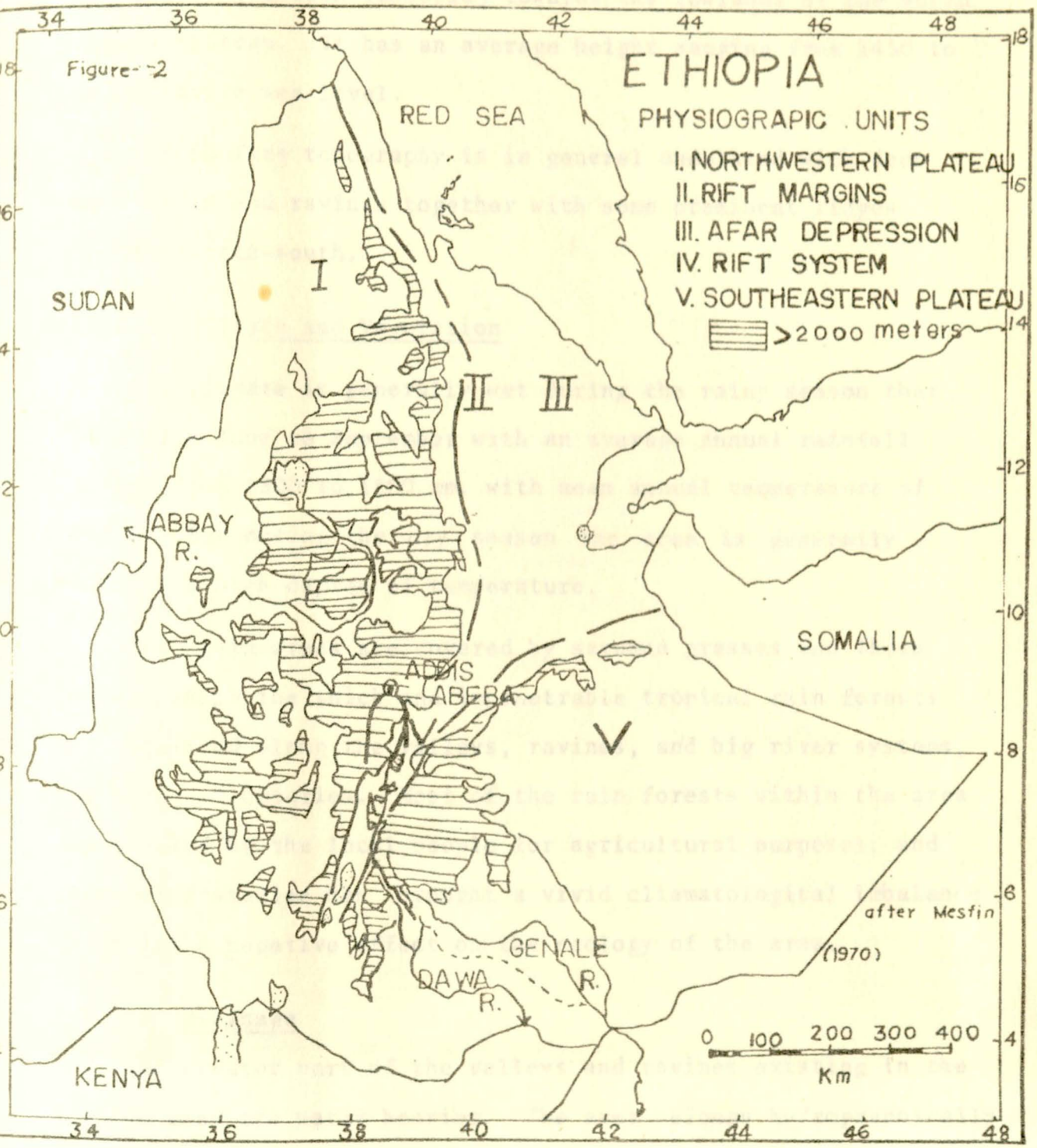
Figure-2
ETHIOPIA
PHYSIOGRAPIC UNITS
I. NORTHWESTERN PLATEAU
II. RIFT MARGINS
III. AFAR DEPRESSION
IV. RIFT SYSTEM
V. SOUTHEASTERN PLATEAU
>2000 meters
RED SEA
SUDAN
SOMALIA
KENYA
ABBAY R.
ADDIS ABEBA
GENALE R.
DAWA R.
after Mesfin (1970)
0 100 200 300 400
Km
34 36 38 40 42 44 46 48
18 16 14 12 10 8 6 4

1.3.2 Local

The project site described is found in Wollega Administrative region (Western Ithiopia) towards the lowlands of the North Western plateau. It has an average height ranging from 1450 to 1660 m. above sea level.

The surface topography is in general undulated with deep cut valleys and ravines together with some prominent ridges trending north-south.

1.3.2.1 Climate and Vegetation

The climate is generally wet during the rainy season that lasts from June to September with an average annual rainfall ranging from 1500 to 1800 mm. with mean annual temperature of 20.2^{o}C. But during the dry season the area is generally hot with a high degree of temperature.

The plain areas are covered by savanna grasses and thorn bushes, while the thick and impenetrable tropical rain forests are localized along the valleys, ravines, and big river systems, and their tributaries. Most of the rain forests within the area are cleared by the local people for agricultural purposes; and this deforestation has brought a vivid cliamatological imbalance which has a negative effect on the ecology of the area.

1.3.2.2 Drainage

The greater part of the valleys and ravines existing in the studied area are water bearing. The area belongs hydrographically

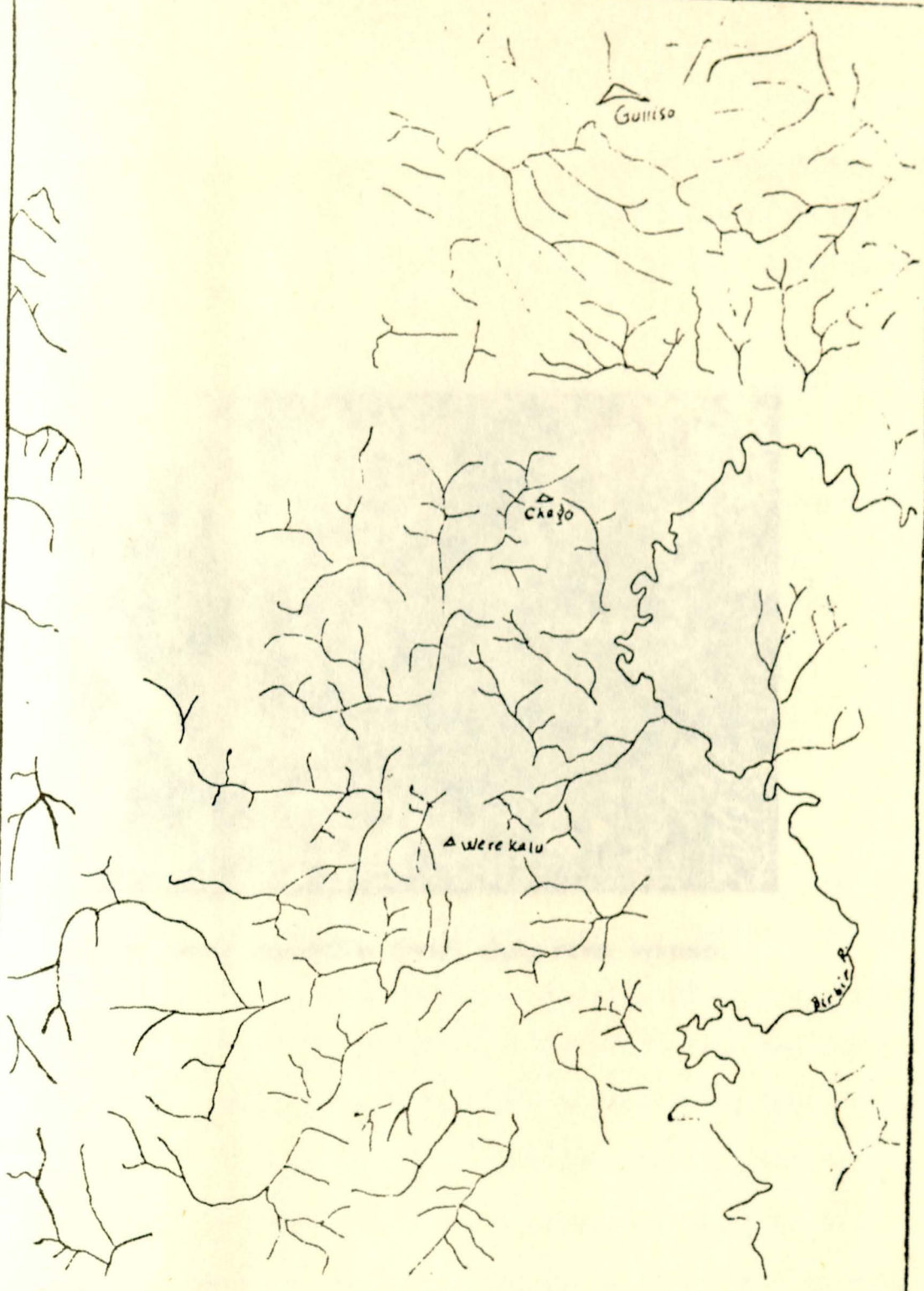

Fig. 3 Drainage pattern of the area

Fig. 4 : Dense vegetation covers along river systems.

to the Birbir drainage system. With numerous meanders the river Birbir, surrounded with thick and dense jungle, flows on the eastern border of the prospected area and discharged into river Baro, which is the tributary of Nile.

As clearly seen in Fig. 3 the drainage pattern of the area is well developed within the metasedimentary units according to a dendritic-angular system. The plutonic rocks which cover the north-western and south-eastern part of the studied area are more or less poorly drained, showing the strong control of the lithology over the development of the drainage system.

1.4 Methods of Approach

Geological mapping was carried out by the author on a scale of 1:50,000 covering an area of about 231 sq. km. Petrographic studies were made on samples collected from the surface outcrops and trenchs to determine variations in mineralogical composition, texture, and structure of the rocks. Ore microscopy was carried out on representative polished sections to determine type, texture, and structure of the ore minerals. Determination of silicate forming oxides and trace elements was conducted using Atomic absorption and Emmission spectrophotometer on more than 78 rock and ore samples, and the results obtained are statistically and graphically treated. Coupled with the field and petrographic data the subsequent discussions were drawn.

There was no regular spacing practiced during sampling operations. The spacing could vary depending on three factors:

i) intensity of weathering
ii) intensity of mineralization
iii) variation in lithology.

The greater the intensity of weathering the wider will be the spacing; and greater the intensity of mineralization, closer is the spacing. For the same lithology the spacing is wider and whenever quick variation occurs, the spacing becomes closer.

1.5 Previous Work

Indications of mineralized zone, specially gold, in Wollega were first discovered in 1880s during which I. Combul prospected the region and formed " the Societa Anonyme des Mines d'or du Wollega" (Jelenc, 1966).

Ancient usage of the iron ore cropping out at Chago and Worekalu, by the local people specially prior to the Italian occupation is evident from the tale of the people living around the area, and they call it " Gordana" which means iron ore in their language. Besides their tale, traces of former mining activities are clearly seen within the prospected area.

After some silent years of exploration, in the mid-sixties and early seventies work resumed by the United Nations and

Ithiopian Institute of Geological Surveys (EIGS) and Cu-Zn-Pb geochemical anomalies were discovered.

Rudis Yugoslavia (1964) in agreement with the Ethiopian Government, Ministry of Mines and Energy carried out geological and geophysical explorations. Hunting Geology and Geophysics Ltd. (1969) made a photogeological survey of the Wollega area.

Kochemasov (1970) has made a follow-up geochemical programme at the middle Birbir basin, Wollega, under the supervision of the United Nations-Ethiopia Mineral Survey, and an extract has been made from the main report which indicates the geochemical surveys over the iron deposits around Chago, Werekalu, etc.

Then Belay Desta, et.al. (1980) made a short review on the geology and iron ore occurence at Chago.

Recently a joint project labelled as "Ethio-Korean Project' has started its exploration programme on iron deposits and their associates around the western part of Wollega.

GEOLOGY

2.1 Regional

2.1.1 Previous Work

The Ethiopian basement has been studied for the last 15 years, mostly by the geological survey of Ethiopia (EIGS), United Nations Mineral Survey, and other different workers. Due to its infant stage in systematic geological exploration, recent knowledge of the Precambrian in Ethiopia is not well developed. However, the most common and plausible view includes the Precambrian of Ethiopia in the PanAfrican Mozambique belt which is the structural zone, streching from Mozambique to Sudan, Egypt, and probably even to Saudi-Arabia (Fig. 5). At different time many workers have attempted to describe and give explanation of this belt. Holmes (1951) described the Mozambique belt as a late Precambrian geosyncline so deeply eroded that its inner highly metamorphosed parts are exposed on the surface. The same view was expressed by Cahen and Snelling (1966), but later in 1970, Clifford, considered and explained it as a 'vestigeosynclinal or mobile belt built up of remobilized ancient material'.

important contributions to the basement geology of Sidamo specifically the Gariboro area in southern Ethiopia were made by Gilboy (1970) and Chatter (1971) and to that of Keffa, Gamo Gofa, and Illubabor by the Ethiopian-Canadian Omo River Project (1973-1976). An important compilation of all the available data was made by Mohr (1971). But later on, Kazmin's (1971, 1972, 1975,

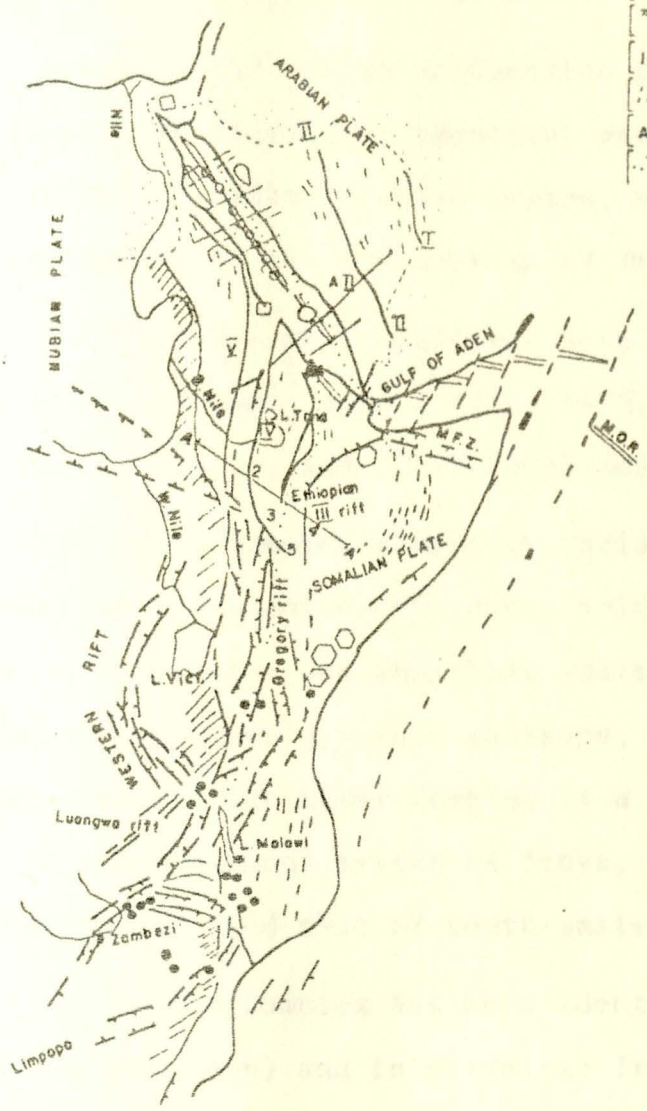

MOZAMBIQIAN FEATURES

Ophiolite zones

- I Idas
- II Nabitah
- III Adola
- IV Western Ethiopian
- V Eastern Sudan
- CA Calcalkaline Volcano Plutonic belt
- Phanerozoic cover
- Mozambiqean foreland
- I-5 Tectonostratigraphic zones of Eth.
- Structural trend
- A-A' Cross sections
- Main inferred suture

PHANEROZOIC FEATURES

- Main rift faults
- Carbonatites
- Pb-Zn deposites
- Mn deposites
- Metaliferous sediments (Brine pools)
- A II Atlantic II deep
- Fe-Mn-Ba deposites
- M.F.Z. Merda fault zone
- M.O.R Mid ocean ridge

Fig. 5 after Dewit & Senbeto

1976, 1978) works provided a better understanding of the stratigraphy and possible manner of evolution of the Ethiopian basement. Senbeto and de Wit (1980) have tried to fit the available data into the scheme of plate tectonics.

Recently the Ethiopian-Canadian crew under the 'Gore-Gambella Project' have started an important geological investigation within the Illubabor Administrative region, which could bring a better understanding of the Precambrian of Ethiopia.

So far three main Complexes have been recognized in the Ethiopian Basement (Kazmin 1971, 1975; Kazmin, et.al., 1978) as the Lower, Middle, and Upper Complexes.

The Lower Complex comprises various high grade gneisses and migmatites representing the older (older than 2500 my) cratonic Basement. Biotite and amphibole gneisses predominate with subordinate quartzo-feldspathic gneisses, calc-silicate rocks and amphibolites. The Lower Complex is a direct northward continuation of the Basement system of Kenya, the Basement of the north-eastern Uganda and that of south-eastern Sudan.

The Middle Complex has been identified in Sidamo Province (The Wadera group) and in Harrergie Province (The Boye Series), and possibly occurs in western Ethiopia. In Sidamo and Harrergie, it is represented by psammitic and pelitic metasediments (biotite and quartzo-muscovite schists, meta-arkoses, quartzites) with subordinate marbles, calc-silicate rocks and amphibole schists. In Western Ethiopia, these rocks are intercalated with amphibole schists and amphibolites.

gure-6; PRECAMBRIAN BASEMENT OF ETHIOPIA

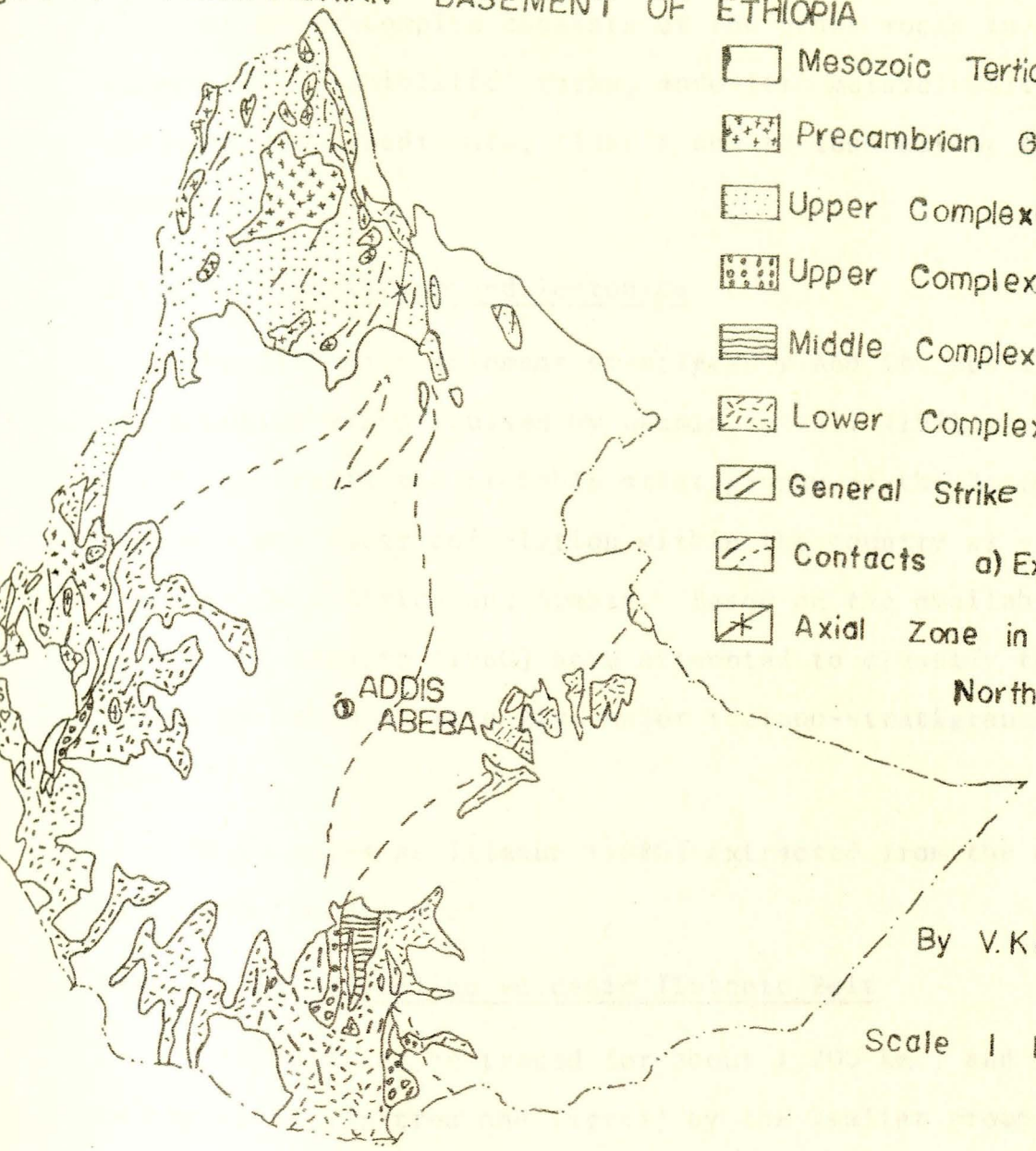

Mesozoic Tertiary Rocks

Precambrian Granitoids

Upper Complex (post-Adola Gp.)

Upper Complex (Adola Gp.)

Middle Complex (Wadera Gp)

Lower Complex

General Strike

Contacts a) Exposed b) Inferred

Axial Zone in Tigrai, Northern Ethiopia

By V. Kazmin

Scale 1 10,000, 000

The Upper Complex consists of low grade rocks in following succession: 'ophiolitic' rocks, andesitic metavolcanics and associated metasediments, clastic and to less extent carbonate sediments.

2.1.1.1 Stratigraphy and Tectonics

The Ethiopian Basement stratigraphy and its possible manner of evolution was discussed by Kazmin, et.al. (1978). Tables 1 and 2 represents the probable stratigraphy of the Basement of Ethiopia and their correlation within the country as well as to those of East Africa and Arabia. Based on the available data, de Wit and Senbeto (1980) have attempted to classify the Ethiopian basement into five major tectono-stratigraphic zones (Fig. 7).

These zones as Tilahun (1980) extracted from the works of deWit and Senbeto are:

Zone 1. Calc-alkaline Volcanic Plutonic Belt

This belt can be traced for about 1,200 km., and represented in the north (Eritrea and Tigrai) by the Tsaliet group. The belt comprises a volcano-sedimentary succession of metavolcanics of andesitic and dacitic composition, various volcano-clastic rocks, tuffs, rhyolitic agglomerates, phyllites, schists, quartzites and arkoses with intercalations of cherts, marbles and granite intrusions. Strongly deformed bodies of early diorite and granodiorites gave an age of upto 700 my. with K/Ar method and even 800 my.

Table 1. Precambrian Units in Ethiopia

Age	Abs. Age m.y.	Southern Ethiopia	Western Ethiopia	Northern Ethiopia	Harar and Aisha	Complex
	500					
Ecoambrian				Matheos Fm		
	700			Shiraro Fm		
				Dadikama Fm		
				Tambien Gr: Amota Fm		
				Tambien Gr: Mai Kenetal Fm		
				Tambien Gr: Arequa Fm		
Upper Proterozoic		Mormora Group and Kajimiti Beds	Birbir Group	Tsaliet Group	Soka and Boje Series	Upper
	1000	Adola Group	Greenstones and Amphibolites			
	1600					
Lower-Middle Proterozoic						Middle
	2500	Burji Gneiss				
		Arero Group: Yavello geneiss	Gneisses undifferentiated	Gneisses undifferentiated	Mica schists	
		Arero Group: Awata gneiss				
		Arero Group: Alghe gneiss			Gneisses undifferentiated	
Archaean		?				Lower
		Konso gneiss	Granulities of the Beles Basin			

Table 2. Correlation of Some Precambrian Units in East Africa and Arabia

Age		Abs. Age	Saudia-Arabia	Egypt	Sudan	Ethiopia	Somalia	Kenya	Tanzania
Infracambrian or Eocamberian		500	Fatima, Abla Formations	Hammamat Series	Awat Series	Shiraro Fm. Matheos Fm.			
Upper Proterozoic	Upper Part		Murrdama Formation Halaban Formation	Schist-mud Stone-grey-wake Series Dokhan Series	Upper Part Nafirdeib Series Lower Part	Tambien Group Tsaliet Group Birbir Group	Inda-Ad Series		
	Lower Part	1000	Beish; Lit Complexes	Shadli Series Barramia Rocks	Primitive System	Adola Group	Green-rock Series in The Basement System	Some green rock complexes in Western Kenya (?) Embu and Ablun Series in central and Eastern Kenya	Ukinga, Konse, Ndembera Series
Middle? Lower Proterozoic		1600 2500	?	?		Wadera Group	?	Turoka Series	Limestone Graphite Series
Archaean			Ancient Gneiss	Orthogneisses of "Basement" Mitiq Series		Burji) Awata) Alghe) Konso) - Gneiss	Gneisses of the Basement system	Basement System	Usagaran System

Zone 2

This belt runs through south-west Ethiopia for some 500 km. from the Kenya border to the Blue Nile and possibly further north. It consists of metagabbaro-serpentinized ultramafic Complex, unconformably overlain by a sequence of probable deep water metasediments and ultramafic meta-volcano-clastics and metasilicic volcanics. It represents the lower part of the Birbir group.

Zone 3

This belt is observed north east of Lake Rudolf and constitutes rocks comprising a series of mafic gneisses and granulites, layered biotite and hornblende gneisses, quartzo feldspathic gneisses and migmatites and paragneisses. It represents Konso gneisses of the Lower Complex.

Zone 4: Eastern Metamorphic Belt

This belt consists of high grade gneisses and migmatites and ophiolitic rocks.

Zone 5: South Western Cataclastic Belt

This belt is a mega shear along the Sudanese border and can be traced into a wide North-West striking intracontinental rift in the Sudan which is filled with upto 15 kms. thick phanerozoic sediments.

The tectonostratigraphic zones described above as fitted into the scheme of plate tectonics (Kazmin, et.al. 1980, deWit and Senbeto, 1980) are:

MAJOR TECTONO - STRATIGRAPHIC UNITS OF THE ETHIOPIAN PRECAMBRIAN

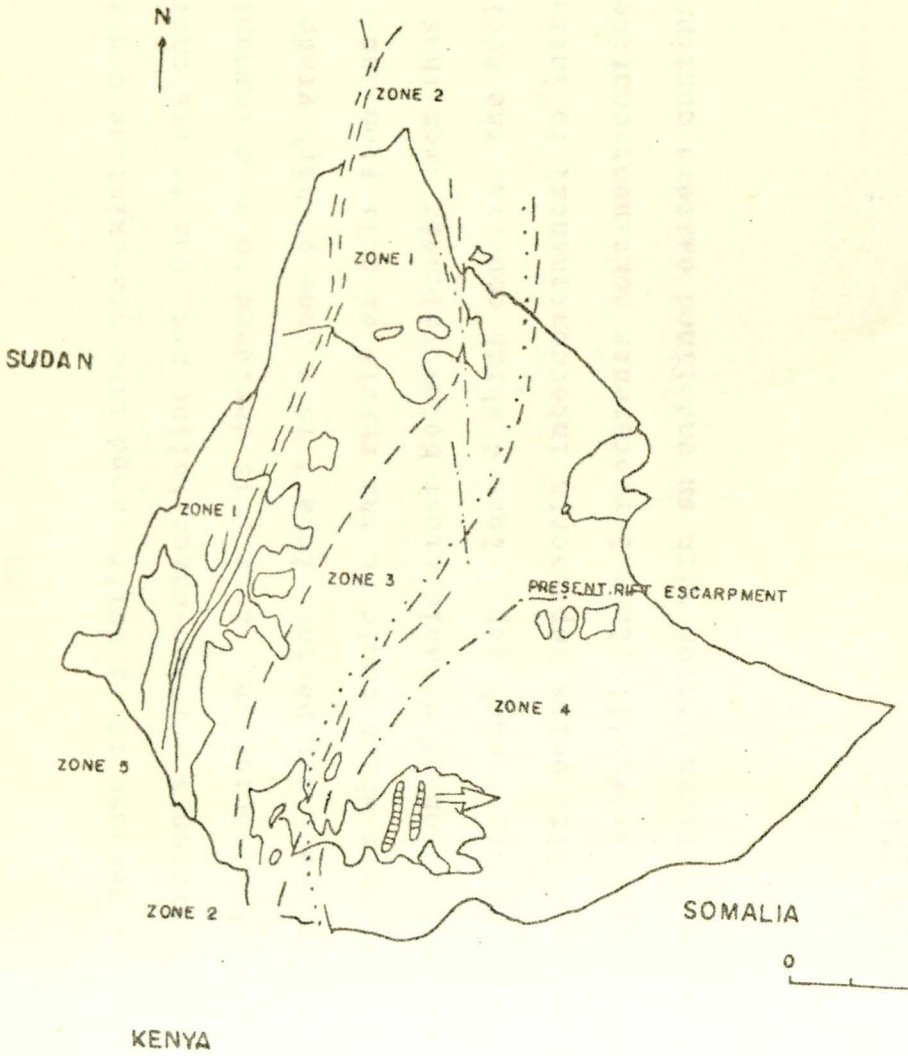

ZONE 1 CALC ALKALINE VOLCANIC PLUTONIC BELT
ZONE 2 WESTERN OPHIOLITIC SUTURE ZONE
ZONE 3 CENTRAL HIGH GRADE AREA
ZONE 4 EASTERN METAMORPHIC BELT
ZONE 5 SOUTHWESTERN CATACLASTIC BELT

LEGEND

INFERRED POSITION OF MAJOR SUTURE ZONE
TECTONIC TRANSPORT DIRECTION IN ZONE 4
BASEMENT IN ZONE 1
OPHIOLITE IN ZONE 4
BOUNDARY BETWEEN ZONES

FIGURE 7 AFTER DEWIT & SENBETO

Zone 1 because it is built on and into pre-existing continental crust represents a paleo-calcalkaline arc; due to its characterstic rock association; Zone 2 is designed to be a remnant inter-arc or back arc basin; Zone 3 is a zone of high grade metamorphic belt which could be the result of collision and subsequent subduction of oceanic crust below volcanic arcs-thus represents an arc trench gap; Zone 4 which contains the Adola and Kenticha ophiolite belts represents intercontinental to intracontinental rifting; finally,Zone 5 represents continent-continent collision of African Craton with an undefined eastern continent.

2.2 Local

2.2.1 Introduction

The rock of the studied area forms part of the Upper Complex of the Wollega Birbir group consisting a series of pelitic and subarkosic Proterozoic rocks of low metamorphic grade. The Birbir group forms part of the Nedjo-Metti belt and is correlated with the Tsaliet group of Northern Ethiopia, Mormora group and Kajimiti beds of Southern Ethiopia, Soka and Boje Series of Harrar and Aisha, the Halaban formation of South Arabia, the Dokan Series of Egypt, and lower part of the Upper Proterozoic of Sudan (Kazmin, 1972).

To the west of the mapped area, the Proterozoic sediments rest unconformably on diorites and to the east on weakly deformed granite-quartzdiorite plutons. Most of the south western part of

the area is covered by basalts, probably of Tertiary age, which are weathered and crumbled to a silicified limonitic laterite. Further to the south east, the area is bordered by ultrabasic rocks, which are hydrothermally altered.

In the metamorphic Proterozoic sediments a nearly north south extending iron bearing horizon was outlined (Rudis, 1964) in which large iron outcrops in the Guji-Worabu area while detrital magnetite-hematite floats can be recognized at Worekalu. The existence of these iron ore was known already in the past and was being exploited by open pit, which is evident by the presence of mining prints of large excavations.

The mineralogical assemblage of the metamorphic rocks indicates a low grade metamorphism of the green schist facies. Field and microscopic studies reveal the occurrence of at least two episodes of deformational processes which are evident by the existence of foliation surfaces which in most cases are produced by the allignment of micaceous minerals and faint segregation of mafic and felsic minerals. The second episode of deformation is recognized by fold fabric both in macro and micro scale.

2.2.2 Stratigraphy

The rocks of the project area are covered by thick lateritic soils and exposed rocks are very limited and even when encountered they appear to provide little information. Moreover, outcrops in these localities are scarce due to the presence of thickly wooded

vegetation specially along rivers and streams which hinders mass movement of loose materials even on very steep slopes.

Limited natural outcrops were observed along hill tops, in some accessible stream beds, and at the peaks of intrusive bodies which support very scanty vegetation.

The mapping was facilitated by artificial exposures such as road sections and trenches. Based on field observation and petrographic studies an attempt was made to establish a tentative vertical sequence of the area. From top to bottom the stratigraphy is:

8.	Residual limonitic laterite	Tertiary
7.	Olivine basalt	
	UNCONFORMITY	
6.	Sericite-chlorite-muscovite schist	
5.	Quartz-sericite-chloritoid schist	
4.	Quartz-muscovite-sericite schist	
3.	Ferruginous quartzite	Upper
2.	Quartziferous-micaceous schist	Proterozoic
	UNCONFORMITY	
1.	Plutonic rocks	

2.2.3 Plutonic Rocks

2.2.3.1 Biotite Granite

This rock unit is exposed in the south eastern part of the studied area along the Birbir River. It is leucocratic to mesocratic in colour, massive to weakly foliated, coarse to medium grained, and strongly weathered. The rocks sometimes grade at the marginal part into biotite-orthogneiss (Rudis, 1964).

Petrographic study of these rocks indicated the presence of quartz, microcline, orthoclase, plagioclase, muscovite, sericite, and subordinate amounts of biotite, chlorite, and epidote.

The quartz grains are very extensively recrystallized forming a mosaic of granoblastic texture and are to some extent oriented. Some of the equant grains of quartz appear surrounding a relict crystal of feldspars showing mortar texture.

The alkali feldspar is dominantly constituted by microcline with a subordinate occurence of orthoclase. The microcline with its typical polysynthetic twinning forming the gridiron structure apnears as megacrysts and is less transformed as compared to the plagioclase feldspars. All the megacrysts are fractured and broken (porphyroclasts). There exists also perthite resulting from the intergrowth of microcline and albite.

The plagioclase feldspars show a low angle of extinction with an index of refraction less than balsam. It is in the albiteoligoclase range in composition. They are highly transformed to muscovite

and sericite especially along the grain boundaries forming belts of secondary minerals. In some of the plagioclase crystals the transformation of the original mineral to the metamorphic ones is oscillatory indicating original zonning of the crystals. Most of the megacrysts are almost transformed into minute metacrysts of muscovite and sericite, and are preferentialy oriented especially those which are formed along grain boundary; this contributes to the weak foliation of the rock.

The epidotes are also formed by the transformation of the plagioclase by the saussuritization process and to a very limited extent from biotite. All the secondary minerals which have been derived from the plagioclase feldspars have filled the fractured parts of the plagioclases.

The biotites are present in a subordinate amount constituting about 2-3% of the rock and are less altered or transformed, keeping their original igneous character. They are slightly transformed along the grain boundaries to chlorite which is partially oriented.

Due to the presence of extensive recrystallised quartz grains, weak foliation and mineral lineation, abundant occurence of relict minerals, secondary muscovite, sericite, chlorite, and epidote the rock can be said to be a low grade weakly metamorphosed pretectonic granite.

2.2.3.2 Quartz Diorite

A wider belt of massive to weakly foliated, mesocratic, medium to coarse grained quartz diorite occurs in the north eastern part of the studied area, which appears as elongated body trending north-south.

Due to the intense tropical weathering, it was immpossible to delineate the contact between the quartz diorite and the granitic bodies. It is highly fractured and locally faulted with a lot of veinlets running east-west crossing the general trend of the rock unit.

Petrographic study disclosed the existence of feldspars, quartz, biotite, amphiboles, pyroxenes, epidote, zircon, apatite, sphene, magnetite with rims of hematite, muscovite, sericite and minor chlorite.

The plagioclase feldspars are andesine in composition and some of them are zoned and are variably affected by metamorphic transformation, where some of the megacrysts are transformed to sericite, muscovite and epidote. Alkali feldspar dominantly perthitic microcline, are few when compared with plagioclase. Some of the feldspar grains are surrounded by oriented epidote and other minute metacrysts of muscovite and sericite.

The pyroxenes are extensively transformed, especially at the rim, to a new metamorphic mineral of pale-green amphibole with relict features at the core. The original magmatic amphi-

Fig. 8 : Biotite granite: alteration of plagioclose feldspars, biotite and recrystallized quartz.

X-nicols, magnification 35X.

Fig. 9 : Quartz diorite. Recrystallized quartz, altered plagioclase and biotite.

X-nicols, magnification 35X.

boles which appear to be pale-brown to deep green are also transformed to a new pale-green metamorphic amphibole.

The biotite is less affected by the metamorphic effect and there exist only very few secondary products and chlorite is the dominant one. Biotite shows a parallel orientation along a particular direction except along shear zones where disorientation of minerals is exhibited.

The equant granoblastic aggregates of quartz grains show undulose extinction in a cloudy appearance and are extensively recrystallized with lenticular and subspherical shape occupying the interstitial position surrounding some of the feldspar grains forming mortar texture.

There exist lot of sphene which could probably be of metamorphic origin, zircon and apatite as accessories, together with magnetite and hematite which are remnants of the original magmatic rock.

The dark mineral of the rock is constituted by biotite, amphiboles, pyroxenes, oxides, and epidote, where biotite is dominant over the others. They totally make about 15% of the rock.

Texturally the rock is subgranular with relict megacrysts of feldspars and exhibits idiomorphic to hypidiomorphic porphyroclasts in a matrix of microlites of muscovite, sericite and chlorite.

The existence of weak foliation, recrystallized quartz, secondary minerals of metamorphic origin (chlorite, sericite, epidote

and pale-green amphibole), and abundant relict crystals indicate a low grade regional metamorphism of a pre-existing plutonic rock.

2.2.3.3 Meta-micro Diorite

The western part of the studied area is covered by dark-grey, massive to weakly foliated, medium to fine grained dioritic body. It shows no flow structure, and at some limited localities there exists concentrated amphiboles which is quite big in crystal size without any preferred orientation. These amphibole rich, melanocratic small bodies within the diorite could be xenoliths.

The section study showed two compositionally distinct types of dioritic bodies.

2.2.3.3.1 Pyroxene-hornblende-biotite-diorite

This rock unit is finer in grain size than the biotite-pyroxene-hornblend-diorite. It is mainly constituted by plagioclase, biotite, amphiboles, pyroxenes, alkalifeldspars and epidote, sericite and chlorite of metamorphic origin.

The dusty plagioclase, which is greater in abundance than the alkalifeldspars appears as stumpy, rectangular forms forming orthophyric textures. They are slightly altered to sericite.

The pyroxenes and the primary brown amphiboles are altered to a certain degree to pale green amphibole.

Biotite, which is the dominant coloured mineral is slightly transformed to chlorite.

There is a tendency to porphyritic texture formed by micro-megacrysts of plagioclase feldspars associated with small crystal inclusions of pyroxenes and brown amphibole exhibiting poikilitic texture.

The rock is poorly metamorphosed with well preserved igneous textures. The metamorphic effect is revealed by the presence of few epidote, some sericite inside plagioclases, very few chlorites from biotite, and pale-green aggregates of amphiboles, which are products of metamorphic transformation of pre-existing mafic minerals.

2.2.3.3.2 Biotite-pyroxene-hornblende-diorite

This rock unit is coarser in grain size than the previously discussed rock.

It is mainly constituted by plagioclase, amphibole, pyroxenes, few biotite, epidote, sericite, apatite and opaques.

The plagioclases are partly transformed to sericite and epidote, while the mafic minerals, pyroxenes and brown amphiboles are variably transformed to pale-green amphibole. The pyroxenes are constituted by both ortho and clino-pyroxenes.

The opaque minerals might be magnetite and there are very few squarely sectioned opaques which are probably sulphides. Among the accessories apatite is very abundant.

Some of the megacrysts of plagioclase are poikilitic as they contain small crystal inclusions of pyroxenes and amphiboles. The order of crystallization is given by pyroxene, then amphibole followed by plagioclase. The conclusion is derived from the fact that the amphiboles are present surrounding the pyroxenes, while both the amphiboles and pyroxenes occur within the plagioclase as small inclusions.

Most of the mineral grain in this rock assume a parallel direction of orientation.

Though both rocks are affected by a low grade metamorphism, the metamorphic transformation is more pronounced in this rock than in the previously discussed dioritic body.

2.2.3.4 Meta Gabbaro

This rock type is exposed west of Gulliso town forming a continuous ridge known as 'Sololo Ridge'. It is dark to green in colour, coarse grained, massive to weakly foliated and hard to break.

The rock is mainly composed of plagioclase of labradorite composition, green and brown amphiboles, red to brown biotite, pyroxene, and secondary minerals resulting from metamorphic transformation.

Along a fracture zone there exist equigranular, well packed, polygonal quartz grains associated with calcite forming granoblastic texture, which probably be a secondary hydrothermal filling.

Opaques, presumably magnetite, occur in a subordinate amount with a cloud of sericite and chlorite microlites surrounding plagioclase and biotite respectively, resulting from a later event which is related to the partial or complete retrogression of high temperature minerals. A lot of epidote is scattered within the rock, resulting from metamorphic transformation of plagioclases.

The clino-pyroxenes which exist in the rock are highly transformed along the border with relics at the core into an acicular aggregate of pale-green amphibole. The original brown amphibole of the rock are also transformed into pale-green amphibole of metamorphic origin.

Some of the feldspar laths present are totally engulfed by pyroxenes forming blasto-ophitic texture, while in some cases the the average length of the plagioclase laths exceeds that of the pyroxene grains, and the latter only partly enclose a number of the former forming a blasto-subophitic texture.

The mineral assemblage resulting from the metamorphic transformation indicate a low grade metamorphism.

2.2.3.5 Pyroxenite

This rock unit is exposed at the south eastern margin of the studied area. The exposures are restricted along hill sides around Limo and along Birbir River.

It is grey-greenish in colour with dark weathering surface, very coarse grained, massive to weakly foliated and highly fractured and altered. A big prominent quartz vein has dissected this rock prior to deformation and has been deformed together with the host rock keeping the same strike.

The rock is mainly composed of clino-pyroxene, amphiboles, and serpentine.

Though the pyroxene grains are highly transformed around the rim to an acicular aggregate of pale-green amphibole, in some of the thin sections there exist well preserved crystals.

Amphiboles are also transformed to new pale-green and colourless acicular amphiboles. Serpentine might be derived from amphiboles alteration. This is ascertained by non-existent of relict minerals of olivine and by the fact that some of existing amphiboles and serpentine occupy interstitial positions.

The accessories are constituted by some iron-oxides (opaques) and a lot of inclusions some of which are apatite.

2.2.4 Volcanic Rock

2.2.4.1 Olivine Basalt

The vast portion of the south-western part of the area is covered by a melanocratic, fine grained, massive and lustrous olivine basalt. These rocks in outcrop are found along hill tops and river beds as remnants from the lateritization effect which

crumbled down everything to lateritic soil and silicified crustal limonitic material.

The weathering product of the basalt can clearly be seen at some localities in succession from lateritic soil to unweathered fresh rock. At station A-14, South-west of Andu Village, near Gojeme River, the upper part of the slope is totally covered by a well developed soil, next to the soil is yellow to reddish, easily friable crustal limonitic material which rests on partly weathered rock material with a lot of cavities on the surface, and these parts of the rock grade to unweathered, lustrous fresh rock, which make the bed of the River Gojeme (Fig. 12).

The studied thin sections range from aphyric to subporpyritic, with micro-phenocrysts of olivine and clinopyroxene. The ground mass is constituted by euhedral to subhedral grains of plagioclase laths, pyroxene, and olivine enclosed in black to brown glassy mesostasise which is often devitrified. The few phenocrysts and some of the micro phenocrysts of olivine and pyroxene are resorbed and have reaction rim with the ground mass resulting in a contorted boundaries. These phenocrysts, the other unaltered grains of olivine, and pyroxene could be xenocrysts of older material.

The clinopyroxene is usually much more abundant in the matrix than olivine. The plagioclase in the ground mass vary from non-oriented to weakly aligned; compositionally they are predominantly in the sodic labradorite range.

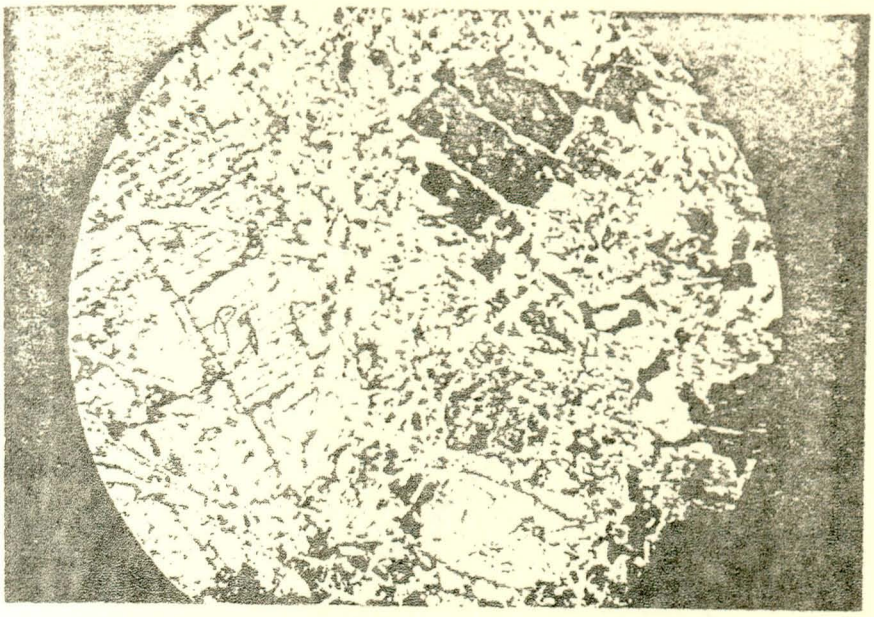

Fig.10: Pyroxerite: megacrysts of altered pyroxene (Py) and serpentine (Srp).

X-nicols, magnification 35X.

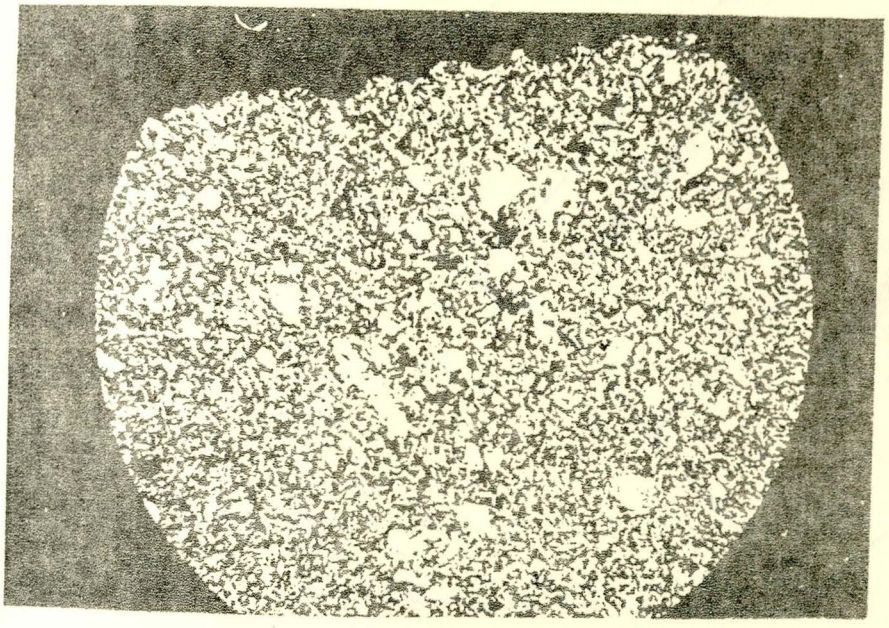

Fig.11: Olivine Basalt: olivine micro phynocryots (Ol) in plagioclose laths; some of the olivine grain are resorbed.

X-nicols, magnification 35X.

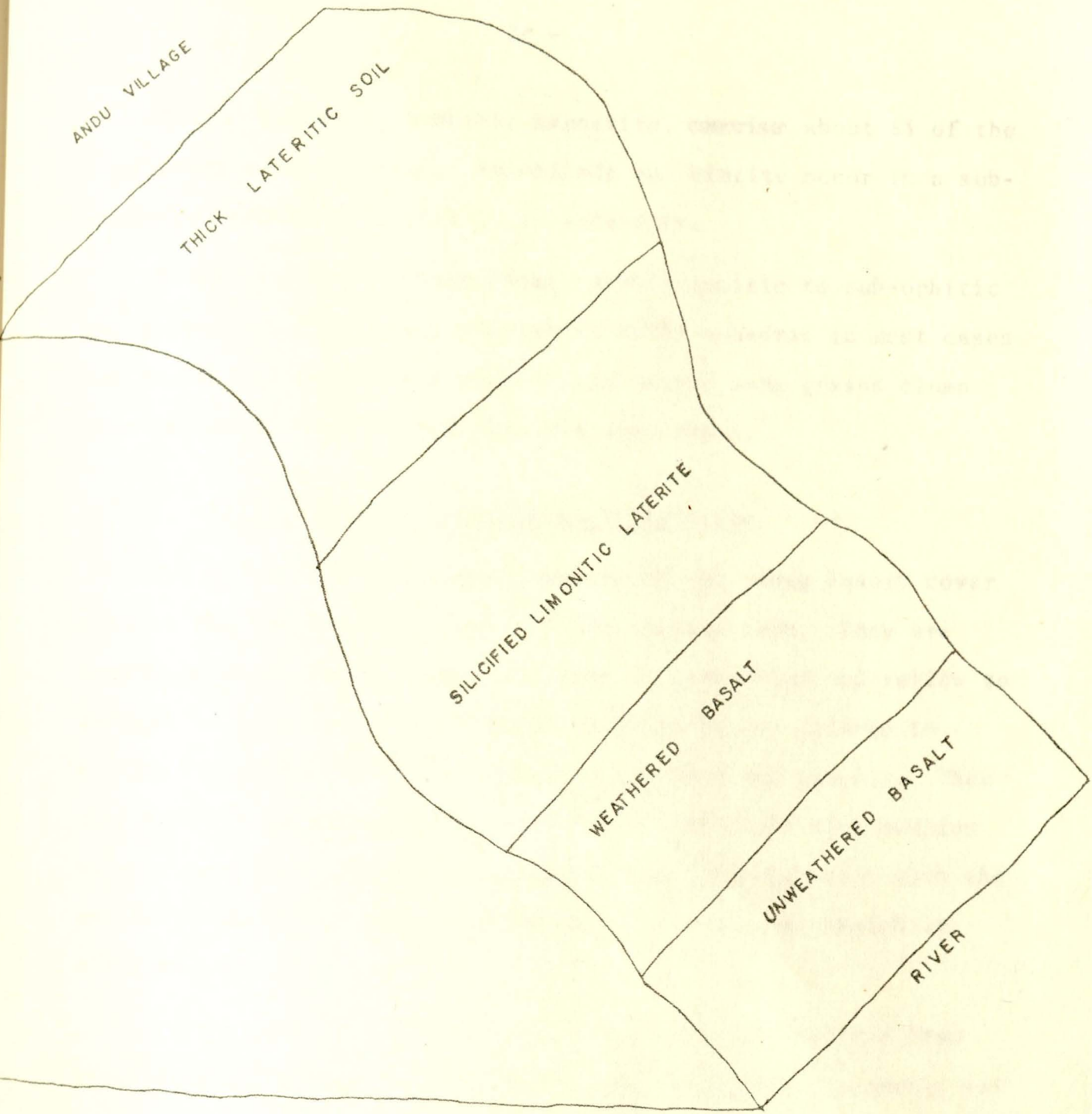

Fig. 12 SKETCH SHOWING THE RELATIONSHIP OF THE BASALT & THE LIMONITIC LATERITE.

Opaque minerals, probably magnetite, comprise about 5% of the constituents of the rock. Hornblende and biotite occur in a subordinate amount while apatite is accessory.

Texturally some plagioclases exhibit ophitic to sub-ophitic relationship with augite; olivine is fully euhedral in most cases but rounded or partly resorbed grains occur; some grains clump together to give glomeroporphyritic aggregates.

2.2.4.2 Silicified Residual Limonitic Laterite

The lateritic weathering products of the young basalt cover most of the south-western part of the studied area. They are heterogenous in appearance, and light to dark-brown and yellow to reddish in colour. In most cases these rocks are friable to earthy material and very seldom they are hard and compact. They show concentric laminated texture containing small dark nodules associated with vesicular structures. Their association with the unaltered basalt is discussed under 2.2.4.1 and the sketch is given in Fig. 12.

It was impossible to make thin and polished sections from these rocks, but chemical analysis for seven selected samples was made for both major and trace elements and the data are discussed under Chapter 5.

2.2.5 Meta Sedimentary Units

2.2.5.1 Quartziferous Micaceous Schists

This rock unit is exposed along stream beds covering a larger area. Most of the outcrops are highly weathered, easily friable, soaked with water and covered by stream side small plants.

The fresh outcrop varies from grey to blue and to pale-green in colour, and is fine grained, soft, and slightly talcous. The rock is at places interlayered with very small dark graphitic material and is well foliated and crenulated with moderate segregation of minerals.

Petrographic study showed the presence of muscovite, chlorite, and very few biotite, and quartz. The quartz is fine in grain size, but elongated along the direction of foliation and is extensively recrystalized with some of the grains forming granoblastic textures. Quartz and mica minerals form alternating layers, which are parallel to one of the schistosity planes. The quartziferous layers contain minor amounts of muscovite, which has parallel orientation whereas the micaceous layers have very few, if any quartz minerals. The micaceous minerals constitute the foliation of the rock forming ribbon texture with that of quartz (Fig. 13).

The number of deformational episodes should at least be two where one is to form the foliation (S_1) parallel to the original stratification (S_o) and the other is to form the fold fabric (S_2) which cuts S_1 and S_o at an angle of about 45-50°.

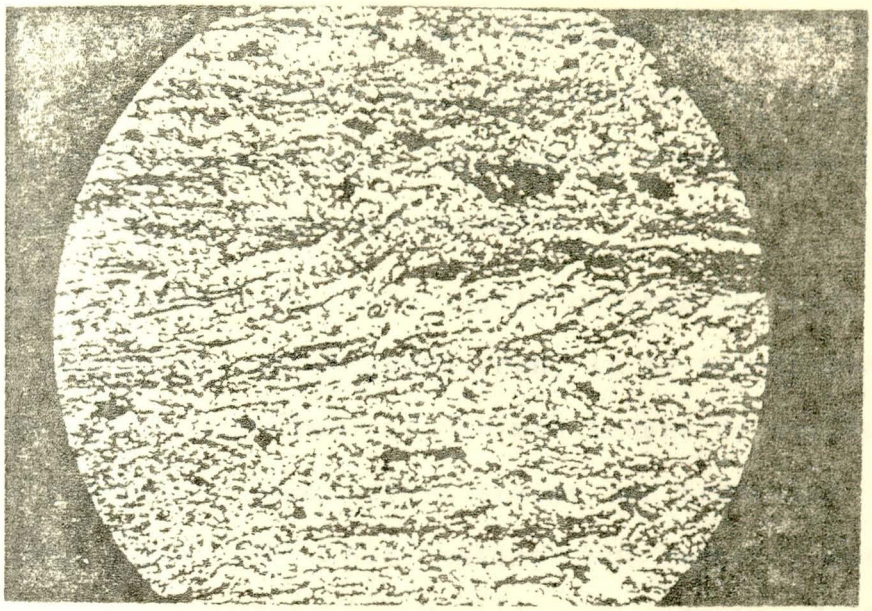

Fig. 13: Quarziferous-micaseous schist showing inter banding of Quartz (Q) and micaseous minerals (mic) and crenulated foliation.

Crossed nicols-magnification 35 X.

2.2.5.2 Ferruginous Quartzite and Associated Magnetite/Hematite Lenses

The ferruginous quartzites with their magnetite-hematite lenses appear in a lithologically well determined horizon belonging to the sequence of the Precambrian metasedimentary units. The fine grained, schistose and red brown ferruginous quartzites crop out in a narrow belt striking north-south. The quartzites seldom change heteropically into magnetite-hematite lenses; as it can be seen at Chago and Worekalu.

The iron ore horizon is mostly covered by thick lateritic soils. Due to the thick overburden, it is impossible to determine the exact dimensions of the ore lenses by surface geology without conducting geophysical survey and trenching. Rudis (1964) and Belay (1980) have carried out magnetic survey and made some trenching both along and across the strike of mineralization.

At Worekalu, which is south of Chago there is a large trench with fine to medium sized detrital floats of iron ore. The position of the mineralized zone is parallel to the main ferruginous quartzites trending north-south. At Chago the ore occurs in large and small blocks with some detrital floats mixed with soil (Fig. 14). The magnetite-hematite lenses show similar features throughout the explored area. It is dark grey to nearly black in colour with a metallic luster. The ore is usually compact, massive and hard to break.

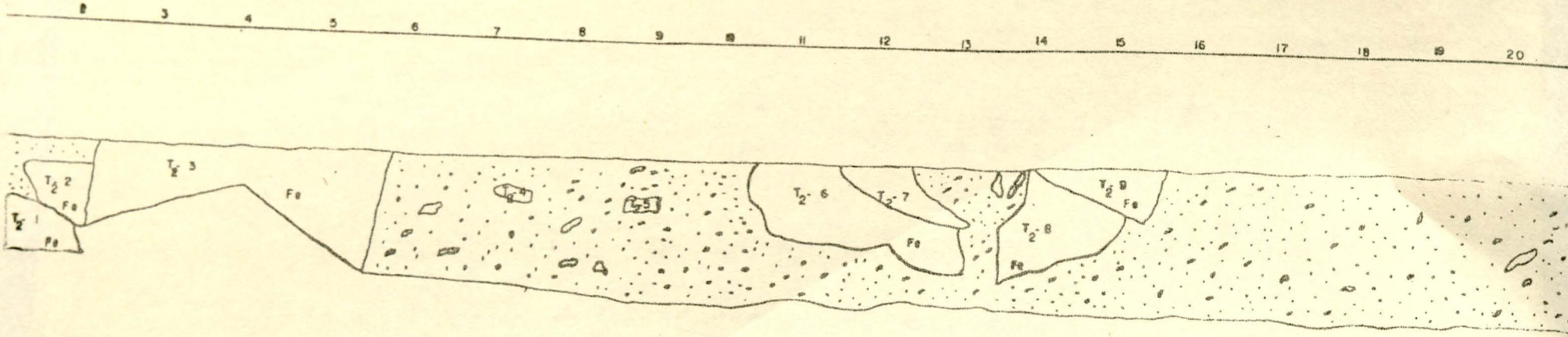

LEGEND

SOIL & FERRUGINOUS FLOATS

Fe IRON (Mag/hematite)

TOP & BOTTOM SURFACE

SCALE

2

CHAGO - IRON, TRENCH NO.2 CROSS - SECTION SOUTH FACE

FIGURE 14

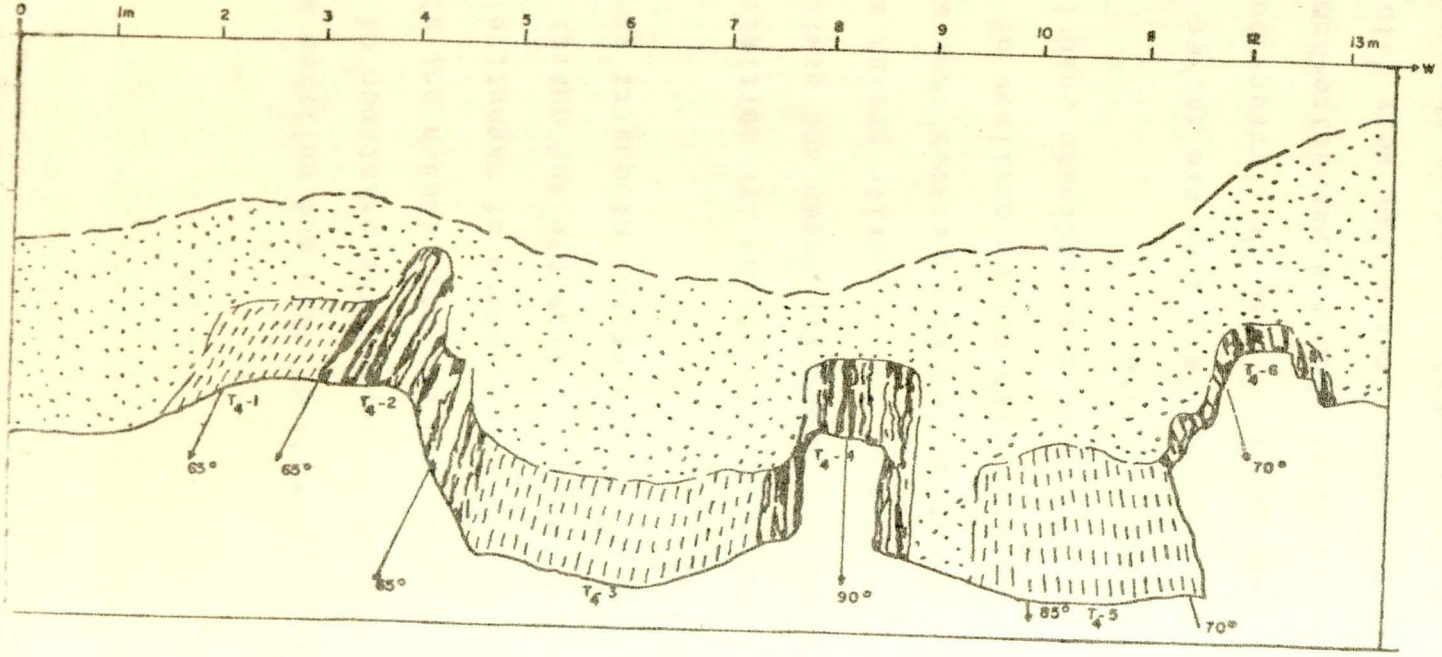

fig. 16 CHAGO IRON, Trench No.4, cross section south face, on profile 180s, 20w.

AFTER TEKLU BEKELE, et al TIR 28,'98)

Petrographic study of thin and polished sections of the ferruginous quartzites revealed the existence of magnetite, hematite, hydroxides of iron, and quartz. Though not all, some of the sections show clear interbedding of magnetite and quartz. Preferential growth of both the iron ore and quartz can be seen in some of the sections where the grains of quartz are fractured and show wavy extinction.

Most of the magnetite grains are martitized and changed into hematite, especially along fractures and grain boundaries. A considerable portion of the magnetite grains show a very advanced stage of martitization, where sometimes they are completely transformed into hematite, with relict outlines of the previous magnetite. Limonite occurs in a subordinate quantity mainly as goethite and seldom as lepidocrocite.

The magnetite-hematite lenses are rather more compact with less quartz, when compared with the ferruginous quartzites. The quartz grains are finer than the magnetite-hematite minerals. In some sections the quartz grains show very faint segregation with preferred orientation, while in others they are disseminated forming clustered aggregates, and in some of the samples investigated they appear in a very well developed interbanding with magnetite-hematite and barite. This feature can be seen both microscopically (Figs. 17-18) and macroscopically (Figs. 20-22).

Magnetite grains are rarely unaffected, they show a more or less high degree of martitization. Hematite originated by martitization is present surrounding magnetite grains, especially

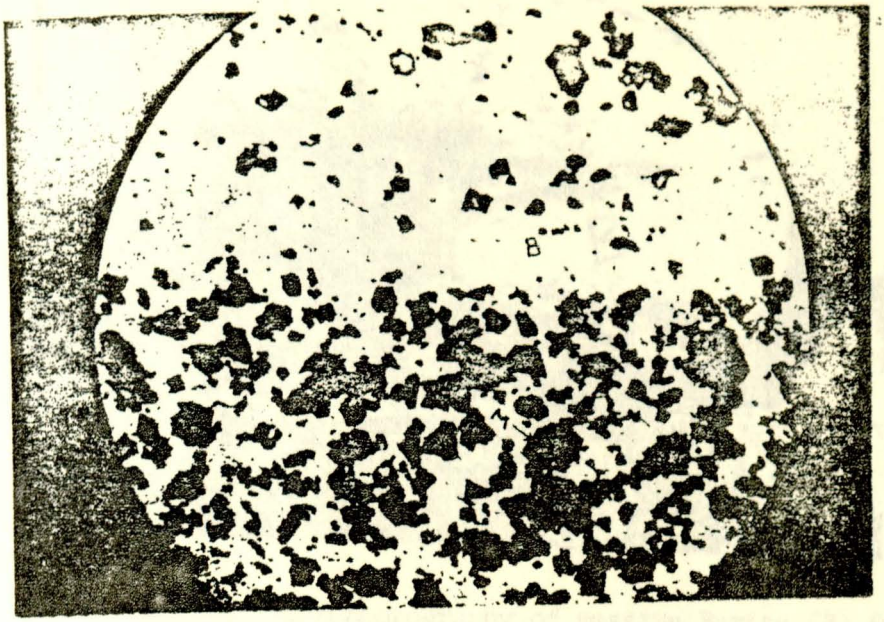

Fig.17: Interbanding of massive barite and magnetite.

Parallel-nicols, magnification 35X.

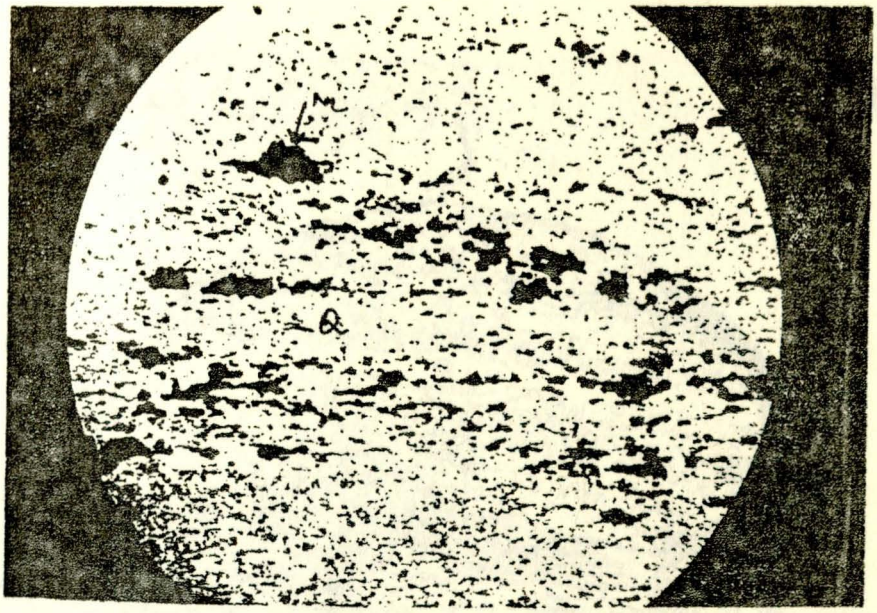

Fig.18: Quartzite: faint banding of quartz and magnetite.

Parallel-nicols, magnification 35X.

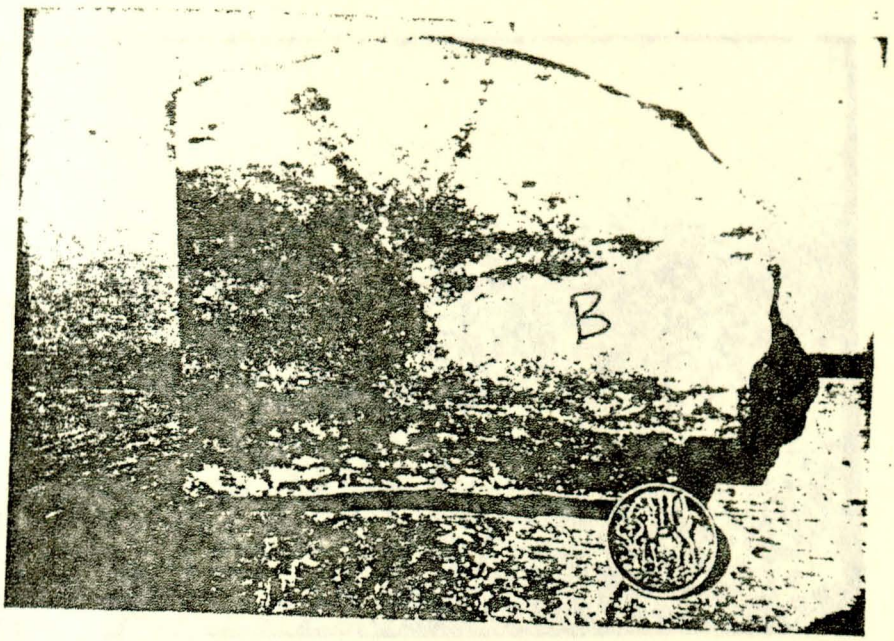

Fig.19: Barite: macrophotography of massive Barite (B) from St. 29.

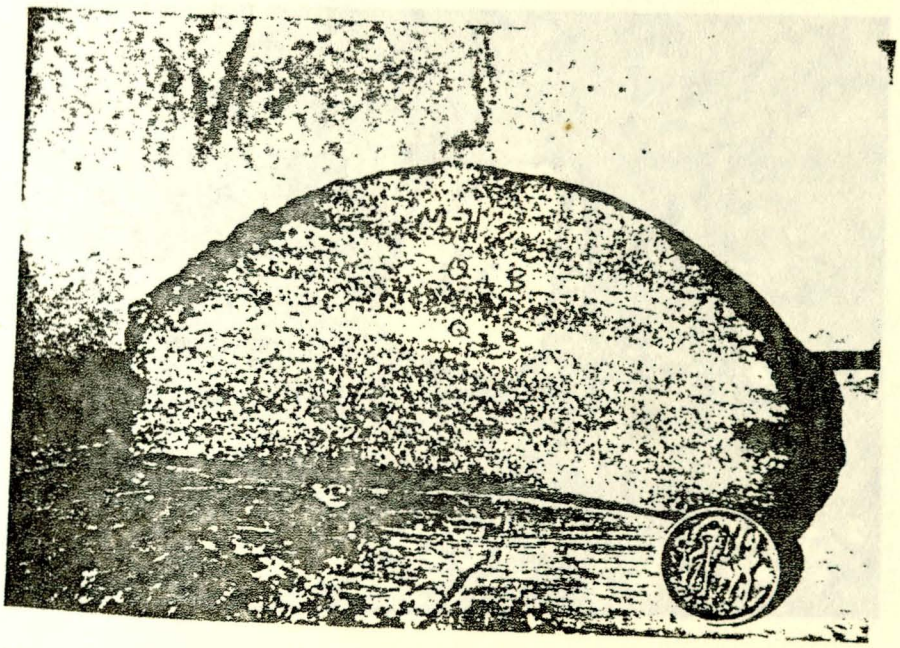

Fig.20: Macrophotography of interbanding of magnetite-hematite (M), Quartz (Q) and Barite (B).

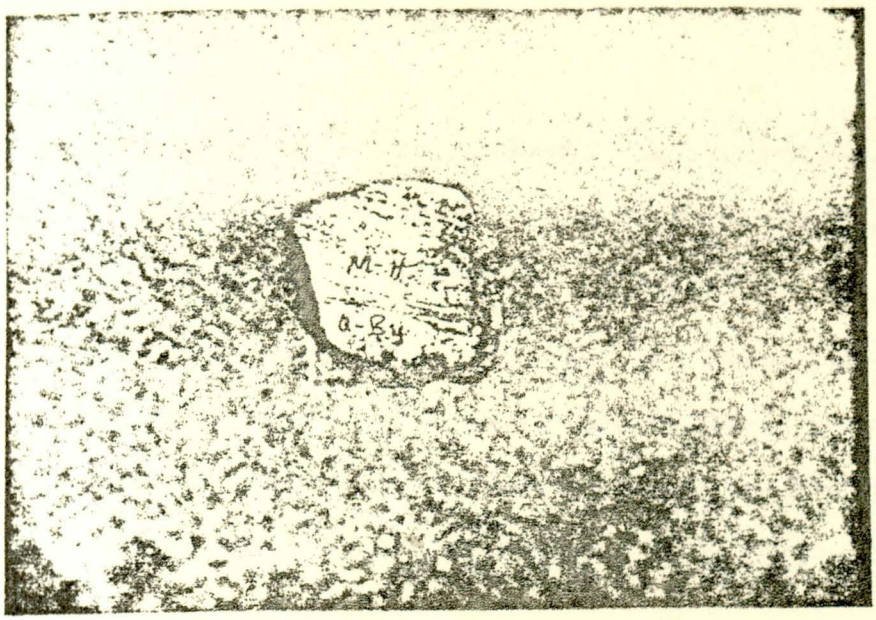

Fig.21: Macrophotograph of interbanded Quartz (Q) barite, (B) and magnetite-hematite (M)

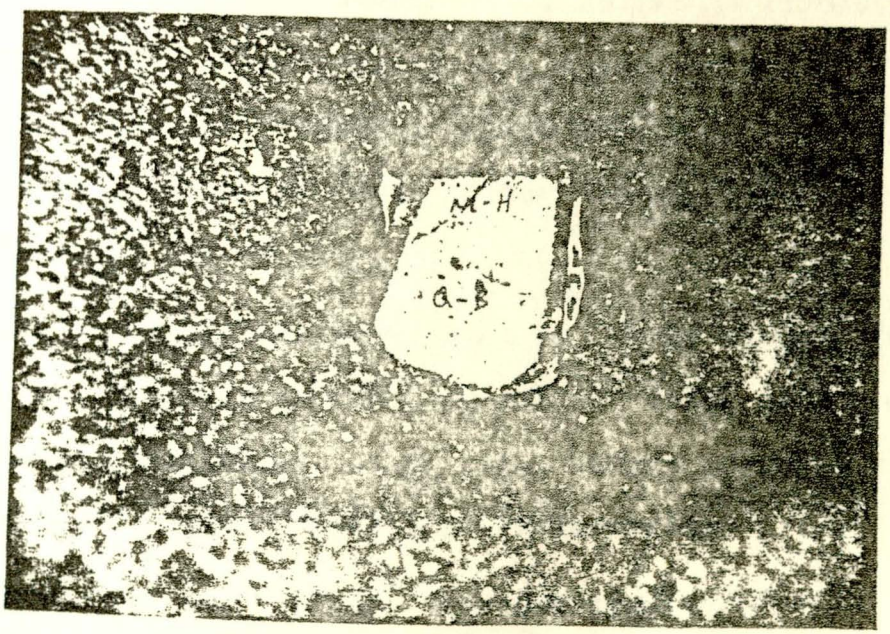

Fig.22: Macrophotograph of interbanded Quartz (Q) barite (B) and magnetite-hematite (M).

along fissures and faces of octahedron. In the polished sections all stages of martitization may be seen from the initial stage to the complete replacement of magnetite by hematite.

At one locality near Chage (Station 29) there exists an outcrop of barite interbanded with magnetite-hematite ore and quartz. A polished section study made at some part of the barite revealed the presence of sulphides; namely galena, sphalerite, chalcopyrite and covellite.

Galena with its white reflection colour appears surrounding sphalerite (Fig. 28). Within the sphalerite there are disseminated exsolution products of chalcopyrite with light yellow colour and high luster. As can be seen from the section, there are two generations of chalcopyrite, where one is formed as exsolution product from sphalerite (Chalcopyrite II), while the second one is syngenetic with the other sulphides (Chalcopyrite I, Fig. 28). Covellite is present surrounding Chalcopyrite showing its secondary development from the latter (Fig. 28).

The order of formation might be: first Chalcopyrite I, then sphalerite followed by Chalcopyrite II, which is the exolution product of sphalerite; galena comes before covellite which is the last product from weathering of chalcopyrite.

Both thin and polished sections studied on some of the samples of trench-3 indicated the existence of spheroidal materials, which appear in solitary, in pairs, and in most cases as colonies. These

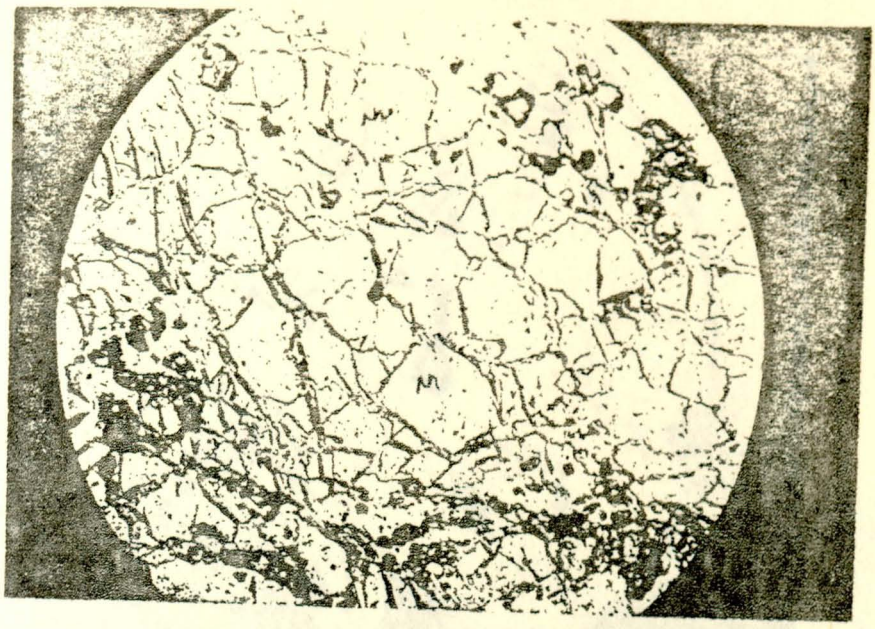

Fig.*23*: Net of martifization developing along the fractured margins of magnetite (m).

parallel-nicols, magnification 240X.

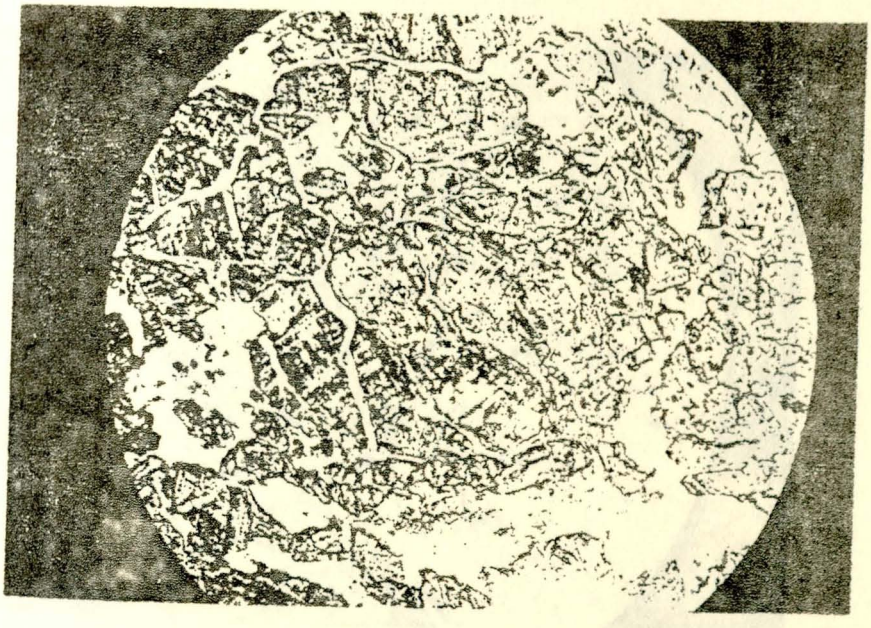

Fig.*24*: The above section in semicrossed-nicols. Magnification 240X.

Fig.25: Relics of magnetite (m) in crystals partly martitized and surrounded by Fe-hydroxides (Fe-hy)

Parallel-nicols, magnification 240X.

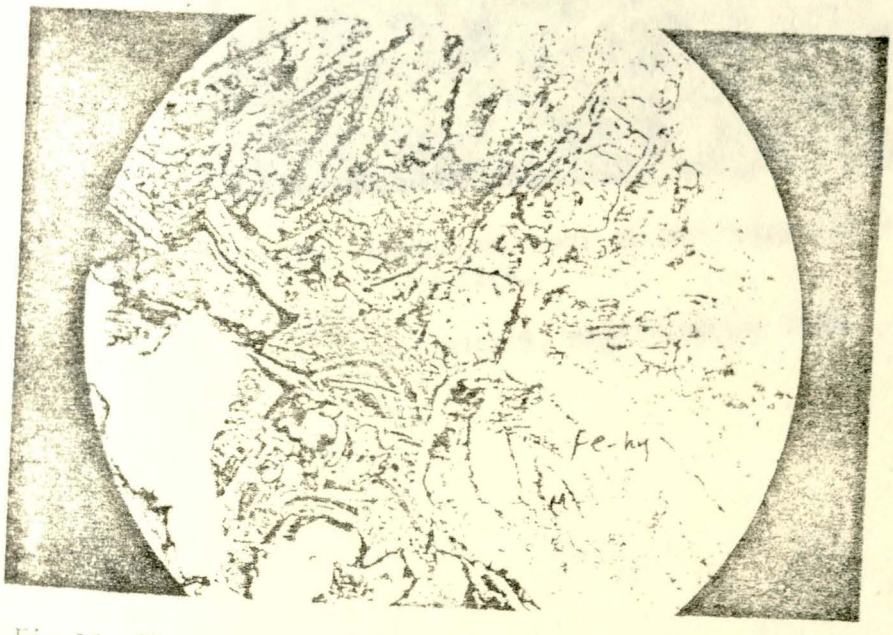

Fig.26: The above section is semicrossed-nicols. Magnification 240X.

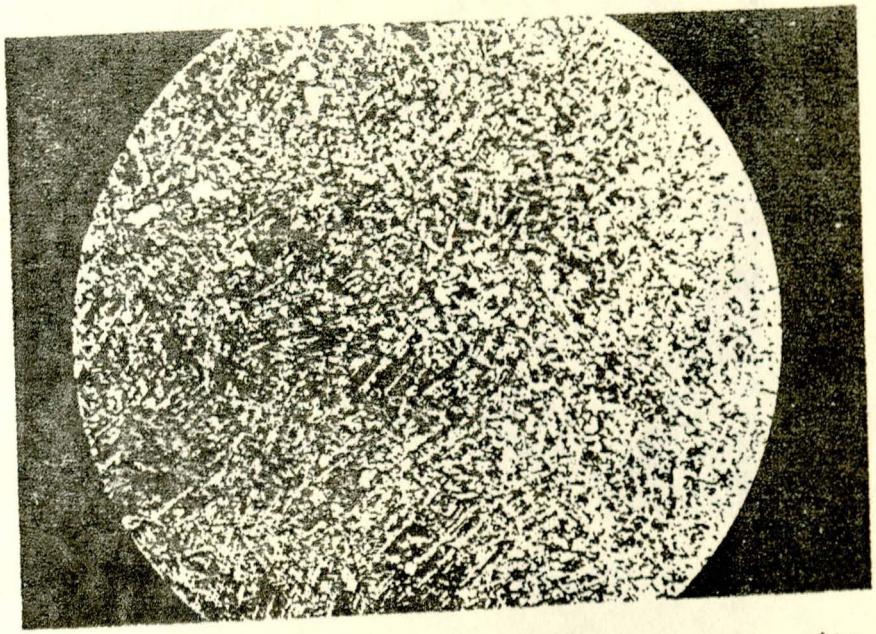

Fig.27: Fibrous net work of martitization of magnetite to hematite.

X-nicols, magnification 240X.

Fig.28: Microphotography of sulphides in polished section. Galena (G), Sphalerite (Sp), Chalcopyrite (Ch) and Covellite (C). The background is Barite (B).

Parallel-nicols, magnification 240X.

very small magnetite-hematite grains are suspected to be fossils of micro-organisms and are discussed in Chapter 4 under micro-paleontology (Fig. 33).

2.2.5.3 Quartz-muscovite-sericite Schist

This rock unit covers a large portion of the metasediments and is pink in colour, lustrous, soft with dusty powder of red paint, fine grained and at various localities of its exposure, especially to the northern part, it is strongly weathered and totally crumbled to soil keeping its strike and dip featuring the original position.

The rock is intercalated with a series of ferruginous metasediments associated with minor graphitic phyllites in the upper part. It is well foliated and strongly deformed and folded particularly at the southern part of the studied area, and also dissected by prominent quartz veins at various localities.

Thin section study revealed the existence of quartz, muscovite, sericite, chlorite and very few biotite with some accessory opaque minerals, possibly magnetite.

Quartz occurs in the groudmass and in a very few case as porphyroblasts. They are elongated and recrystallized along the direction of foliation. The foliation is formed by parallel alignment of chlorite, muscovite, and sericite which have made alternating stratification with the quartz grains, hence forming

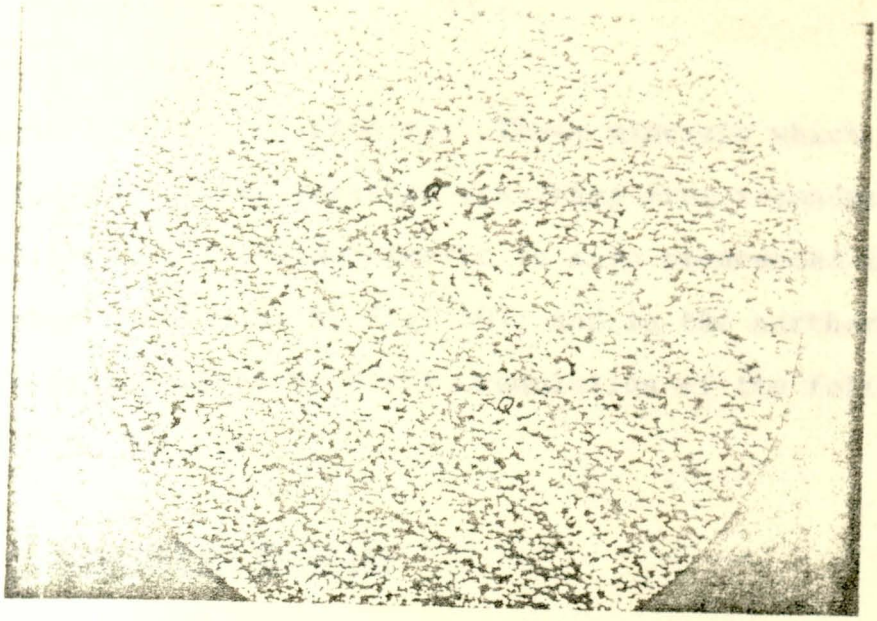

Fig.29: Quartz-muscovite sericite schist: the foliation is formed by alignment of muscovite, chlorite and sericite. Shows crenulated foliation. (Q= Quartz).

X-nicols, magnification 35X.

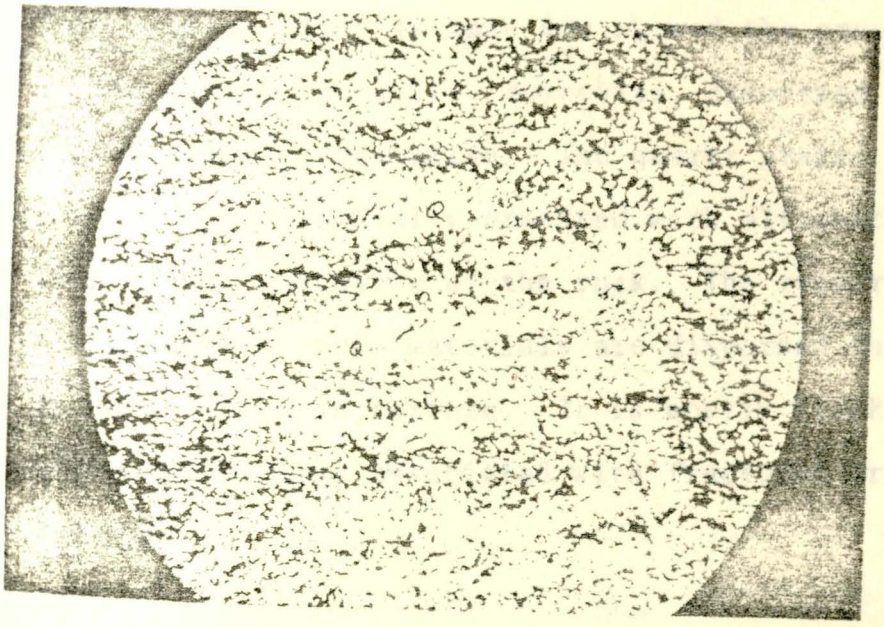

Fig.30: The same rock type as Fig.29. It shows intense deformation than the above one. The fold fabric is more pronounced.

X-nicols, magnification 35X.

the lepidoblastic schistosity. These minerals which form the foliation are folded together resulting from secondary stage of deformation. This folded fabric is more pronounced in the southern part (thin section 51-b, Fig. 30), and in the northern part of the area it is expressed by minor crenulation of the foliation (thin section 2a, Fig. 29).

2.2.5.4 Graphytic Phyllite

A small road side exposure near Chago along the main route to Aira. It is a thin intercalation within the quartz-muscovite-sericite schist. It is pale blue in colour, easily friable, very soft and shinny, fine grained with silt size materials.

Thin section study (sample 40) showed the presence of very fine quartz grains, sericite, muscovite, dispersed organic matter, and opaques probably magnetite. The quartz grains are uniformly dispersed and preferentially oriented with alternating sequence with that of the muscovite of the rock. The rather uniformly distributed tiny organic materials are dispersed throughout the rock and are dotted in texture. It is mostly black and dark-brown in colour, while those associated with fractures are dark-brown with red shade.

2.2.5.5 Quartzite

This rock unit is exposed at the southern part of the studied area. It is a very small road side exposure and slightly affected by weathering.

Petrographic study both in thin and polished sections (sample 58) revealed the existence of quartz, very few feldspars, magnetite and hematite.

The grains of quartz are well packed and show some degree of recrystallization. They show a preferential growth and some of the grains are fractured and show wavy extinction.

Minor interbandings of magnetite and quartz are visible. Magnetite is concentrated at a particular level and also disseminated in the quartz grains. Here the amount of quartz is dominant over opaques (Fig. 18).

The rock shows an elongated, seriate granoblastic texture.

2.2.5.6 Quartz-sericite-chloritoid Schist

This rock unit is exposed at the side of a prominent ridge west of Chago and along the main road to Aira where rock materials have been excavated for road construction. It is light greyish, well foliated, fine grained rock overlying conformably the quartz-muscovite-sericite-schist.

This section study disclosed the presence of quartz, feldspars, sericite, chloritoid, chlorite, muscovite and very few epidote, biotite, and pale-green to yellowish amphibole.

Quartz grains are angular to sub-angular, recrystallized and elongated along the direction of the foliation. Dark to green chloritoid minerals exist in the rock in equal amount with quartz

and are fragmented, massive, tabular to acicular in appearance, and are well dispersed throughout the sections (Fig. 31). The foliation is produced by the presence of stretched micaceous minerals along the original bedding plane where it is constituted by muscovite, chlorite, sericite, and few biotite. Faint to moderate segregation of minerals can be observed parallel to schistosity and the foliation is slightly crenulated.

The quartz and the chloritoid are dominant over the micaceous minerals which exist in a subordinate amount.

At least two deformational episodes can be recognized from the thin section study:

a) The parallel orientation of the chlorite and sericite with the original bedding (S_o) forming the foliation plane (S_1).

b) The second foliation plane (S_2) is produced by the chloritoid which has grown at about 70^o to the chlorite orientation.

The dominant texture is lepidoblastic with minor granoblastic features.

2.2.5.7 Sericite-chlorite-muscovite Schist

This rock unit is exposed on a small hill top along the road to Aira. It is fragmented and scattered on the hill-top and probably lies conformably on the quartz-sericite-chloritoid schist. But it is very difficult to get a direct contact of the two litho-

units due to the intense weathering and thick soil cover.

The rock is pale-blue in colour with pink-greyish weathering surface, has medium grain size, and is well foliated.

The petrographic study showed the presence of quartz, muscovite, chlorite, sericite, few epidote and apatite and some opaque minerals, which probably are magnetite.

The quartz grains are fine to medium with some degree of recrystallization and most of them show very irregular boundaries and are dispersed within the section. Quartz contain several solid inclusions and some of them are apatite and opaques.

The muscovite appear in large crystal and are elongated along two schistosity planes which cross at an angle of about 45^{o}. Sericite constitutes the fine grained matrix enveloping the quartz grains and is not oriented, which could probably indicate its formation by secondary transformation process. Chlorite is associated especially with unoriented sericite and also occur with muscovite crystals along schistosity planes.

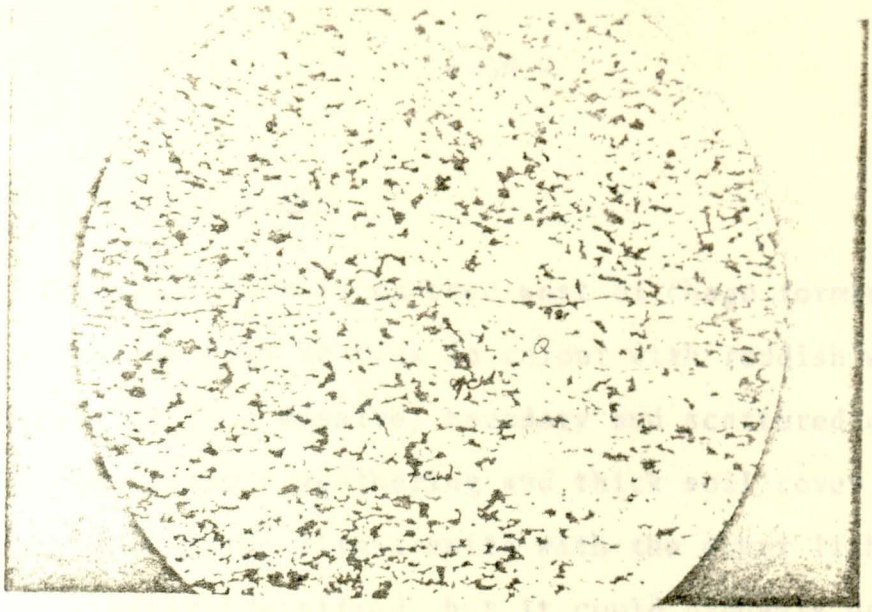

Fig. 31: Quartz-sericite-chloritoid schist: alignment of Quartz (Q) and sericite (Sr). The chloritoid (Chd) is inclined at an angle to the foliation (S_1).

X-nicols, magnification 35X.

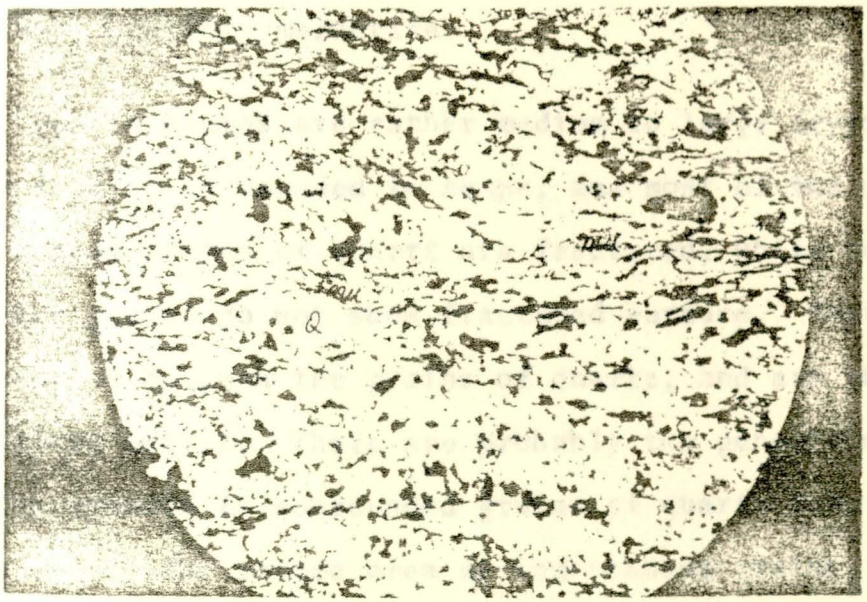

Fig. 32: Sericite-chlorite-muscovite schist: coarse grains of Quartz (Q) and muscovite (mu). They are elongated along the shistosity plane.

X-nicols, magnification 35X.

2.2.5.8 Lith-Arenite

This rock unit is exposed west of Chago forming a prominent ridge, and is grey to pink in colour with reddish weathering surface. It is a massive, boundery and scattered outcrop, and due to the intense weathering and thick soil cover of the area the contact of the lith-arenite with the other litho-units cannot be clearly identified, but it could probably be an intercalation within the schists.

Thin section study showed the existence of quartz, sericite, feldspar, subordinate amount of chlorite and biotite with some opaques, probably magnetite.

Quartz grains are rather medium to large crystals and range from angular to rounded in shape, and most of the rounded and subrounded grains of quartz are fractured, while some of the angular grains do not show fractured surface. Mostly there is no contact between the grains of quartz, and are embedded in the sericitic matrix, There are probably two generations of quartz, as the rounded to subrounded grains of quartz have been derived from a very far source area as independent grains, while the angular and unfractured quartz grains could be added to the basin from neighbouring area without long distance of transportation; or could have been released from rock fragments within the basin. They are rather uniformly distributed and could have been settled in agitated water.

There is no well developed foliation, the sericitic material does not show any preferential orientation rather differently oriented enclosing the quartz grains. Its appearance as a pseudomorph could indicate a probable transformation product from feldspars.

METAMORPHISM AND STRUCTURE

3.1 Metamorphism

As observation on metamorphic mineral assemblages indicated, the explored area has been affected by regional metamorphism which involved both the plutonic and sedimentary rocks.

The mineral assemblages found in both rock types are:

muscovite-sericite-chlorite-epidote;

Quartz-sericite-muscovite-epidote-pale green amphibole-chlorite;

pale green amphibole-chlorite-epidote-sericite;

serpentine-pale green amphibole;

pale green amphibole-chlorite-sericite-epidote

Quartz-sericite-chlorite;

Biotite-muscovite-chlorite-quartz;

Quartz-chloritoid-chlorite-muscovite;

Sericite-chlorite-muscovite.

The rocks have undergone low grade regional metamorphism of greenschist to lower amphibolite facies. The metamorphism and degree of deformation seem to increase to the southern part of the studied area. Some of the rocks exposed around Werekalu are highly deformed and folded with segregation of minerals forming thin bands.

3.2 Structure

The structural study of the area has suffered from lack of outcrops, intense weathering and very thick soil cover, which made almost impossible to make an accurate structural reconstruction and interpretation.

Foliation and/or faint gneissic layering is the dominant planar feature in the studied area. The foliation is defined by the parallel preferred orientation of platy minerals whereas the gneissic layering is defined by faint segregation of dark and light minerals. These features have a general NNE-SSW and NNW-SSE trend with moderate to steep dips towards west or east.

In the eastern half of the area, these planar features predominantly dip to the east with average dip angle of 65^{o}, whereas, in the western half of the area, the planar features with minor variation dip to the west with average dip angle of 60^{o} defining a major antiform.

At least two phases of deformation are recognized in the rocks. The early phase, producing the regional foliation (S_1), is axial planar to the tight isoclinal folds and often completely transposes the original sedimentary layering (S_0). The second phase of deformation (S_2) is expressed by the formation of the fold fabric, resulting in a series of isoclinal folds with southerly plunging fold axes.

Mineral lineation due to alignment of prismatic minerals is the dominant linear feature in the rocks of the studied area. These linear features have a pronounced nearly north-south trend with plunge 05^{o} - 20^{o}.

Systems of quartz veins trending north-south and E-W cut the rocks at different localities.

NW-SE trending fractures and minor faults are observed on air photographs and some are confirmed in the field (Belay, et.a., 1980).

4. Micro Paleontology

Micro paleontological investigations carried out on samples No. T_3-7 both in thin and Polished sections have revealed the occurrence of large populations of spheroids of certain biological origin. Such organisms which have a medium size of 7.8^{-4}mm occur as solitary individuals but, most commonly, occur in populations of a few to several dozen cells in close proximity. When in large populations, individuals are closely packed (generally the sphericity is not lost due to the material compaction), but adjacent cells in most cases are separated by a few microns of space. Such spheroidal bodies, in many of which dark inclusions (nuclei?) are observed, strongly suggest algal origin (cynobacteria) particularly in their size range. At the scope of the present study it is not possible to state whether the dark inclusions are real nuclei (and hence eucaryotic cells) or not; because such inclusions can be also satisfactorily explained as procaryotic cells, which have undergone plasmolitic degradation.

Incomplete preservation, mostly due to diagenetic alteration, mineralization, and metamorphism a detailed taxonomic interpretation cannot be given. As a preliminary study it can be stated as undifferentiated biospheroids. However some similarities with the blue-green algal genera Myxoccocoides and Gloedionopsis are observed.

Fig.33a: Undifferentiated biospheroid(?) in Solitary and Co1eny.

X-nicols, magnification 1280X.

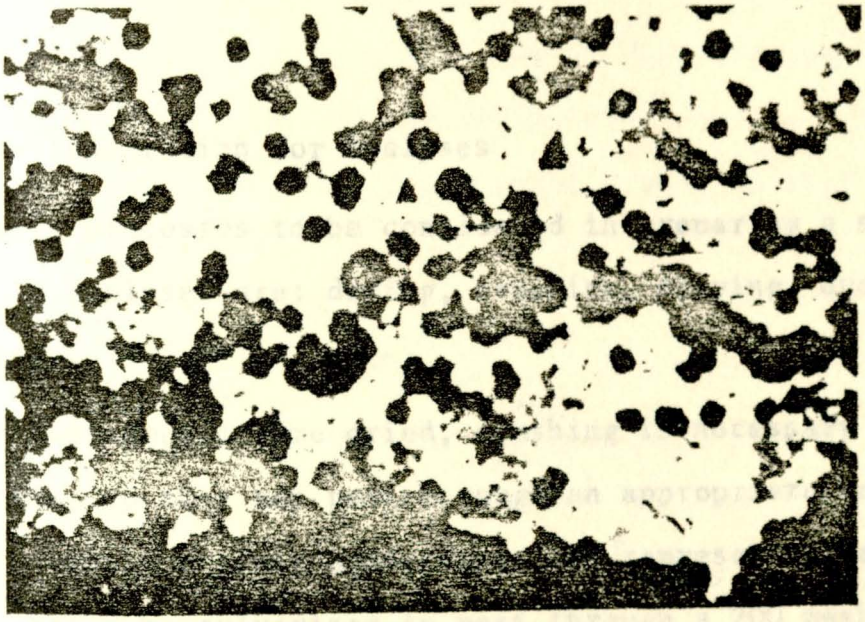

Fig.33: Undifferentiated biospheroid (?) in Solitary and Co1eny.

X-nicols, magnification 512X.

GEOCHEMISTRY

5.1 Introduction

Chemical analyses for 78 rock and ore samples were conducted at the Chemical Laboratory of Ethiopian Institute of Geological Survey. Both major and trace element determinations have been carried out. The analyzed major elements are SiO_2, Al_2O_3. Fe_2O_3, FeO, CaO MgO, Na_2O, K_2O, MnO, TiO_2 and P_2O_5, while the trace elements are Co, Ni, Cr, Pb, V, Zr, Ba, Mo, Mn and Ti.

The results have been treated graphically, and an interpretation was extracted in order to determine the environment of formation of the various rocks, their relationships, and source of materials for the various lithounits, and age of rocks and mineralization.

5.2 Sample Preparation for Analyses

The main processes to be considered in preparing a sample for chemical analyses are: drying, crushing, sieving, quartering and grinding.

After the samples were dried, crushing is necessary to reduce the rock size, so they may pass through an appropriate screen. In order to obtain a truly homogeneous and representative sample, the rocks should be pulverized to pass through a 200 mesh screen.

Two stages of crushing were used; the first one was to reduce the big samples into small fragments, the second stage of crushing

further reduced the small fragments into finer ones prior to quartering.

After crushing the samples were mixed and quartered in order to obtain a representative portion of a large sample. Following the quartering process a small portion (10-15 gms) of the rock, was taken and grinded by means of a non-contaminating mill, to ensure a representative homogeneous sample.

Two methods of grinding were used in order to avoid contamination of the samples.

a) Cobalt-Tungsten, and

b) Chromium-Iron.

The cobalt determination was carried out from the samples grinded by the chromium-iron mill; while the chromium and iron analyses were made from the samples prepared by the cobalt-tungsten mill. The method has contributed a lot, to minimize the risk of analytical errors.

5.3 Methods of Analyses

The test samples which were prepared according to the methods explained under 5.2, were analyzed using instrumental and chemical methods of analyses for major and trace elements.

The instrumental methods of analyses include

1. Atomic absorbtion spectrophotometry, and
2. Optical emission spectrophotometry.

While the chemical analyses include

1. Titrimetric
2. Colorimetric, and
3. Gravimetric

All the oxides, except FeO, TiO_2 and P_2O_5 and some of the trace elements (Co, Ni, Co and Pb) were determined using the atomic absorbtion spectrophotometer; while the analyses for the rest of the trace elements were carried out by optical emission spectrophotometer.

TiO_2 and P_2O_5 were analyzed by colourimetric method, where the absorbance of colour complexes is determined.

Ferrous oxide (FeO) was determined titrimetrically, where the ferrous ion was oxidized to ferric ion by using metavanadate as oxidizing agent.

Moisture content and loss on ignition were determined using gravimetrical method of analyses.

Two methods were adopted in preparing analytical test solutions.

1. Cold HF attack, and
2. Fusion

In both cases 0.2 g. of the sample was accurately weighed to the nearest 0.001 g. In the fusion method lithium metaborate and/or tetraborate were used as flux depending on the nature of the sample.

5.4 Geochemistry of the Plutonic and Basaltic Rocks

5.4.1 Introduction

The data obtained from the chemical analyses of the plutonic and basaltic rocks are attached under Tables 3-18. They were used to plot both binary and triangular variation diagrams; when the results are applied to draw relationship among the different lithounits.

Twenty samples of granite, quartz diorite, diorite; gabbro, and basalt were used to plot the variation diagrams. A mini computer was used for plotting, giving different symbols for the different rock units.

Rock	No. Samples	Symbol Used
Granite	4	+
Quartz diorite	4	x
Diorite	6	*
Gabbro	1	⊕
Basalt	5	◊

The basaltic rocks are used together with the metamorphosed plutonic rocks in order to compare the chemical composition of the original magmatic material of the plutonic rocks with the younger effusive ones.

5.4.2 Variation Diagrams

Chemical variation within the rocks of one magma series, or among the rocks of different petrogenic provinces, can be conve-

TABLE 3 : Major Element Contents of Biotite Granite (Wt %)

Field No.	SiO_2	Al_2O_3	$Fe_2O_3^t$	CaO	MgO	Na_2O	K_2O	H_2O	L.O.I.	MnO	TiO_2	P_2O_5
A-54	77.0	12.5	1.71	0.4	0.2	2.6	5.4	0.1	0.8	< 0.1	0.13	0.07
55	76.0	11.5	2.22	0.6	0.2	2.8	4.8	0.1	0.8	< 0.1	0.32	0.04
56	77.0	10.4	2.22	0.8	0.2	2.8	4.4	0.1	0.8	< 0.1	0.15	0.03
57b	74.0	13.1	2.58	1.6	0.6	3.5	3.4	0.1	0.7	< 0.1	0.20	0.08

TABLE 4 : Major Element Contents of Qu artz Diorite (Wt %)

A-10	57.0	15.5	10.36	5.0	2.5	4.4	2.1	0.2	0.6	0.2	2.00	0.86
59	60.0	15.3	8.10	5.7	3.3	3.1	2.0	0.1	1.0	0.1	1.0	0.20
60	62.0	14.9	7.93	4.4	2.4	3.1	1.5	0.1	2.2	0.1	0.75	0.16
61	55.0	17.3	9.22	7.2	4.0	3.8	1.7	0.1	0.8	0.1	0.75	0.24

TABLE 7 : Major Element Contents of Micro Diorite (Wt %)

Field No.	SiO_2	Al_2O_3	$Fe_2O_3^t$	CaO	MgO	Na_2O	K_2O	H_2O	L.O.I.	MnO	TiO_2	P_2O_5
A- 4	54.0	15.7	10.51	7.2	6.2	3.3	1.6	0.2	0.7	0.1	1.62	0.18
21	53.0	15.9	11.07	7.8	6.2	3.0	1.0	0.1	0.3	0.2	1.53	0.18
74	48.0	15.2	14.01	10.6	5.8	3.1	0.5	0.1	0.4	0.2	1.88	0.47
38	48.0	16.1	12.40	8.8	6.7	2.5	1.3	0.3	1.2	0.2	1.84	0.27
39	50.0	14.8	13.30	10.0	6.6	2.9	0.4	0.1	0.8	0.2	1.71	0.25
7a	48.0	15.6	15.54	6.9	4.8	3.4	1.2	0.6	0.4	0.2	2.29	0.56

TABLE 8 : Major Element Contents of Gabbro (Wt %)

A-38	48.0	15.6	12.01	7.2	9.0	2.7	0.8	0.2	2.5	0.2	0.94	0.29

TABLE 9 : Major Element Contents of Pyroxenite (Wt %)

A-47a	50.0	3.0	9.15	18.6	17.0	0.4	0.1	0.1	1.2	0.2	0.27	0.02
48	50.0	2.6	9.58	12.4	18.0	0.3	<0.1	0.6	2.1	0.2	0.23	0.01
49	48.0	1.1	8.34	12.8	22.4	<0.1	<0.1	0.2	6.1	0.2	0.10	0.02

TABLE 10: Trace Element Contents in PPm of Microdiorite

Field No.	Co	Ni	Cu	Pb	Cr	Mn	Ti	V	Zr	Ba	Mo
A- 4	40	75	170	20	30	1000	3000	300	50	-	0.7
21	20	80	215	20	100	3000	7000	300	200	-	0.5
74	30	50	115	15	150	7000	5000	150	300	300	-
28	30	80	80	20	300	3000	3000	300	20	-	0.5
39	20	30	265	20	500	3000	5000	500	100	500	0.7
7a	50	65	155	20	100	3000	1000	300	70	0.5	0.5

TABLE 11: Trace Element Contents in PPm of Gabbro

A-38	55	150	95	10	215	3000	3000	200	100	2000	0.5

TABLE 12: Trace Element Contents in PPm of Pyroxenite

A-47a	20	70	170	15	500	7000	2000	200	50	-	0.5
48	40	90	55	10	700	3000	2000	200	20	-	0.5
49	45	280	480	30	700	3000	700	100	10	200	0.5

TABLE 13: Major Element Contents of Olivine Basalts (Wt %)

Field No.	SiO_2	Al_2O_3	$Fe_2O_3^t$	CaO	MgO	Na_2O	K_2O	H_2O	L.O.I.	MnO	TiO_2	P_2O_5
A-12a	46.0	12.2	14.58	9.4	8.8	1.4	1.4	1.5	1.9	0.2	2.50	0.74
14b	44.0	13.6	13.87	10.0	8.4	1.8	1.3	1.2	2.1	0.2	2.47	0.70
14c	44.0	14.0	14.01	9.8	8.6	2.0	1.6	1.2	1.7	<0.1	2.42	0.7
45	47.0	14.5	17.16	7.4	5.2	3.5	1.2	0.5	0.4	0.2	2.38	0.51
75	50.0	15.2	14.94	7.6	4.2	3.2	1.0	0.2	1.2	0.2	1.95	0.50

TABLE 14: Major Element Contents of Limonitic Laterite

A-12b	13.0	12.8	58.34	<0.1	0.2	<0.1	<0.1	1.4	12.3	0.1	1.67	0.26
13	11.0	11.3	60.55	<0.1	0.2	<0.1	<0.1	1.9	12.1	<0.1	2.20	0.48
14a	17.0	20.3	41.18	0.6	0.4	<0.1	0.2	4.1	13.6	0.5	2.06	0.87
15	19.0	18.4	45.04	0.4	0.2	0.2	<0.1	1.6	12.5	<0.1	2.41	0.28
16	15.0	12.5	60.80	1.8	0.4	<0.1	<0.1	1.1	7.6	<0.1	1.95	0.2
44	16.0	12.0	57.19	0.3	0.2	0.2	<0.1	0.4	11.2	0.2	1.5	0.41
77b	14.0	10.1	59.90	0.1	2.2	<0.1	<0.1	0.3	10.3	<0.1	1.67	0.63

TABLE 15: Trace Element Contents in PPm of Olivine Basalts

Field No.	Co	Ni	Cu	Pb	Cr	Mn	Ti	V	Zr	Ba	Mo
A-12a	50	130	210	25	1000	3000	3000	300	100	-	2
14b	55	180	130	20	50	3000	300	20	5	-	1
45	40	75	225	25	30	5000	1%	500	500	300	0.5
75	40	35	80	20	30	7000	5000	300	200	1000	0.5
14c	55	140	95	35	300	3000	1000	300	200	-	2

TABLE 16: Trace Element Contents in PPm of Limonitic Laterite

A-12b	40	55	130	60	3	300	700	30	30	-	1
13	35	60	125	40	70	200	1000	30	10	-	1
14a	95	65	110	60	200	5000	5000	7	70	-	1
15	35	60	50	60	200	1000	2000	70	100	-	2
44	30	30	125	40	10	2000	3000	20	200	-	2
77b	45	60	40	40	15	100	2000	10	70	-	-
16	20	40	45	115	-	300	3000	15	50	-	1

TABLE 17: Average Chemical Compositions (Oxides, wt %) of the Flutonic and Younger Volcanic Rocks

Elements (wt %)	1	2	3	4	5	6
SiO_2	76	58.5	50.16	48.0	46.2	49.33
Al_2O_3	11.87	15.75	15.55	15.6	13.9	2.23
Fe_2O_3	2.18	8.9	12.81	12.01	14.91	9.02
CaO	0.85	5.57	8.55	7.2	8.84	16.26
MgO	0.3	3.05	6.05	9.0	7.04	19.13
Na_2O	2.92	3.6	3.03	2.7	2.38	0.26
K_2O	4.5	1.82	1.00	0.8	1.3	<0.1
H_2O	0.1	0.12	0.23	0.2	0.92	0.3
L.O.I.	0.77	1.15	0.63	2.5	1.46	3.13
MnO	0.1	0.12	0.18	0.2	0.18	0.2
TiO_2	0.2	1.12	1.81	0.94	2.84	0.2
P_2O_5	0.055	0.36	0.32	0.29	0.63	0.02
TOTAL	99.75	100.06	100.32	99.44	100.4	100.08

1. Biotite Granite
2. Quartz Diorite
3. Diorite
4. Gabbro
5. Olivine Basalt
6. Pyroxenite.

TABLE 18: Average Values of Trace Element Contents in ppm of the Plutonic and Younger Volcanic Rocks

Elements in ppm	1	2	3	4	5	6
Co	7.5	25	31.66	55	48	35
Ni	10	26.25	63.33	150	112	146.66
Cu	90	216.25	160.0	95	148	235.00
Pb	18.75	26.25	19.16	10	25	18.33
Cr	5	60	196.66	215	282	633.33
Mn	375	1537.5	3333.33	3000	4200	4333.33
Ti	2000	3825	4000	3000	3860	1566.66
V	17.5	237.5	308.33	200	824	166.66
Zr	350	207.5	123.33	100	201	26.66
Ba	5675	675	133.41	2000	260	66.66
Mo	0.85	0.55	0.48	0.5	1.2	0.5

1. Biotite Granite
2. Quartz Diorite
3. Diorite
4. Gabbro
5. Olivine Basalt
6. Pyroxenite

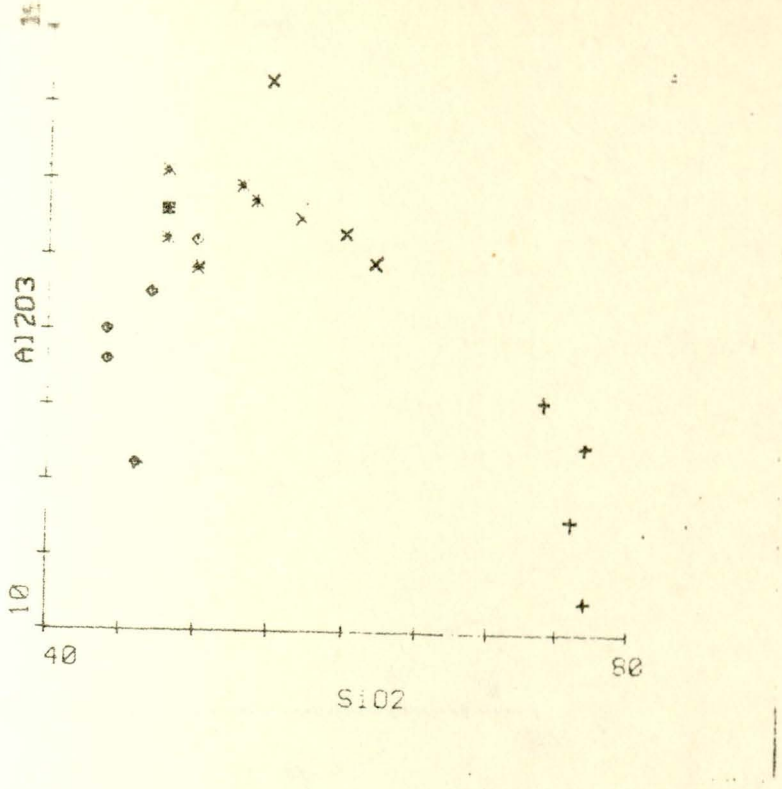

Fig.34 Variation diagram showing Al_2O_3 against SiO_2

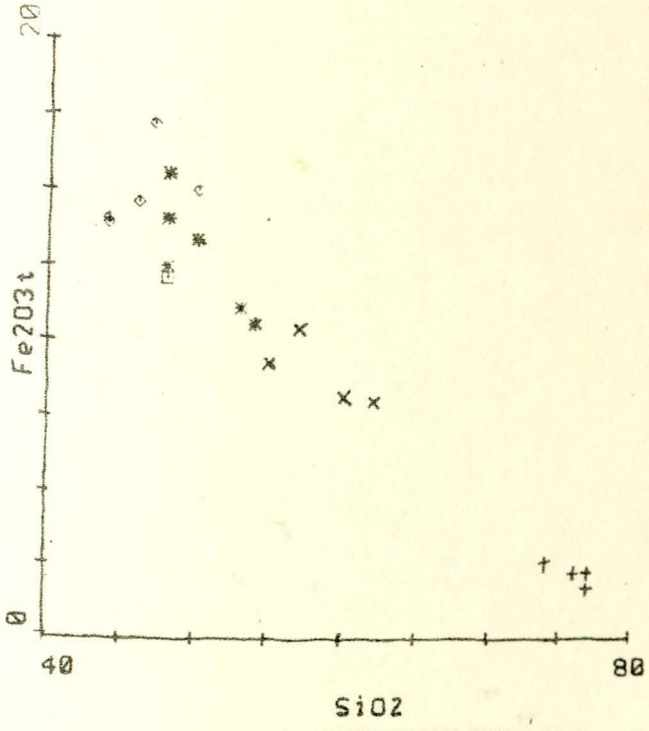

Fig.35 Variation diagram showing Fe_2O_3 against SiO_2

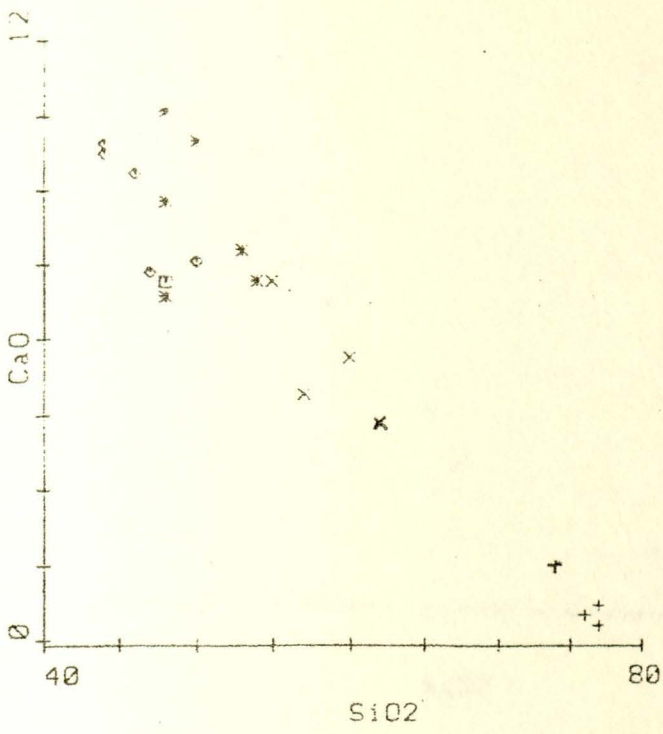

36 Variation diagram showing CaO against SiO2

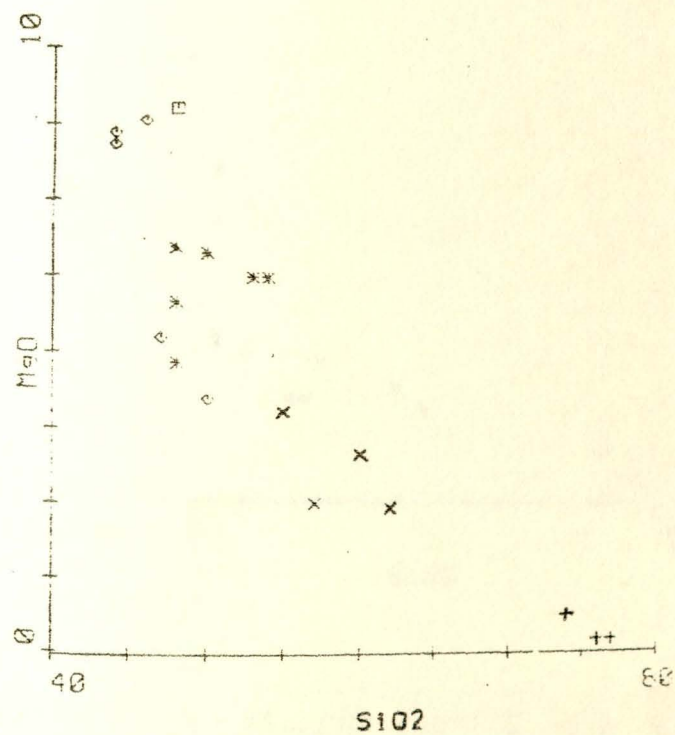

37 Variation diagram showing MgO against SiO2

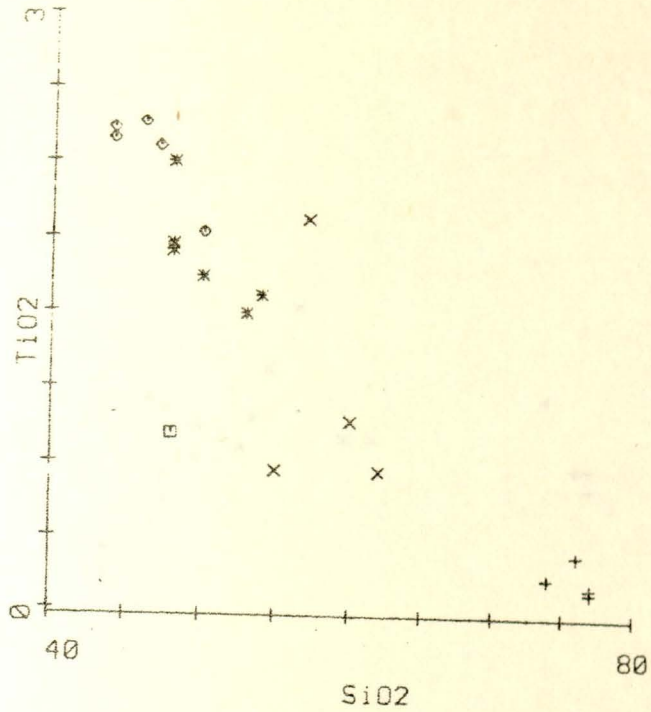

Fig.38 Variation diagram showing TiO_2 against SiO_2

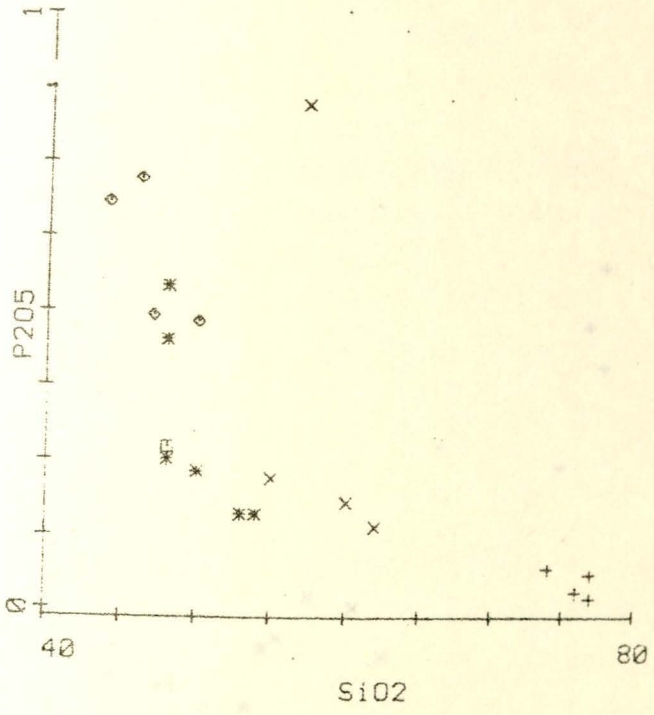

Fig.39 Variation diagram showing P_2O_5 against SiO_2

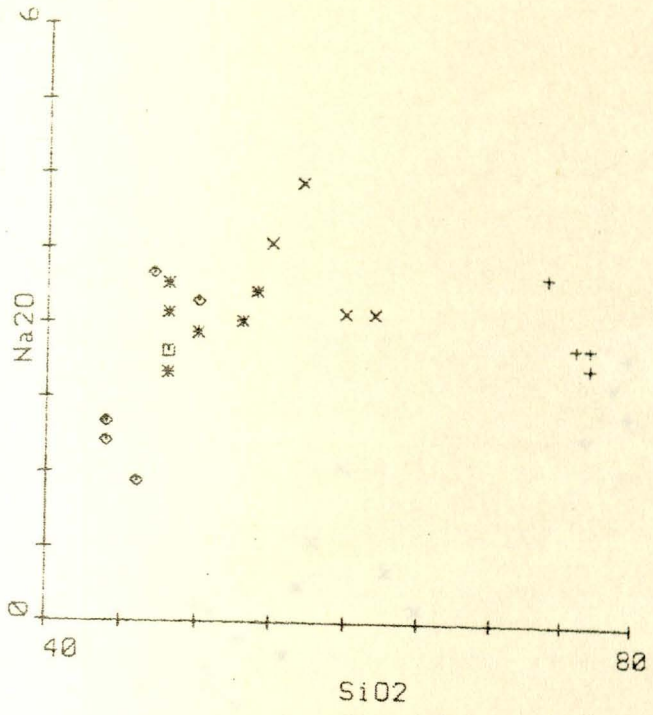

Fig. 40 Variation diagram showing Na_2O against SiO_2

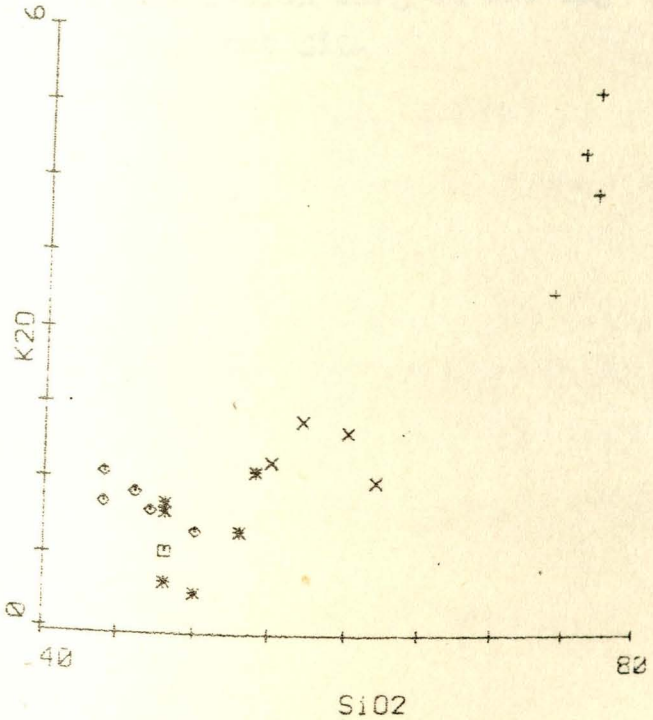

Fig. 41 Variation diagram showing K_2O against SiO_2

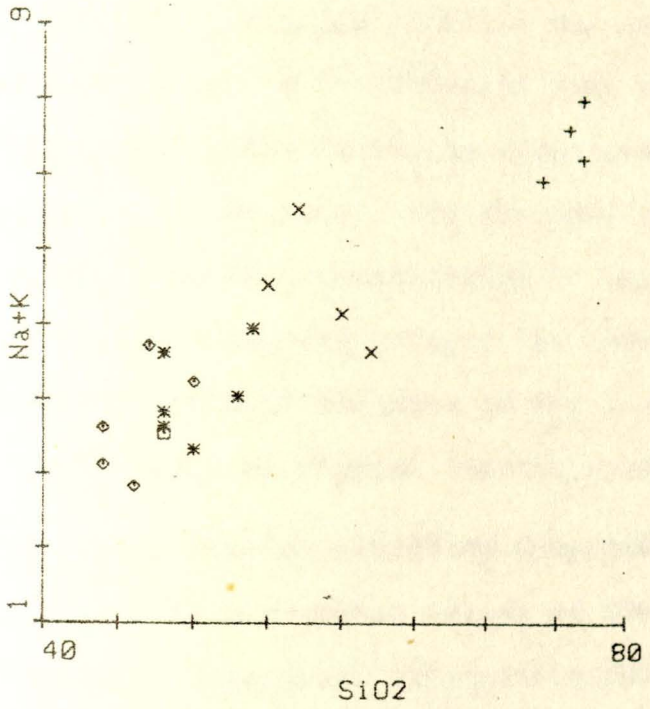

Fig.42 Variation diagram showing $Na_2O + K_2O$ against SiO_2

The granites have an almost constant composition except for K, which shows a rather high variation. In the variation diagrams the granites are plotted with large chemical gap after quartz diorite. The chemical data are in agreement with the derivation of the granite from basic rocks involving separation of mafic minerals, plagioclases and apatite. The presence of chemical gap in magmatic series has been demonstrated by Williams and McBIrney (1979). The existing gap between the granite and the other rocks does not contradict the idea of the derivation of the granites from a basic magma by crystal fractionation.

Generally the major element variation diagrams of the plutonic rocks could indicate a probable origin of the rocks from one parent magma through fractional crystallization. The liquid line of descent shows a linked variation which are consistent with cogenetic rocks, related by crystal fractionation to a common parent magma or by partial melting to a common source.

The basaltic rocks are much younger and are not genetically related with the plutonic rocks of the area. However, they show more or less similar composition with the Gabbroic - dioritic rocks. When plotted on alkali-silica diagram they show a transitional characteristic (Fig. 42). Their similarity in chemical composition could give a primary clue, that the younger basalt and the older plutonic rocks could have emplaced in the same tectonic environment.

From the trace elements determined; Ni, Co, Cu and Pb were used to plot variation diagrams against SiO_2.

The Ni and Co contents are very high in the basic range when compared to the low content of them in the granits.

The high content of nickel drops very sharply (Fig. 43) from Gabbroic to intermediate rocks and continues to fall with a very gentle slope from the intermediate range to the acidic rocks. Cobalt as that of Nickel decrease but not as sharp as the latter one (Fig. 44). The very sharp decrease of nickel at early stage is due to the fractionation of olivine from the magma. It is sharper than cobalt due to its higher value of fractionation coefficient, k, which is defined as

$$K = \frac{\text{PPm in solid}}{\text{PPm in liquid}}, \quad \text{where } K^{ol}_{Ni} > K^{ol}_{co}$$

K = fractionation coefficient

ol = olivine

The negative correlation of both Ni and Co with SiO_2 are in agreement with the previous proposition of the derivation of the rocks by fractional crystallization.

Cu and Pb do not show any regular variation. Their content is highly variable especially in the basic and intermediate rocks.

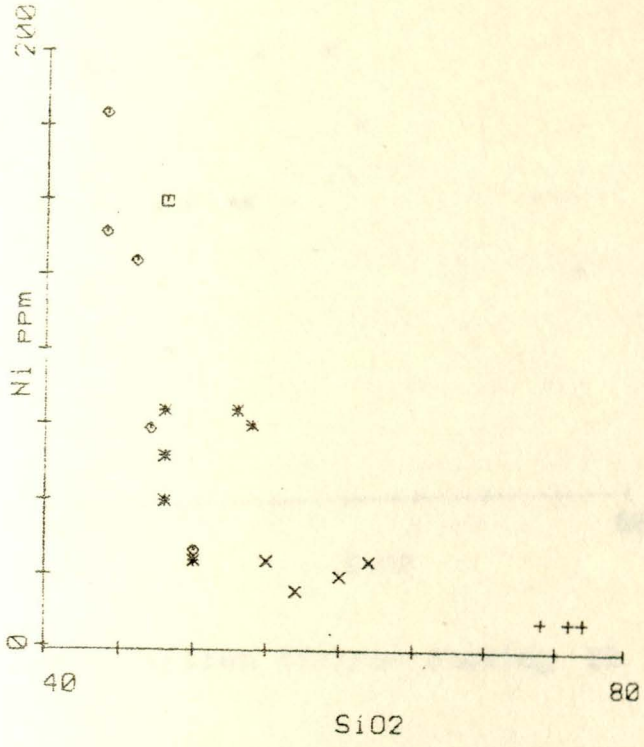

Fig. 43 Variation diagram showing Ni against SiO_2

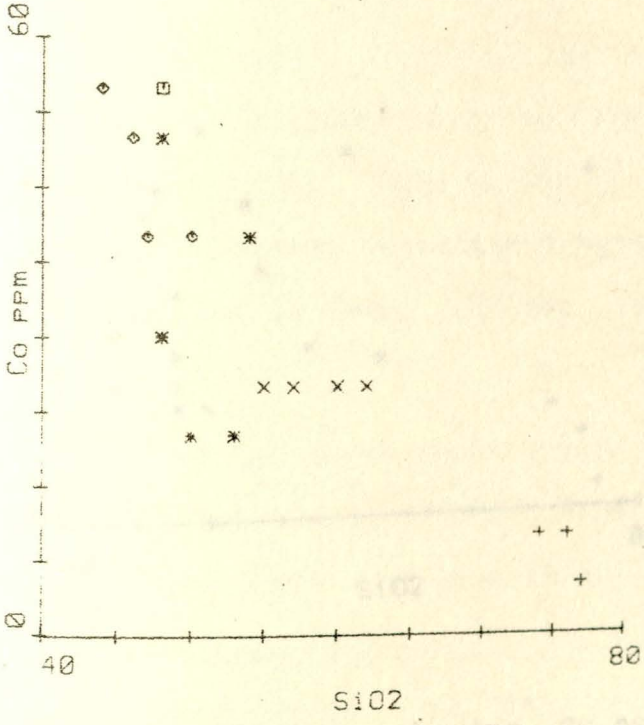

Fig. 44 Variation diagram showing Co against SiO_2

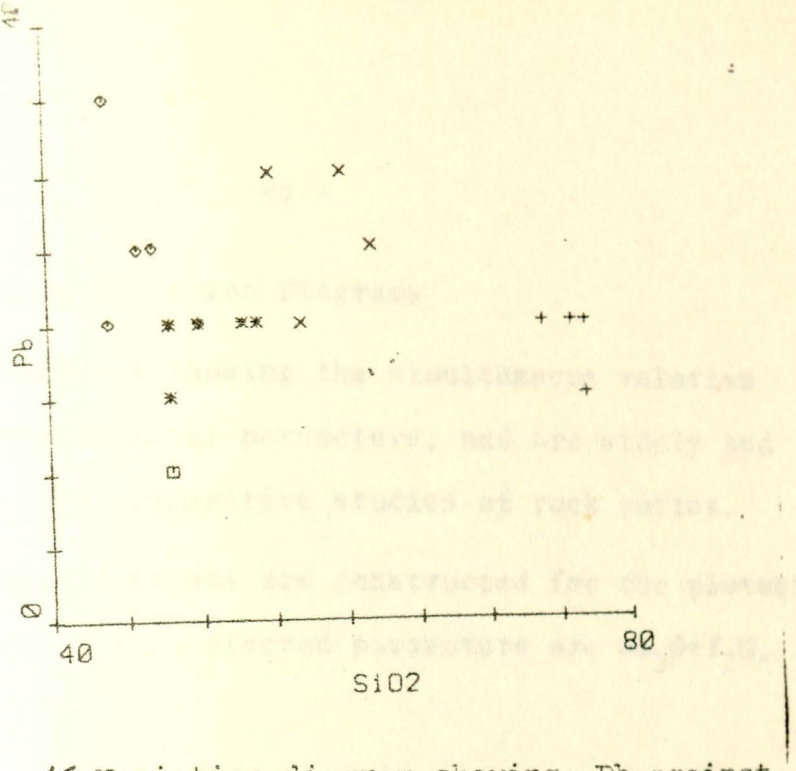

Fig. 45 Variation diagram showing Pb against SiO_2

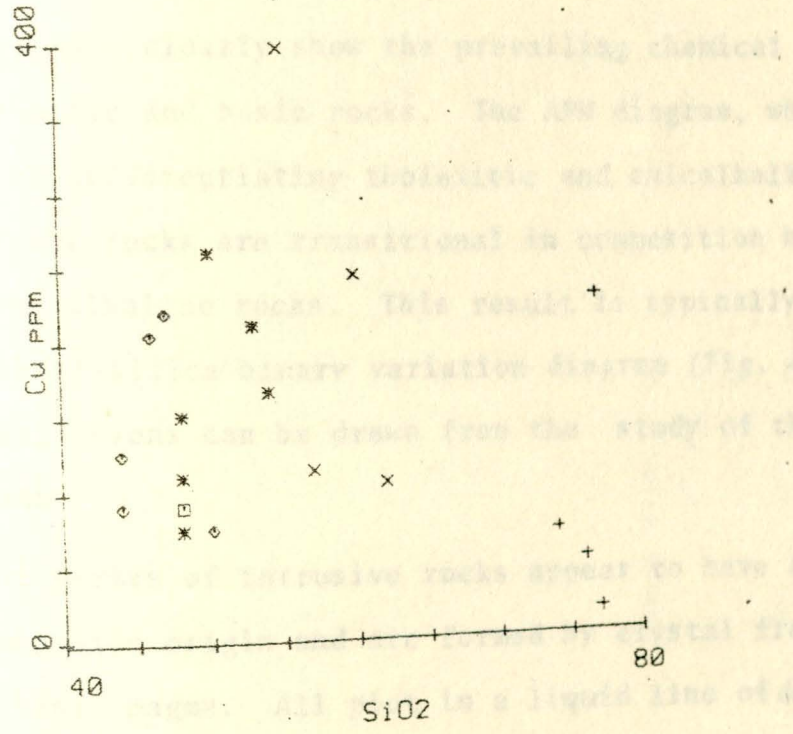

Fig. 46 Variation diagram showing Cu against SiO_2

5.4.2.2 Triangular Variation Diagrams

These are diagrams showing the simultaneous relative variation of three chemical parameters, and are widely and usefully employed in comparative studies of rock suites.

Two triangular diagrams are constructed for the plutonic and effusive rocks. The selected parameters are Na_2O+K_2O, $Fe_3O_3{}^t$, MgO and CaO.

i) AFM Diagram: plotted by using Na_2O+K_2O, $Fe_2O_3{}^t$, and MgO (Fig. 47)

ii) ACF Diagram: erected by Na_2O+K_2O, $Fe_2O_3^t$, and CaO (Fig. 48).

Both the diagrams clearly show the prevailing chemical gap among the granitic and basic rocks. The AFM diagram, where it is employed for defferentiating tholeiitic and calcalkaline series show that the rocks are transitional in composition between the tholeiitic and alkaline rocks. This result is typically the same with the alkali-silica binary variation diagram (Fig. 42). The following conclusions can be drawn from the study of the variation diagrams.

1. The different series of intrusive rocks appear to have a probable comagmatic origin and are formed by crystal fraction from a basic magma. All plot in a liquid line of descent.
2. Mafic minerals, plagioclase, and apatite are the main separating phases during fractionation. The sharp decrease of the

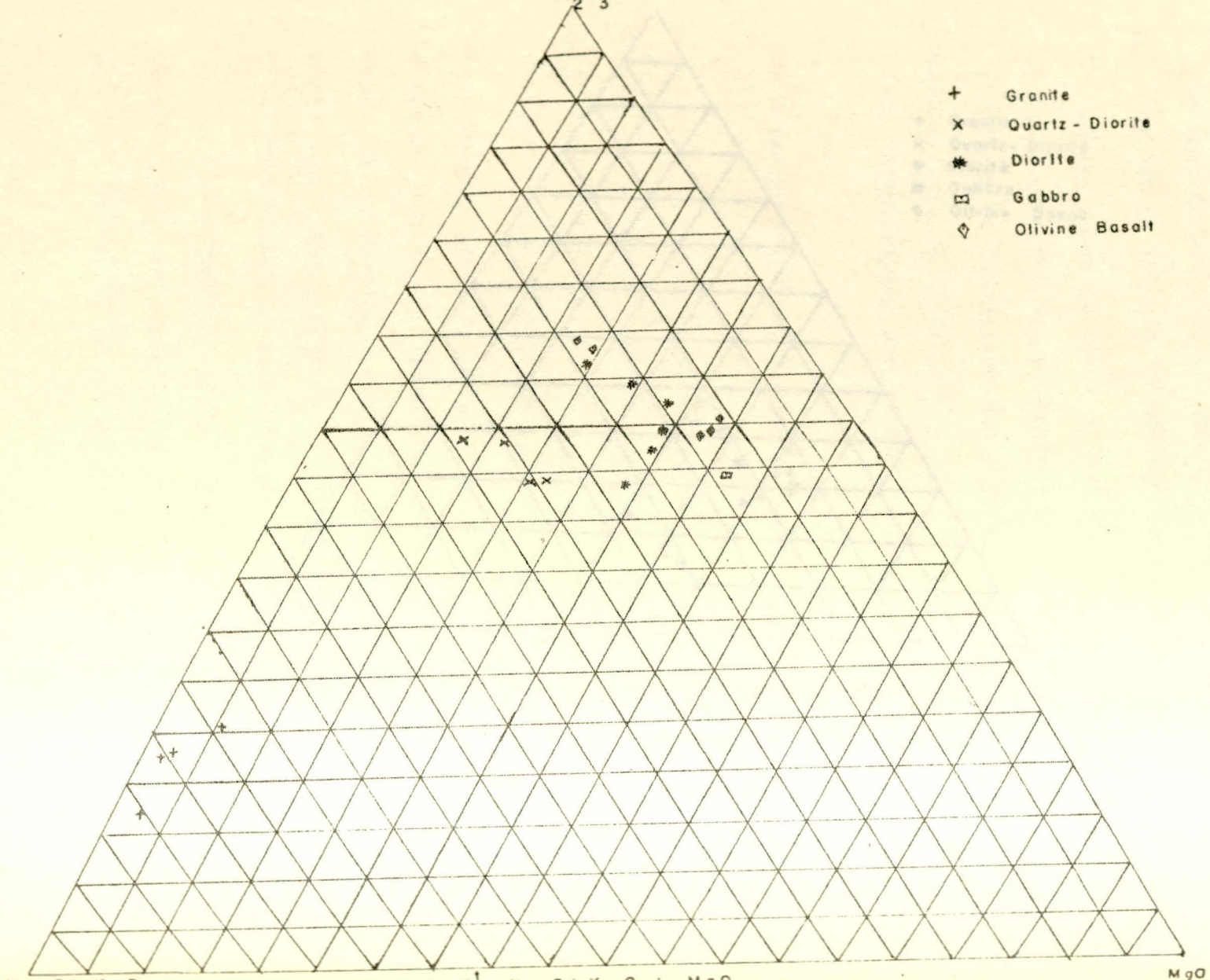

Variation of $Fe_2O_3^t$: $Na_2O + K_2O$: MgO

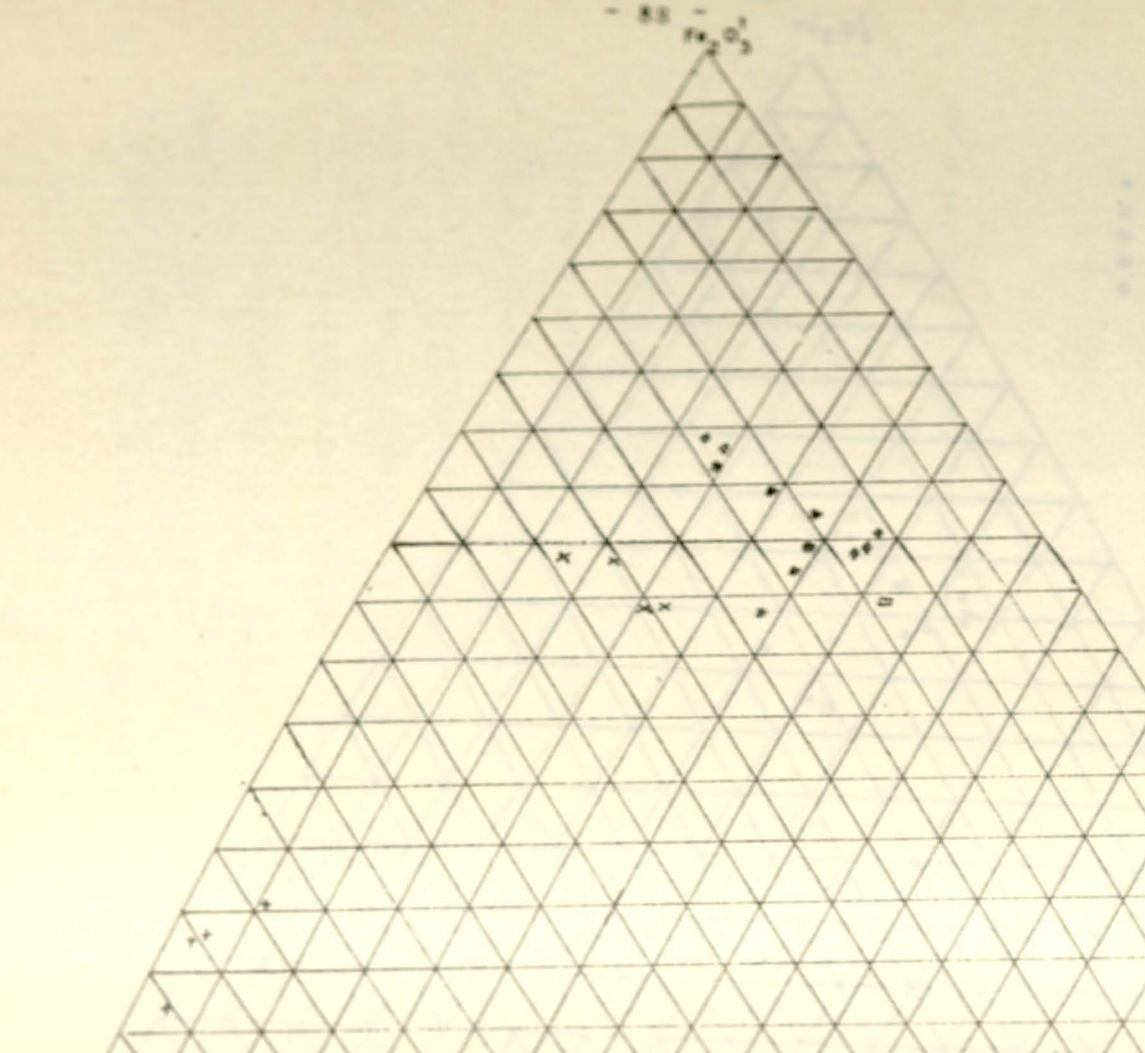
Fe_2O_3
$Na_2O + K_2O$
variation of Fe_2O_3 : $Na_2O + K_2O$: MgO

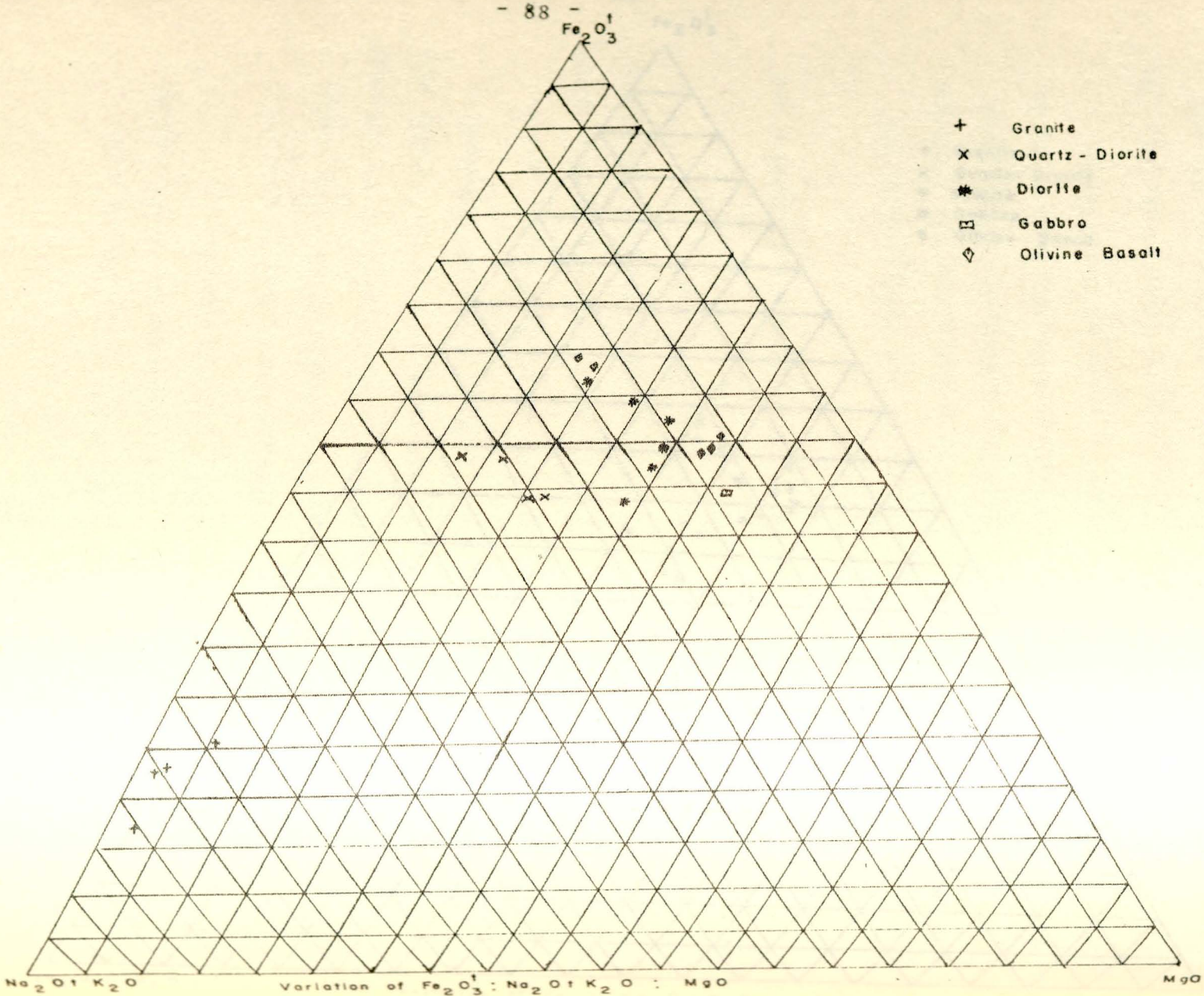

Variation of $Fe_2O_3^t$: $Na_2O + K_2O$: MgO

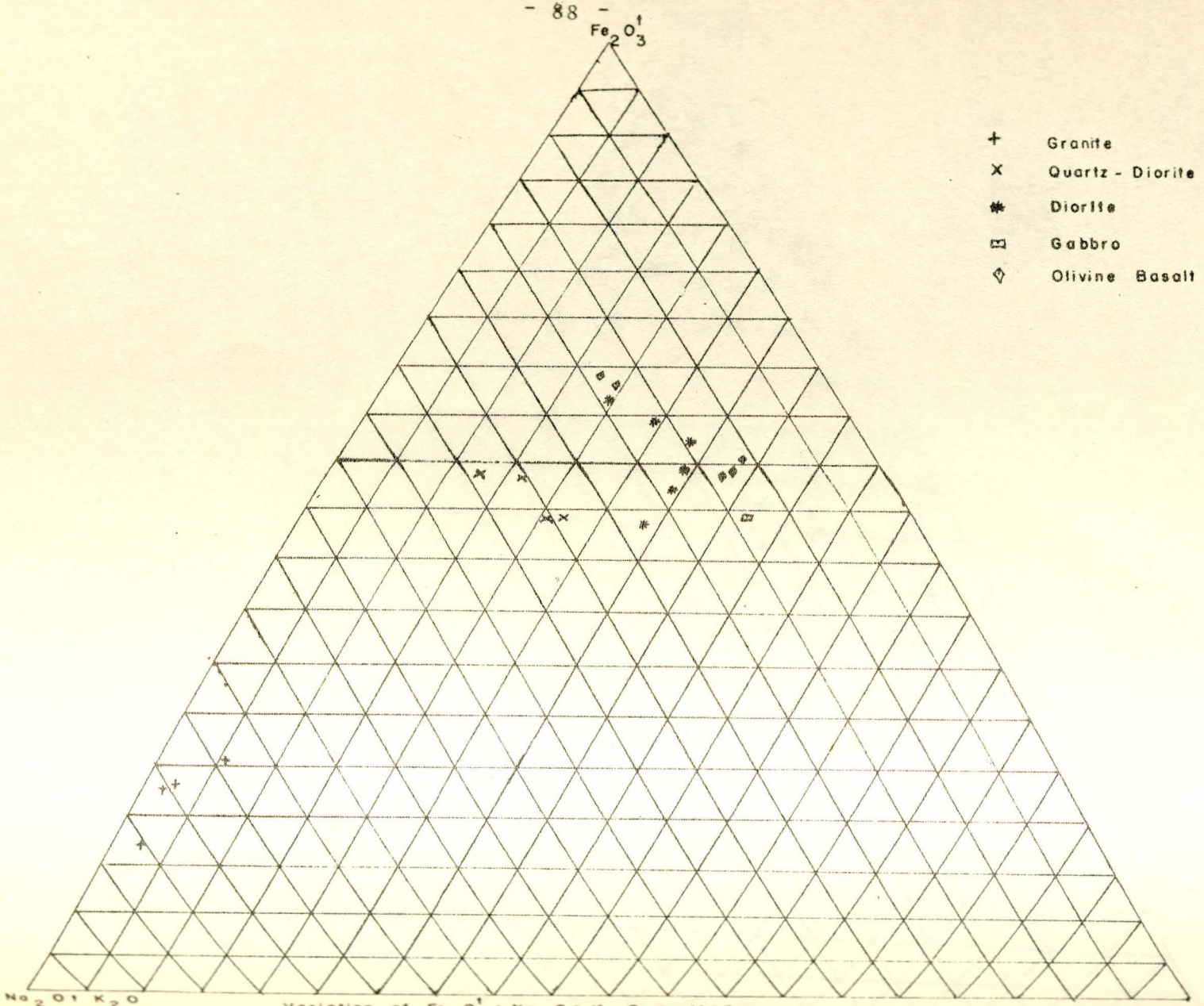

Variation of $Fe_2O_3^t$: $Na_2O + K_2O$: MgO

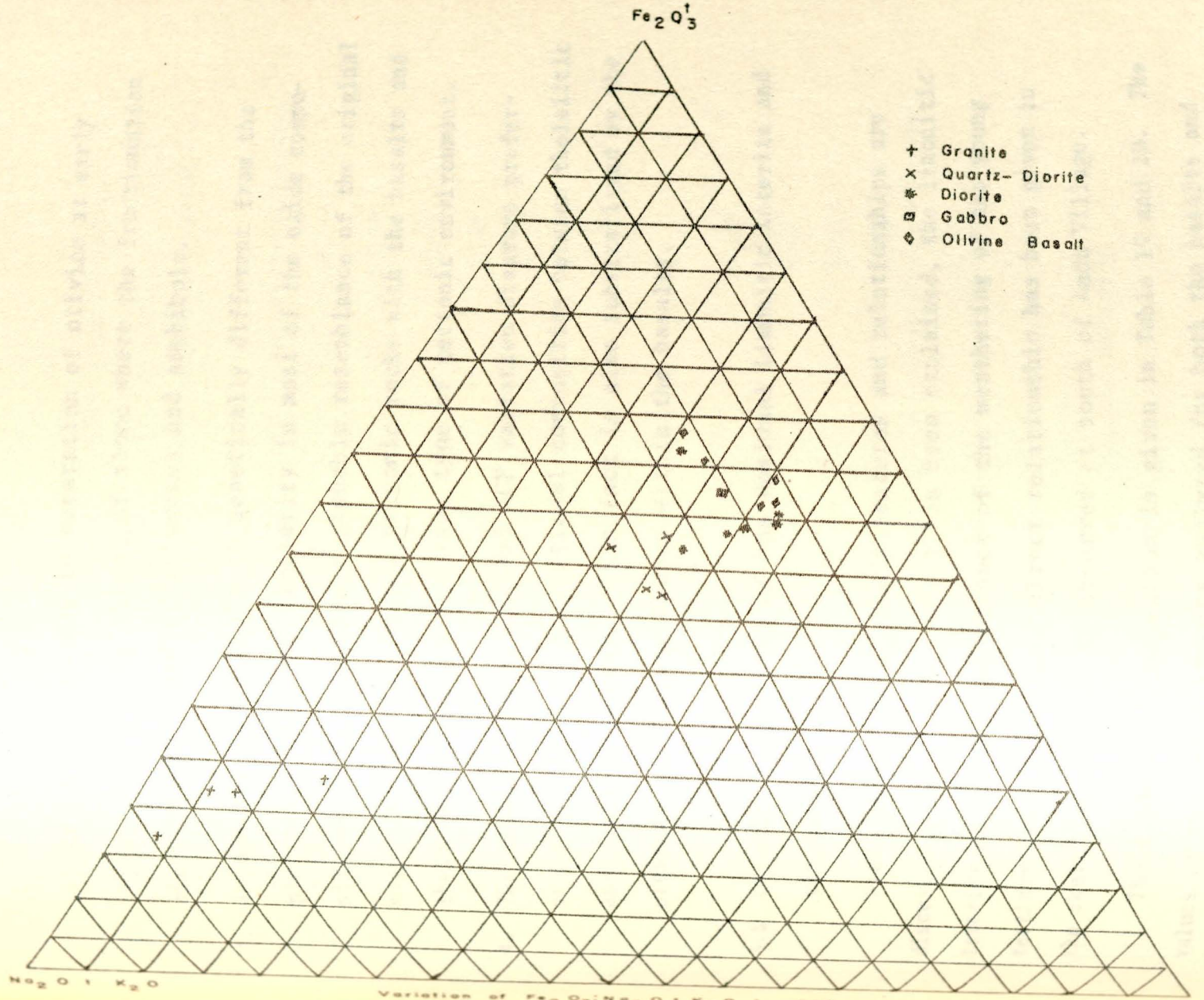
$Fe_2O_3^t$
Granite
Quartz- Diorite
Diorite
Gabbro
Olivine Basalt
$Na_2O + K_2O$
Variation of $Fe_2O_3 : Na_2O + K_2O : CaO$
CaO

nickel content is due to separation of olivine at early stage; followed by change of slope where the fractionation might be continued by pyroxenes and amphibole.

3. Though the young bsalt is genetically different from the plutonic rocks, its similarity in most of the oxide compositions could indicate a probable resemblance of the original magmatic material of the plutonic rocks with the basalts and their generation in the same type of tectonic environment.

4. The alkali-silica, AFM and ACF variation diagrams preferentially indicate transitional composition between tholeiitic and alkaline magmas. This fact is also substantiated by the presence of orthopyroxenes within the basalts.

5.5 Chemical Comparison of the Residual Limonitic Laterite and the Basalts

Field occurrences, their features and relationships are discussed under 2.2.4. As it has been explained, the limonitic laterite is a residual product of the weathering of the young tertiary basalts. Their direct relationship has been given in the sketch of Fig. 12 as observed at south of Andu Village.

Their chemical comparison is given in Table 19 and 20. The values of the total samples analyzed for both the basalts and limonitic laterites is given in Table 13, 14, 15 and 16.

TABLE 19: Average Chemical Compositions (Oxides, wt %) of residual limonitic laterites and basalts

Elements (wt %)	1	2
SiO_2	46.2	15
Al_2O_3	13.9	13.91
$Fe_2O_3{}^t$	14.91	54.71
CaO	8.84	0.47
MgO	7.04	0.54
Ma_2O	2.38	0.1
K_2O	1.3	0.1
H_2O	0.92	1.54
L.O.I.	1.46	11.37
MnO	0.18	0.14
TiO_2	2.84	1.92
P_2O_5	0.63	0.44
T o t a l	100.5	100.24
n	5	7

1 = Basalt

2 = Residual limonitic laterite

n = Number of samples

TABLE 20: Average values of trace element contents in ppm of residual limonitic laterites and basalts

Element in ppm	1	2
Co	48	42.85
Ni	112	52.85
Cu	148	89.28
Pb	25	59.28
Cr	282	71.14
Mn	4200	1271.43
Ti	3860	2385.71
V	824	26.00
Zr	201	75.71
Ba	260	-
Mo	1.20	1.14
n	5	7

1 = Basalt

2 = Residual limonitic laterite

n = Number of samples

There is a wide chemical variation between the unalterned basalt and limonitic laterite in almost all the oxides and trace element values. The variation is more pronounced especially in their contents of

a) SiO_2: It is about 45% in the basalts and 15% in the limonitic laterites, indicating excessive leaching of SiO_2 from the original rock.

b) $Fe_2O_3{}^t$: The total iron content of the limonitic laterites is by far greater than in basalts. There is a general enrichment in the iron content during the leaching and decomposition of the basalt.

c) Oxides of Alkali and Alkali Earth Elements: There is excessive loss of these oxides, namely CaO, MgO, Na_2O and K_2O during the laterilization process. Their value is higher in the undecomposed fresh rock.

d) H_2O and L.O.I.: The water content of the residual material is much greater than the fresh basalt. This is due to the formation of the limonites which are hydroxides of iron and require the presence of water for their formation.

e) The TiO_2 content of the fresh unweathered rock is also greater in value than the laterites. The same is true for P_2O_5 but not that much magnified as compared to the other oxides.

f) There is no difference in Al_2O_3 content between residual limonitic laterites and fresh basalts.

The trace element geochemistry show also some variations specially in their contents of Ni, Cr, Mn, Ti, V, Zr, and Ba. There is a general depletion of these trace elements in the residual limonitic material when compared with the undecomposed rocks.

A variation diagram was made by using SiO_2: $Fe_2O_3{}^t$: $CaO + MgO$, as selected parameters to show their difference in composition prior and after decomposition of the basalts - (Fig. 49). As it is clearly seen from the diagram there is an excessive loss of SiO_2, CaO, and MgO during the lateritization process, while on the contrary it can be seen that there is a tremendous enrichment of $Fe_2O_3{}^t$.

5.6. Geochemistry of the Iron Bearing Horizon

5.6.1 Introduction

Major and trace element analyses for the representative samples of the iron formation were carried out. An account of the analytical work is given under 5.2 and 5.3. Based on Geochemical data, an interpretation is given for:

a) the source of iron and silica,

b) genetic relationships among the recognized lithounits,

c) the probable environment of the depositional basin.

Twenty six samples were collected from three trenches, at Chago, where some of the samples are from lenses of magnetite-

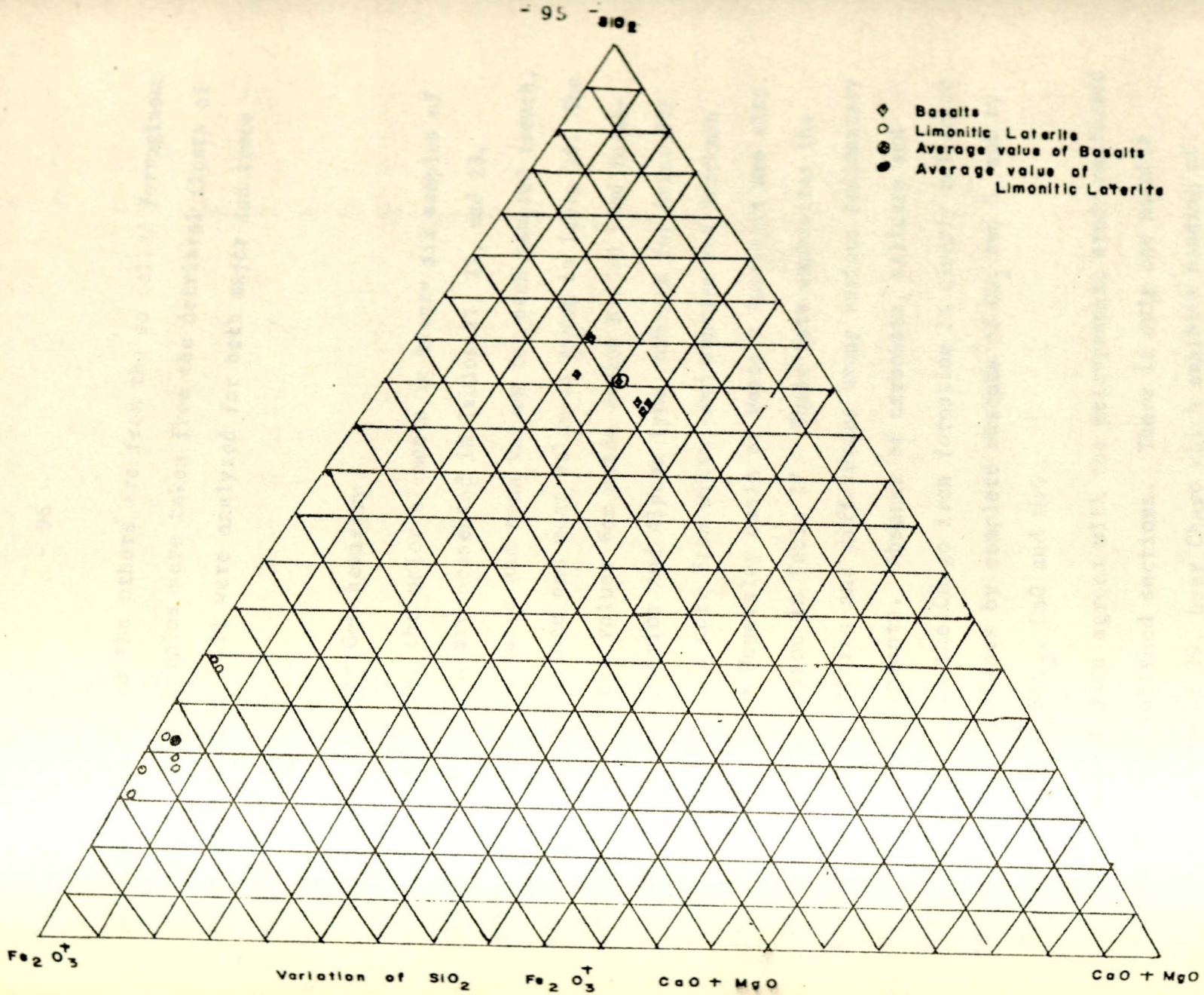

Variation of SiO_2 $Fe_2O_3^+$ $CaO + MgO$

hematite ore, while the others are from the so called ferruginous quartzites. Two samples were taken from the detriatal floats of iron, at Werekalu. All were analyzed for both major and trace element contents.

5.6.2 Major Element Geochemistry

The content for the major elements in twenty six samples of Chago iron formation are presented in Tables 21, 22, and 23. Table 25, gives the range and mean values for each sampled trench, while the over all range and mean value is given in Table 26. The average major element values for oxide facies Banded iron formation of the Lake Superior and Algoma type, average for Orisa BIF (India), interlayered tuff from Orisa, and average for Brockman iron formation from Hamersley basin of Western Australia are also provided for comparison in Table 27. These data emphasizes the geochemical similarities and differences among various sedimentary and volcanic environments. Absence of carbonate, silicate and sulphide minerals in the Chago iron formation is clearly reflected in the chemical analyses by complete absence of CO_2 and S, and by the low values of SiO_2, CaO and MgO.

The chemical data agrees with the petrographic study performed on both thin and polished sections. There is only one notable exception for sample 29, near Chago which exhibits banding of iron together with barite and quartz. This sample within a localized portion of its barite, there is some occurrence of sulphides.

TABLE 21: Major Element Contents of Magnetite-hematite Lenses from Trench - 2

Field No.	SiO_2	Al_2O_3	Fe_2O_3	FeO	$Fe_2O_3^t$	CaO	MgO	Na_2O	K_2O	H_2O	L.O.I	MnO	TiO_2	P_2O_5
T - 1	4.0	3.5	79.71	11.79	91.50	0.1	<0.1	0.1	0.1	0.3	0.8	0.1	0.14	0.04
2	3.0	2.4	73.66	20.24	93.90	0.5	<0.1	0.1	0.1	0.2	<0.1	0.2	0.64	0.23
3	3.0	1.3	75.49	17.51	93.00	0.8	<0.1	0.1	<0.1	0.2	0.4	<0.1	0.12	0.16
4	4.0	1.2	81.17	11.62	92.79	0.1	<0.1	0.2	0.1	0.2	0.4	<0.1	0.10	0.16
5	3.0	2.1	84.26	5.8	90.06	2.4	0.2	<0.1	<0.1	0.4	2.3	<0.1	0.10	0.16
6	1.0	0.7	94.76	2.2	96.96	0.6	<0.1	0.2	<0.1	0.3	1.3	<0.1	0.03	0.03
7	2.0	0.8	90.1	5.8	95.90	0.8	0.2	0.1	<0.1	0.2	1.3	<0.1	0.04	0.01
8	4.6	2.2	75.93	10.03	85.96	0.6	<0.1	<0.1	<0.1	1.2	5.5	<0.1	0.06	0.15
9	2.0	1.2	89.42	5.28	94.70	0.1	<0.1	<0.1	<0.1	0.3	2.1	<0.1	0.06	0.05

TABLE 22 : Major Element Contents of Ferruginous Quartzites from Trench - 3

Field No.	SiO_2	Al_2O_3	Fe_2O_3	FeO	$Fe_2O_3^t$	CaO	MgO	Na_2O	K_2O	H_2O	L.O.I.	MnO	TiO_2	P_2O_5
T_3-1	19.4	9.5	59.96	< 0.09	59.96	< 0.1	< 0.1	0.0	<0.1	1.4	8.2	0.4	0.50	0.18
2	10.0	4.4	69.43	11.0	80.43	0.7	0.2	0.1	0.1	0.3	2.3	<0.1	0.20	0.21
3	21.0	9.5	58.97	0.79	59.76	0.3	0.2	0.1	0.2	1.0	6.9	<0.1	0.32	0.18
4	26.0	14.8	49.02	0.44	49.46	<0.1	<0.1	<0.1	<0.1	1.3	8.2	<0.1	0.56	0.35
5	8.0	4.8	77.25	0.6	77.85	0.3	<0.1	<0.1	<0.1	1.2	7.4	<0.1	0.42	0.34
6	22.6	16.8	43.97	0.35	44.32	0.3	<0.1	<0.1	<0.1	2.1	12.2	<0.1	0.54	0.21
7	21.6	12.9	53.96	0.84	54.80	0.1	<0.1	<0.1	<0.1	1.3	7.4	0.1	0.57	0.15
8	25.0	13.8	45.79	0.6	46.39	0.7	<0.1	<0.1	<0.1	2.0	7.9	1.7	1.72	0.14
9	12.0	8.9	69.29	2.2	71.49	0.1	<0.1	<0.1	<0.1	0.7	4.9	0.2	0.28	0.09
10	28.0	15.5	44.58	0.17	44.75	0.7	0.3	0.1	0.8	1.1	7.6	< 0.1	0.80	0.04
11	21.0	7.5	56.3	0.6	56.90	0.3	0.3	<0.1	0.9	2.0	9.9	<0.1	0.38	0.22

TABLE 23 : Major Element Contents of the Iron Bearing Horizon from Trench - 4

Field No.	SiO_2	Al_2O_3	Fe_2O_3	FeO	$Fe_2O_3^t$	CaO	MgO	Na_2O	K_2O	H_2O	L.O.I.	MnO	TiO_2	P_2O_5
T_4-1	6.0	3.2	73.32	16.54	89.86	<0.1	<0.1	<0.1	<0.1	0.3	0.3	<0.1	0.08	0.14
2	7.0	1.6	82.52	7.56	90.08	0.1	<0.1	<0.1	<0.1	0.4	1.1	<0.1	0.10	0.08
3	8.0	3.5	71.91	12.3	84.21	0.2	<0.1	<0.1	<0.1	0.5	1.9	0.4	0.12	0.27
4	10.0	3.0	76.54	7.39	83.93	0.1	<0.1	<0.1	<0.1	0.5	1.6	<0.1	0.14	0.08
5	7.0	3.2	77.19	9.15	86.34	0.2	0.2	<0.1	<0.1	0.6	1.6	<0.1	0.08	0.09
6	4.0	3.5	76.49	14.26	90.75	0.2	<0.1	<0.1	<0.1	0.4	1.0	<0.1	0.06	0.14

TABLE 24 : Major Element Contents of Magnetite-Hematite Ore from Werekalu

52a	6.0	1.3	n.d.	n.d	87.42	<0.1	<0.1	<0.1	<0.1	0.5	4.1	<0.1	0.26	0.20
52b	8.0	3.7	n.d	n.d	85.22	<0.1	0.2	0.1	<0.1	0.6	2.1	0.1	0.23	0.33

n.d = not determined.

TABLE 25 : Range and Average Chemical Compositions (Oxides, wt%) of the Iron Bearing Trench Samples of Chago and Limonitic Laterites

Element	T_2		T_3		T_4		Limonitic Laterite	
	1	2	1	2	1	2	1	2
SiO_2	1-4	2.95	8-26	19.5	4-10	7	11-19	15
Al_2O_3	0.7-3.5	1.71	4.4-16.8	10.76	1.6-3.5	3	10.1-20.3	13.91
Fe_2O_3	73.66-94.76	82.72	43.97-77.25	57.14	71.91-82.52	76.33	n.d	n.d
FeO	2.2-20.24	10.03	<0.09-11	1.6	7.56-16.54	11.2	n.d	n.d
$Fe_2O_3^t$	85.96-96.96	92.75	44.32-80.43	58.73	83.93-90.75	87.52	41.18-60.8	54.71
CaO	0.1-2.4	0.66	<0.1 - 0.7	0.34	<0.1 - 0.2	0.15	0.1 - 1.8	0.47
MgO	<0.1-0.2	0.12	<0.1 - 0.3	0.15	<0.1 - 0.2	0.11	0.2 - 2.2	0.54
Na_2O	<0.1-0.2	10.12	<0.1 - 0.1	<0.1	<0.1 - 0.1	<0.1	<0.1 - 0.2	0.08
K_2O	<0.1-0.1	<0.08	<0.1 - 0.9	0.24	<0.1 - 0.1	<0.1	<0.1 - 0.2	0.07
H_2O	<0.2-0.4	0.36	0.3 - 2	1.31	0.3 - 0.6	0.45	0.3 - 1.9	1.54
L.O.I.	<0.1-5.5	1.57	2.3- 12.2	7.53	0.3 - 1.9	1.25	7.6 -13.6	11.37
MnO	<0.1-0.2	0.11	<0.1 - 1.7	0.28	<0.1 - 0.4	0.15	<0.1 - 0.5	0.14
TiO_2	0.03-0.64	0.14	0.2 - 1.72	0.43	0.06-0.14	0.1	1.5 - 2.41	1.92
P_2O_5	0.01-0.23	0.11	0.04-0.35	0.19	0.08-0.27	0.13	0.2 - 0.87	0.45

n.d = not determined, 1. Range of values, 2. Average values.

TABLE 26 : Range and Average Chemical Compositions (Oxides, wt%) of all the Trench Iron Bearing Samples.

Elements	Range	Average
SiO_2	1-26	10.9
Al_2O_3	0.7-16.8	5.83
Fe_2O_3	43.97-94.76	70.42
FeO	< 0.09-20.24	6.74
$Fe_2O_3^t$	44.32-96.96	77.15
CaO	<0.1 - 2.4	0.4
MgO	<0.1 - 0.3	0.13
Na_2O	<0.1 - 0.9	0.1
K_2O	<0.1 - 0.9	0.16
H_2O	<0.2 - 2.0	0.78
L.O.I.	<0.1 -12.2	4.02
MnO	<0.1 - 1.7	0.2
TiO_2	0.03- 1.72	0.31
P_2O_5	0.01- 0.35	0.15

TABLE 27: Major Element Contents of Iron-formation of Chago-Werekalu, Wellega and Lake Superior and Algoma Type Oxide Facies BIF of Canada and Others

	1	2	3	4	5	6	7	8
SiO_2	1-26	10.9	47.20	50.50	47.02	30.04	46.86	47.57
Al_2O_3	0.7-16.8	5.83	1.39	3.00	0.70	26.83	0.48	0.08
Fe_2O_3	43.97-94.76	70.42	35.40	26.90	44.16	n.d	24.68	27.01
FeO	<0.09-20.24	6.74	8.20	13.00	8.28	n.d	17.19	14.47
$Fe_2O_3^t$	44.32-96.96	77.15	44.50	41.10	50.00	29.02	43.65	43.00
MnO	< 0.1 - 1.7	0.2	0.73	0.22	0.06	0.69	n.d	n.d
CaO	< 0.1 - 2.4	0.4	1.58	1.51	0.17	0.42	1.49	2.17
MgO	< 0.1 - 0.3	0.13	1.24	1.53	0.13	0.09	2.58	2.47
Na_2O	< 0.1 - 0.2	0.10	0.12	0.31	0.10	0.01	0.16	0.23
K_2O	< 0.1 - 0.9	0.16	0.14	0.58	0.13	0.14	0.10	0.16
H_2O^t	< 0.2 - 2.0	0.78	1.30	1.10	1.94	10.44	0.57	0.56
P_2O_5	0.01- 0.35	0.15	0.06	0.21	0.07	n.d	0.25	0.22
CO_2	-	-	3.00	1.10	-	n.d.	5.81	4.99
S	-	-	0.02	0.29	-	n.d	-	-
FeS_2	n.d	n.d	-	-	-	- -	n.d	0.07

n.d = not determined; t = total

1. Range of major element contents from Chago-Werekalu iron-formation
2. Average of major element contents from Chago-Werekalu iron-formation
3. Average Lake Superior oxide facies BIF 0 (Gross, 1980
4. Average Algoma oxide facies BIF 0 Table 3, p. 226).
5. Average Orisa BIF, India 0 (Majumder, et.al., 1982, Table 1, p. 110).
6. Interlayered tuff from Orisa
7 & 8. Brockman Iron-formation, Hamersley basin, Western Australia (Trendal and Blockley, 1970, Table 11, p. 134.

TABLE 28: Major Element Contents of Quartz-chlorite Sericite Schist (Wt %)

Field No.	SiO_2	Al_2O_3	$Fe_2O_3^t$	CaO	MgO	Na_2O	K_2O	H_2O	L.O.I.	MnO	TiO_2	P_2O_5
A-2a	57.0	20.7	10.15	0.1	1.0	1.1	1.9	0.3	5.2	<0.1	1.86	0.13
22	56.0	18.2	13.44	0.1	1.4	0.6	1.1	0.5	5.3	0.1	1.82	0.38
51b	61.0	15.9	12.08	< 0.1	1.0	0.8	1.6	0.4	5.0	<0.1	1.65	0.08
18	63.0	14.2	11.07	0.3	0.4	0.7	1.6	0.5	4.9	<0.1	2.20	0.18
53	54.0	19.1	12.72	0.2	2.4	0.5	3.1	0.4	5.4	<0.1	1.51	0.10
81	60.0	16.4	12.0	0.1	1.5	0.6	2.2	0.2	5.0	<0.1	1.85	0.2

TABLE 29 : Major Element Contents of Lithic-Arenite (Wt %)

A - 3	60.0	19.8	9.58	0.1	0.4	1.1	2.0	0.7	5.2	<0.1	1.70	0.07
20	60.0	18.4	10.49	0.3	1.6	0.7	1.6	0.4	4.6	0.2	1.86	0.04
73	58.0	17.3	13.08	0.7	0.3	0.4	0.8	1.2	7.0	<0.1	1.40	0.17
26	56.0	22.1	9.44	0.5	1.0	2.1	1.9	0.3	5.1	<0.1	2.0	0.38
35	56.5	20.3	11.79	0.1	1.2	0.8	1.1	0.4	5.2	<0.1	1.32	0.10

TABLE 30: Range and average chemical compositions (Oxide, wt %) of the quartz-muscovite - sericite - schist

Element	Range	Average
SiO_2	54 -63	58.5
Al_2O_3	14.2 -20.7	17.42
$Fe_2O_3{}^t$	10.15-13.44	11.91
CaO	< 0.1 - 0.3	0.14
MgO	0.4 - 2.4	1.28
Na_2O	0.5 - 1.1	0.72
K_2O	1.1 - 3.1	1.92
H_2O	0.2 - 0.5	0.38
L.O.I.	4.9 - 5.4	5.13
MnO	< 0.1 - 0.1	< 0.1
TiO_2	1.51- 2.2	1.82
P_2O_5	0.08- 0.38	0.18

TABLE 31: Range and average chemical compositions (Oxide wt %) of the lithic arenaites

Element	Range	Average
SiO_2	56 -60	58.1
Al_2O_3	17.3-22.1	19.58
$Fe_2O_3{}^t$	9.44-11.79	10.87
CaO	0.1 - 0.7	0.34
MgO	0.3 - 1.6	1.02
Na_2O	0.4 - 2.1	1.02
K_2O	0.8 - 2	1.48
H_2O	0.3 - 1.2	0.6
L.O.I.	4.6 - 7	5.42
MnO	< 0.1 - 0.2	< 1.2
TiO_2	1.32 - 2	1.66
P_2O_5	0.04 - 0.38	0.15

However, such striking features are discussed in Chapter 2 under 2.2.5.1.

At first glance, data from Table 26, points out that the range of variation differs for the different oxides. The general pattern observed is that SiO_2, Al_2O_3, FeO and P_2O_5 contents show wider variations than CaO, MgO, Na_2O, K_2O, MnO and TiO_2 contents.

In order to shed light both on the age and type of the Chago iron formation, a viable approach is to compare the chemical data obtained with those different iron formations which are reported in literatures.

As published by Gross, et.al. (1980) the K_2O, Al_2O_3, Na_2O and P_2O_3 in Algoma oxide facies BIF are at least twice as much as in the Lake Superior oxide facies.

Table 32, 33, and 34 whow the comparison of these oxides of Algoma and Superior type BIF with that of Chago iron formation (the different trench samples are used).

TABLE 32: Comparison with Trench-2 Samples

Element	Chago	Superior	Algoma
Al_2O_3	1.7	1.39	3.00
K_2O	0.08	0.14	0.58
Na_2O	0.12	0.12	0.31
P_2O_5	0.11	0.06	0.21

It is observed that the average values for Al_2O_3, Na_2O, and P_2O_5 of Algoma oxide facies is two fold higher than the Chago iron formation, and that the K_2O value for Algoma is about seven-fold exceeding from Chago formation. While the average values for Al_2O_3, K_2O, Na_2O and P_2O_5 of Superior BIF are more or less similar with the Chago iron formation

TABLE 33: Comparison with Trench-3 Samples

Element	Chago	Superior	Algoma
Al_2O_3	10.76	1.39	3.00
K_2O	0.24	0.14	0.58
Na_2O	0.1	0.12	0.31
P_2O_5	0.19	0.06	0.21

The table points out that in Algoma oxide facies, K_2O and Na_2O are two and three-fold enriched compared to trench-3 samples respectively; while P_2O_5 contents do not show any significant difference. The reverse occurs for Al_2O_3, which is three-fold enriched in Chago samples; thus likely suggesting that the latter samples could contain some amount of aluminosilicate minerals. The K_2O and Na_2O content of the Chago trench-3 samples are similar with the superior BIF type; whereas the Al_2O_3 and P_2O_5 content of the former samples are ten and three-fold greater than the contents of the latter respectively.

Data for the samples from Trench-4 are listed in Table 34.

TABLE 34: Comparison with Trench-4 Samples

Element	Chago	Superior	Algoma
Al_2O_3	3.0	1.39	3.0
K_2O	0.1	0.14	0.58
Na_2O	0.1	0.12	0.31
P_2O_5	0.13	0.06	0.21

As displayed by the above set of data it can be observed that the oxide contents for Algoma BIF facies exceeds those shown by trench-4 samples. Al_2O_3 contents, however, are quite comparable for both localities. The K_2O and Na_2O values of trench-4 samples are also less than the superior oxide facies; whereas the Al_2O_3 and P_2O_5 contents of Chago (Trench-4) Iron formation exceed that of the superior BIF. Inspite of the existing difference in values, the oxide contents of K_2O, Na_2O and P_2O_5 of Chago is closer to the Superior type than the Algoma oxide facies.

It is worthy to note that all samples from Chago are at least two-fold Fe-enriched when compared with Banded iron formations reported in Table 27. At Chago, SiO_2 content is very low. Such feature is more evident for the magnetite-hematite lenses. A review of the published data reveals that in Chago samples, SiO_2 is about five-fold depleted than the classical Banded iron formations.

Al_2O_3 content of Chago samples is rather high, especially those collected from trench-3. Here the samples are constituted by ferruginous sediments which are richer in clayey material than the magnetite-hematite lenses. The samples from trench-2 (magnetite-hematite lenses) are quite comparable in their Al_2O_3 content, with the Superior oxide facies BIF.

CaO and MgO contents are highly depleted in the iron ore of Chago as compared with other BIF. Such a feature is a reliable indication that the iron formation of Chago is carbonate facies-free.

The value of the three components Al_2O_3, Fe_2O_3, and SiO_2 of Chago iron formation when plotted in the Govett's triangular diagram (1966, Fig. 50) lie outside the field of the precambrian Banded iron formation (Fig. 51). Such a behavior is due to its extreme low silica and high Fe_2O_3 content. The field occupied by the Chago iron formation is similar to that of Oolitic Precambrian and post Precambrian iron formations and non Oolitic post Precambrian iron formation (Fig. 50, 51). Except for the existence of some undifferentiated biospheroids, the question of Oolitic iron formation is ruled out by petrographic study. The problem of the iron formation being Precambrian or post Precambrian is attempted to be solved by considering other factors.

Lepp and Goldich (1964) have given a comparison between the chemical composition of Precambrian and post Precambrian iron formations (Table 35).

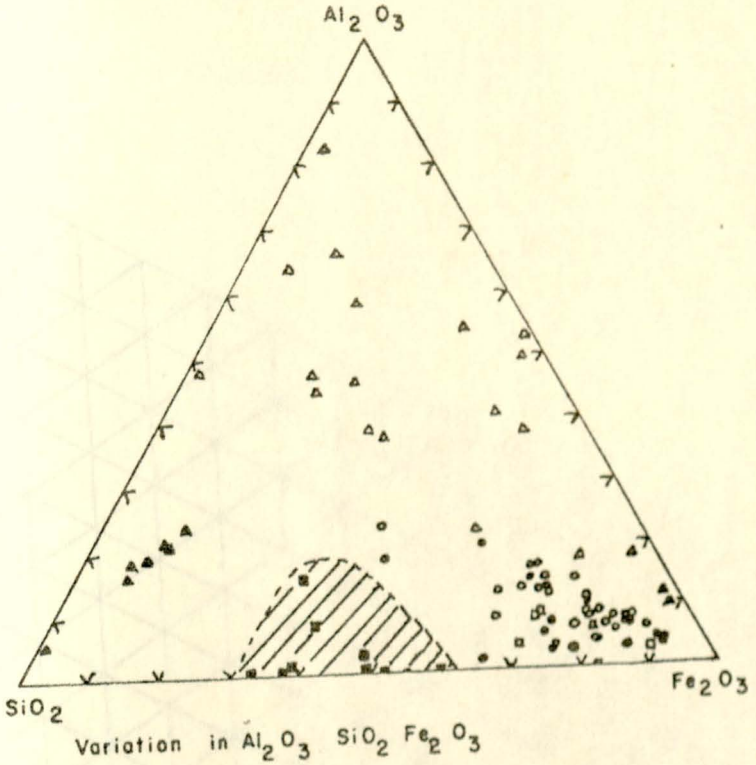

Fig. 50

- Banded iron formation — Precambrian
- Oölitic iron formation
- Non Oblitic iron formation — Post - Precambrian
- Oölitic iron formation
- Recent lake and bog iron formation
- Laterite and bauxite
- Sedimentary rocks and recent sedements
- Banded iron formation field of composition

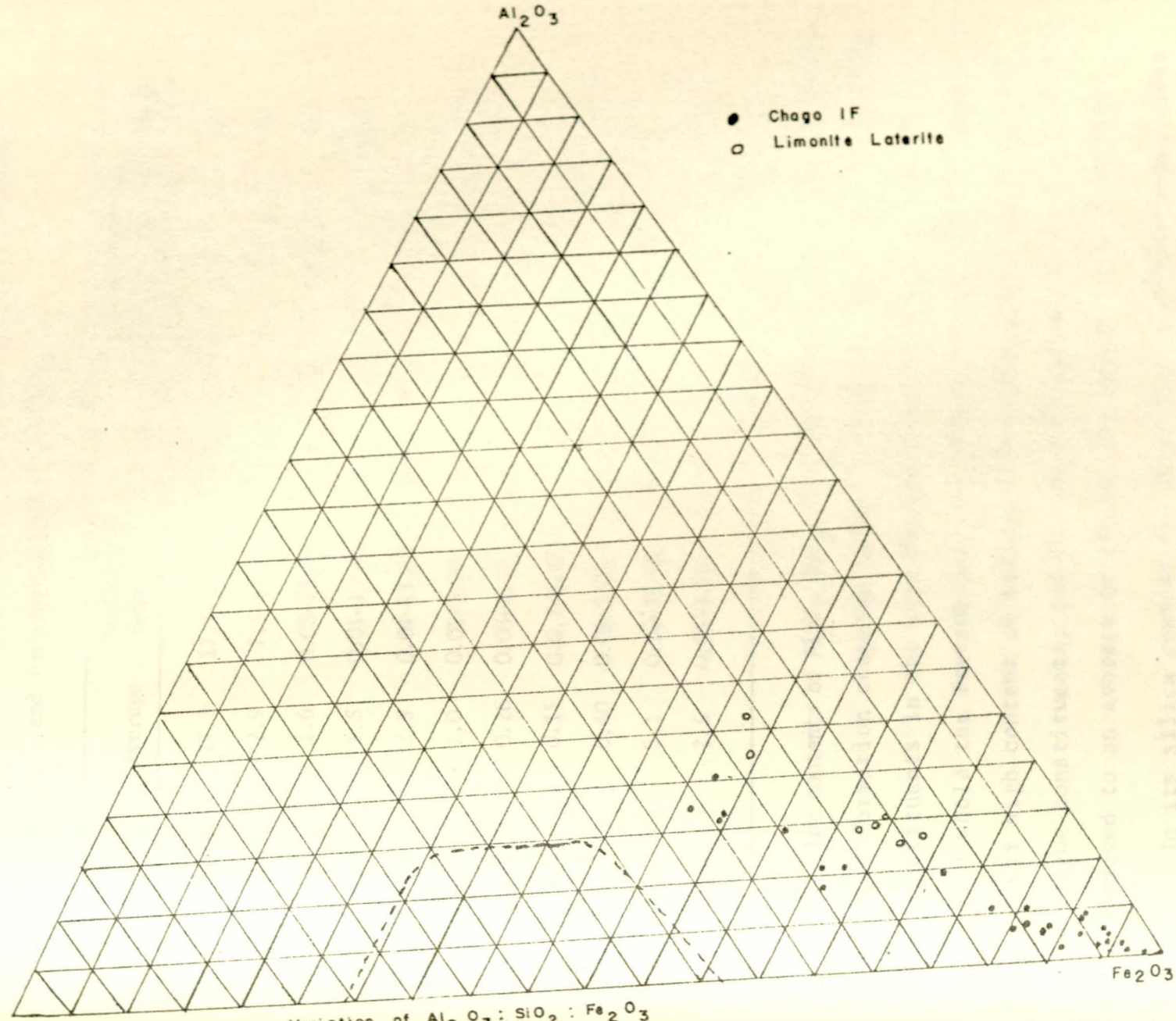

Variation of Al_2O_3 : SiO_2 : Fe_2O_3

Fig. 34

§ TABLE 35: Comparison of the Chemical Composition of Precambrian and Post-precambrian Iron-formation

	Precambrian			Post-Precambrian		
	Average	Range	No. Sample	Average	Range	No. Sample
Total Fe	27.8	17.1-44.2	158	29.0	15.2-47.9	118
SiO_2	42.9	7.3-64.6	158	12.9	4.5-55.7	100
Al_2O_3	1.6	0.03-13.93	153	6.1	0.24-16.8	100
CaO	1.5	0.01-10.48	148	14.3	0.10-33.0	108
MgO	2.8	0.04-11.22	148	2.9	0.45-7.84	59
MnO	1.0	0.01-5.06	108	0.34	0.02-1.80	57
P_2O_5	0.26	0.03-4.02	87	0.86	0.14-2.20	86
TiO_2	0.15	0.0.2-0.53	37	0.45	0.17-2.44	12
C	0.40	0.01-3.05	57	1.11	0.58-2.55	5
Co_2	8.1	0.10-31.56	143	17.8	1.50-30.32	31
H_2O^+	2.5	0.05-9.29	97	4.7	0.26-15.1	23

Low contents of Al_2O_3, TiO_2, P_2O_5 and CaO characterize the Precambrian iron formation compared to the relatively large amount of these constituents in the post Precambrian iron bearing sediments. As a whole the Precambrian iron formations are characterized by their high content of silica. Chert and quartz are the chief gangue constituents, and the average content of SiO_2 is 43% as opposed to an average of 13% for the younger iron formation.

In its silica content the Chago iron formation shows close

proximity to the post Precambrian iron formation. The most striking chemical difference between Precambrian and post Precambrian iron formation is in CaO content, that for the former formation averaging 1.5% while in contrast 14% for the latter formation. Hence, owing to the CaO content of Chago iron formation (0.4%) a Precambrian age can be inffered.

Lepp and Goldich (1964) reported the distribution of silica and the great difference in CaO contents of Precambrian and post Precamberian iron formation (Fig. 52). The author has plotted the percent of SiO_2 and CaO + MgO against percent of total sample (Fig. 53).

Further important differences between Precambrian and Younger iron formations are the low Al_2O_3 and P_2O_5 contents that characterize the older iron formation. The average Al_2O_3 content for the Precambrian iron formation is 1.6%, whereas for the post Precambrian is 6.1%. The overall average Al_2O_3 content for Chago iron formation is about 6%. This figure is quite comparable with post Precambrian iron formation. By considering the average Al_2O_3 content for the magnetite-hematite lenses from Chago (T_2-samples), the value, (1.7%) is in strong agreement with that of the Precambrian iron formation (Table 32).

The P_2O_5 content for Precambrian iron formations is low averaging 0.26% compared to the average value of 0.86% for post Precambrian formations. The average P_2O_5 content for the Chago iron

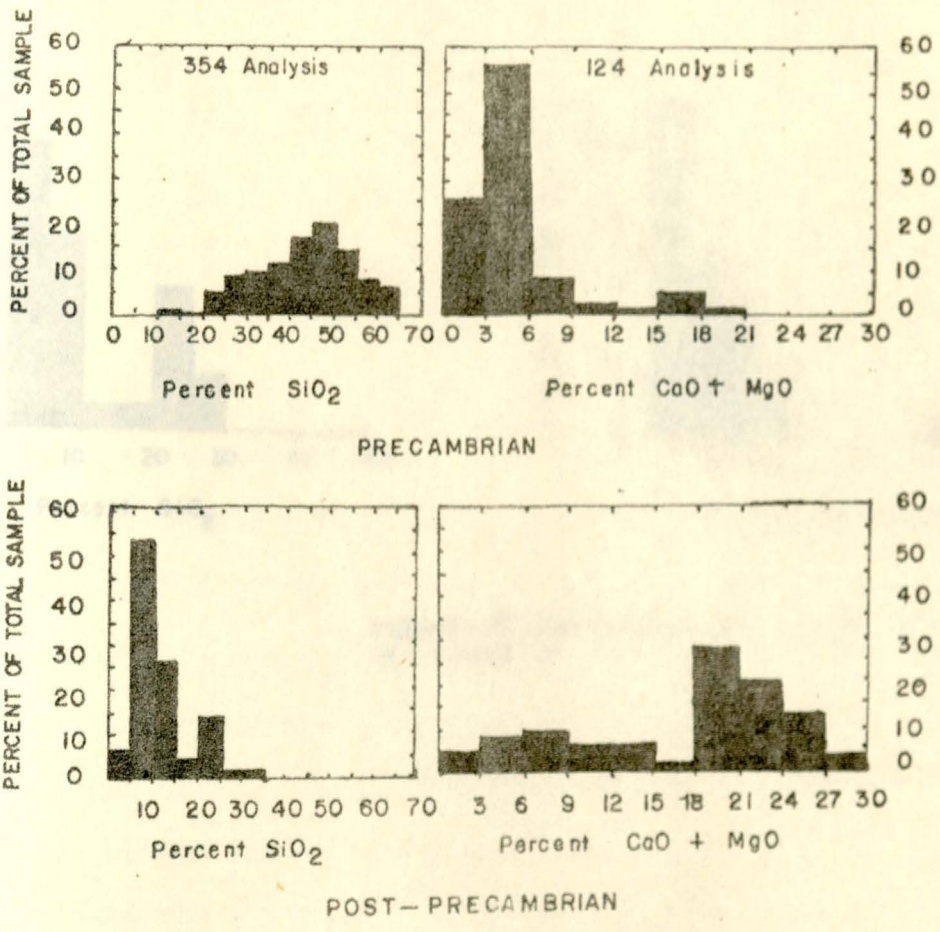

Fig. 52 (After LEPP & GOLDICH, 1964) DISTRIBUTION OF SiO_2 AND CaO + MgO IN PRECAMBRIAN & POST-PRECAMBRIAN IF.

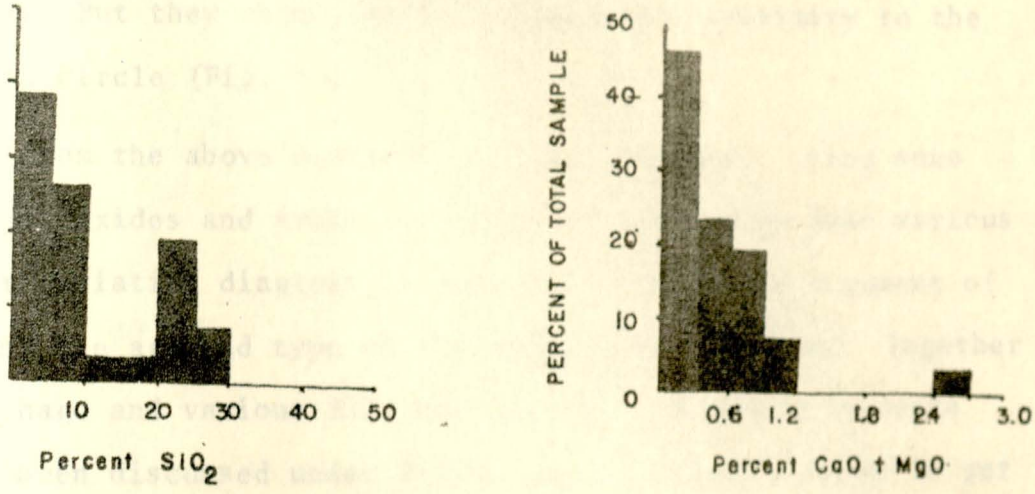

FIGURE. 53. DISTRIBUTION OF SiO_2 & CaO + MgO IN CHAGO IF.

formation is 0.15%, thus close to the average value of the Precambrian iron formation. Further-more the value of the three components of total Fe, CaO+MgO and SiO_2 of Chago when plotted in the Lepp and Goldich triangular diagram (Fig. 54) they lie outside the field of both Precambrian and post Precambrian iron formations. But they show a more or less close proximity to the Precambrian circle (Fig. 55).

Apart from the above mentioned ternary diagrams, using some of the major oxides and trace elements the author has made various triangular variation diagrams in order to broaden the argument of determining the age and type of the Chago iron formation. Together with the Chago and various BIF, the residual limonitic laterite which has been discussed under 2.2.4.2 was plotted in order to get various indications it could possibly offer.

a) P_2O_5 - Na_2O - K_2O diagram: The plottes are dispersed with some degree of alignment above the 45% P_2O_5 content (Fig. 56). The average value of the Algoma, Superior and Orissa Banded iron formations lie within 25-15% of P_2O_5, 40-55% K_2O and 25-40% Na_2O. On the other hand the average value of Chago and the two available data for the Brockman iron formation from Hamersley basin of Western Australia fall within 35-50% of P_2O_5, 20-30% K_2O and 30-40% Na_2O. The graph points out a strong similarity between the Chago and Brockman iron formations with respect to the mentioned parameters. The difference in contents of these oxides of Chago and the other Banded iron formation is not wide, specially the Na_2O content.

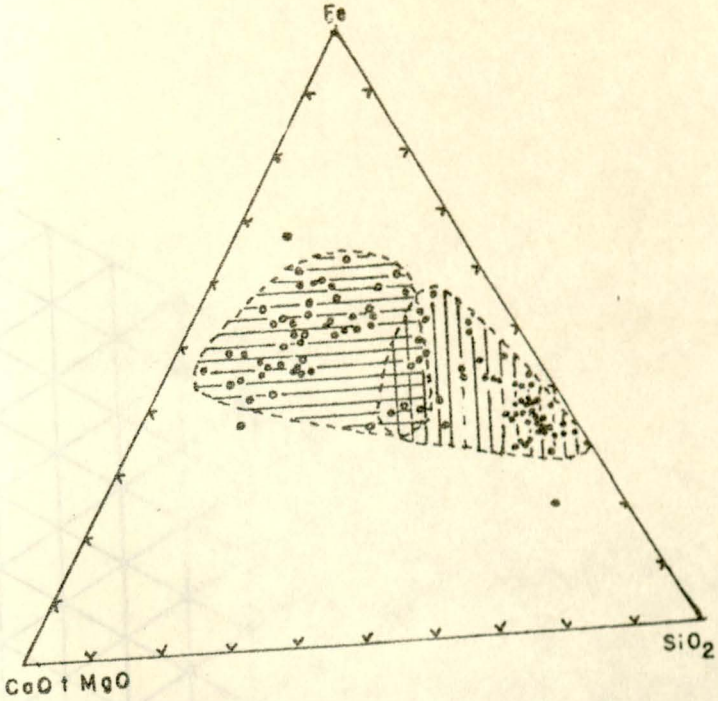

Fig. 54 Variations of Fe : SiO_2 : CaO + MgO

Precambrian

Post-Precambrian

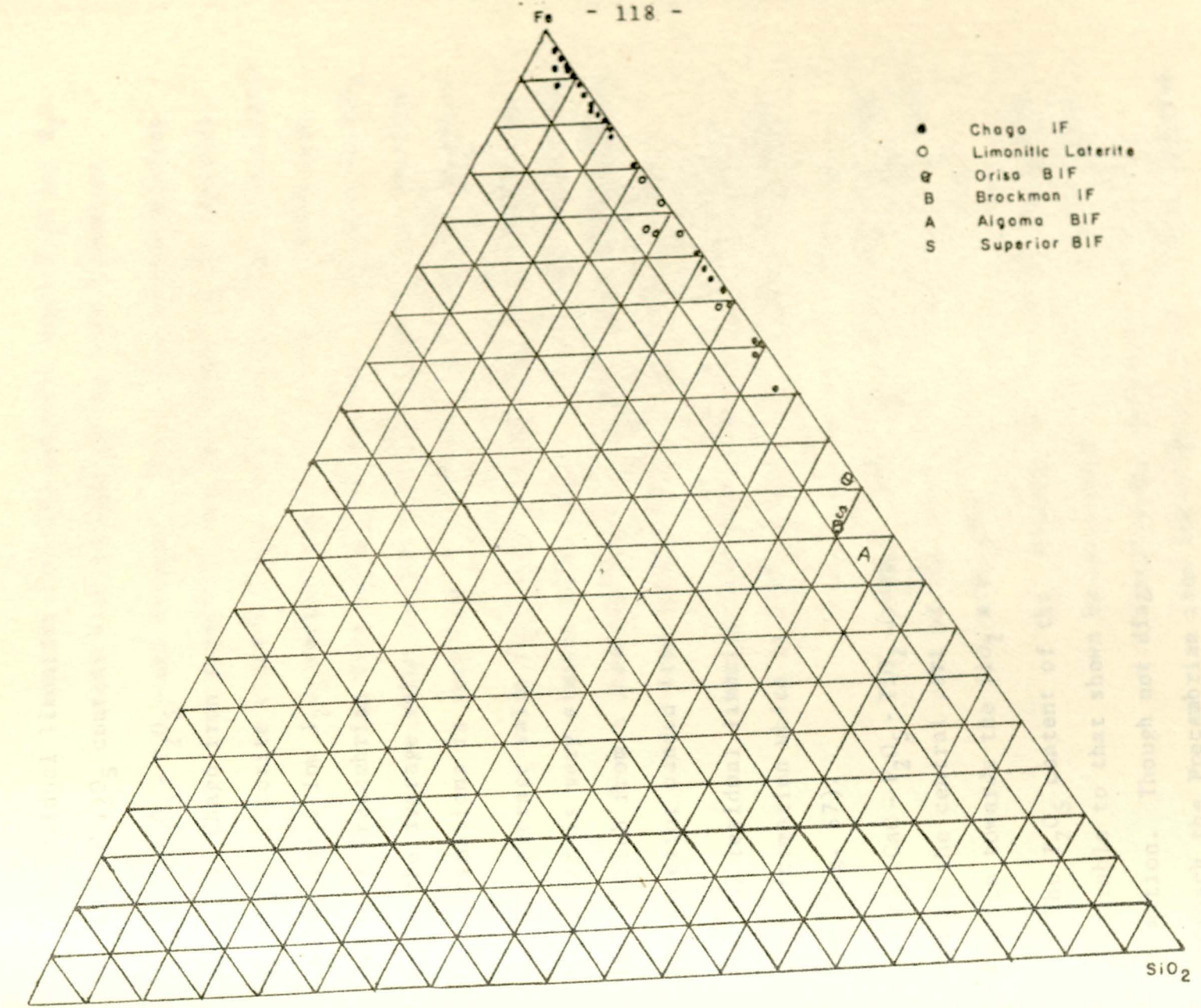

Variation of Fe : CaO t MgO : SiO_2

Fig. 55

The residual limonitic laterite exhibits lower Na_2O and K_2O and higher P_2O_5 content with respect to the iron formations.

b) $Al_2O_3 - P_2O_5 - CaO$ diagram: The various average plottes used, the Chago iron formation, and the points of the residual limonitic laterite cluster along the line $Al_2O_3 - CaO$, thus clearly indicating a low P_2O_5 content (Fig. 57). Both the Precambrian and post Precambrian iron formations plotted are depleted in P_2O_5 while the average value for CaO of post Precambrian and Brockman iron formations is very high compared to the Chago iron formation.

The average value for Al_2O_3, CaO and P_2O_5 of the Chago iron formation is very similar with that of Orissa Banded iron formation, which from a chemical stand point resembles in many aspects the superior banded iron formation (Majumder, et.al., 1982).

The residual limonitic laterite appears to be analogous to Chago formation which is high in Al_2O_3 and very low in P_2O_5 and CaO (Fig. 57).

c) $CaO - P_2O_5 - TiO_2$ diagram: Here the points are clustered around the central part of the graph with a preferential concentration towards the TiO_2 side (Fig. 58).

The P_2O_5 content of the Precambrian iron formation is quite comparable to that shown by the average value of the Chago iron formation. Though not diagnostic the values of CaO and TiO_2 approach the Precambrian iron formation than the post Precambrian iron formation.

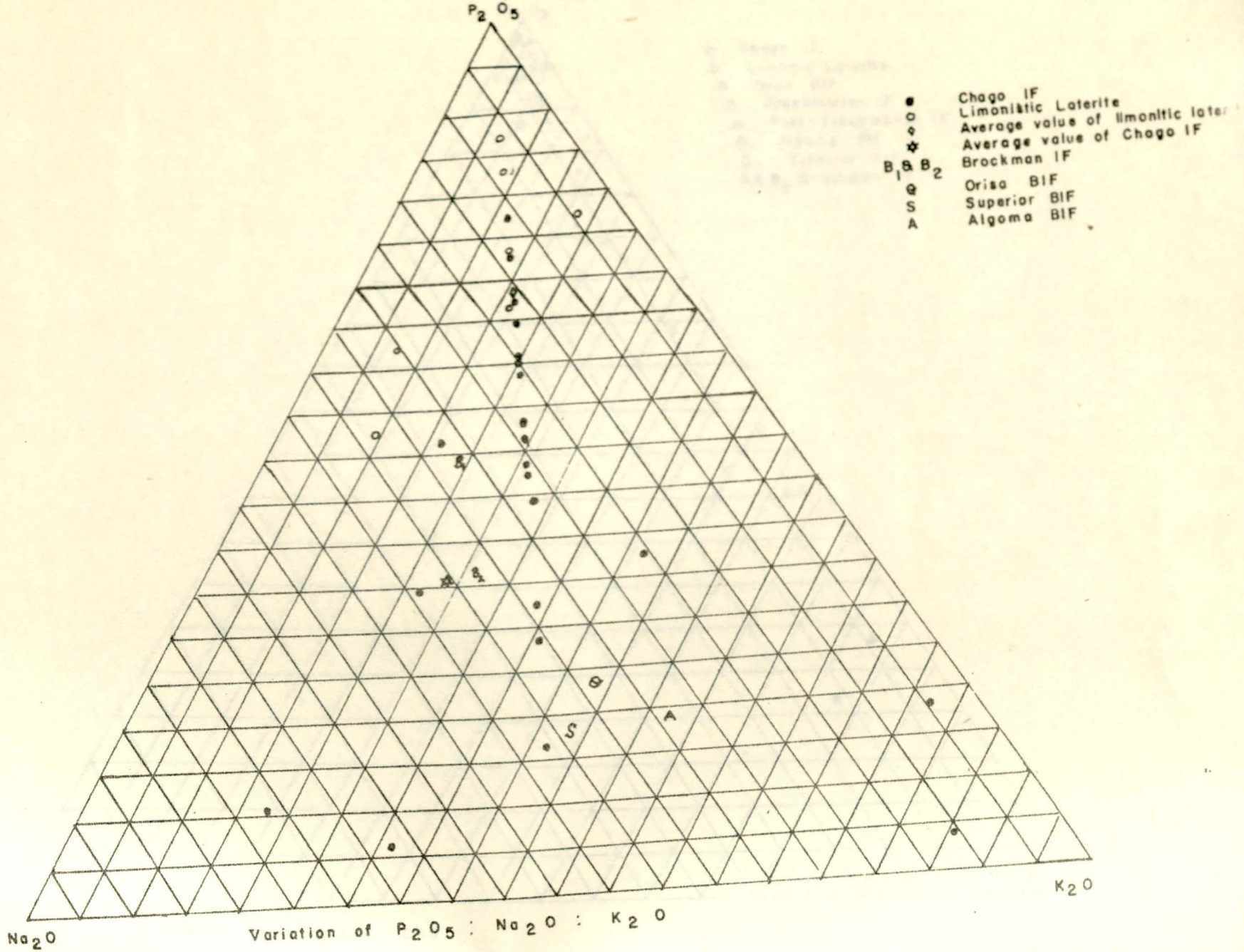
P_2O_5
Na_2O
K_2O
Variation of P_2O_5 : Na_2O : K_2O
Chago IF
Limonitic Laterite
Average value of limonitic late
Average value of Chago IF
B_1 & B_2 Brockman IF
Q Orisa BIF
S Superior BIF
A Algoma BIF

Fig. 56

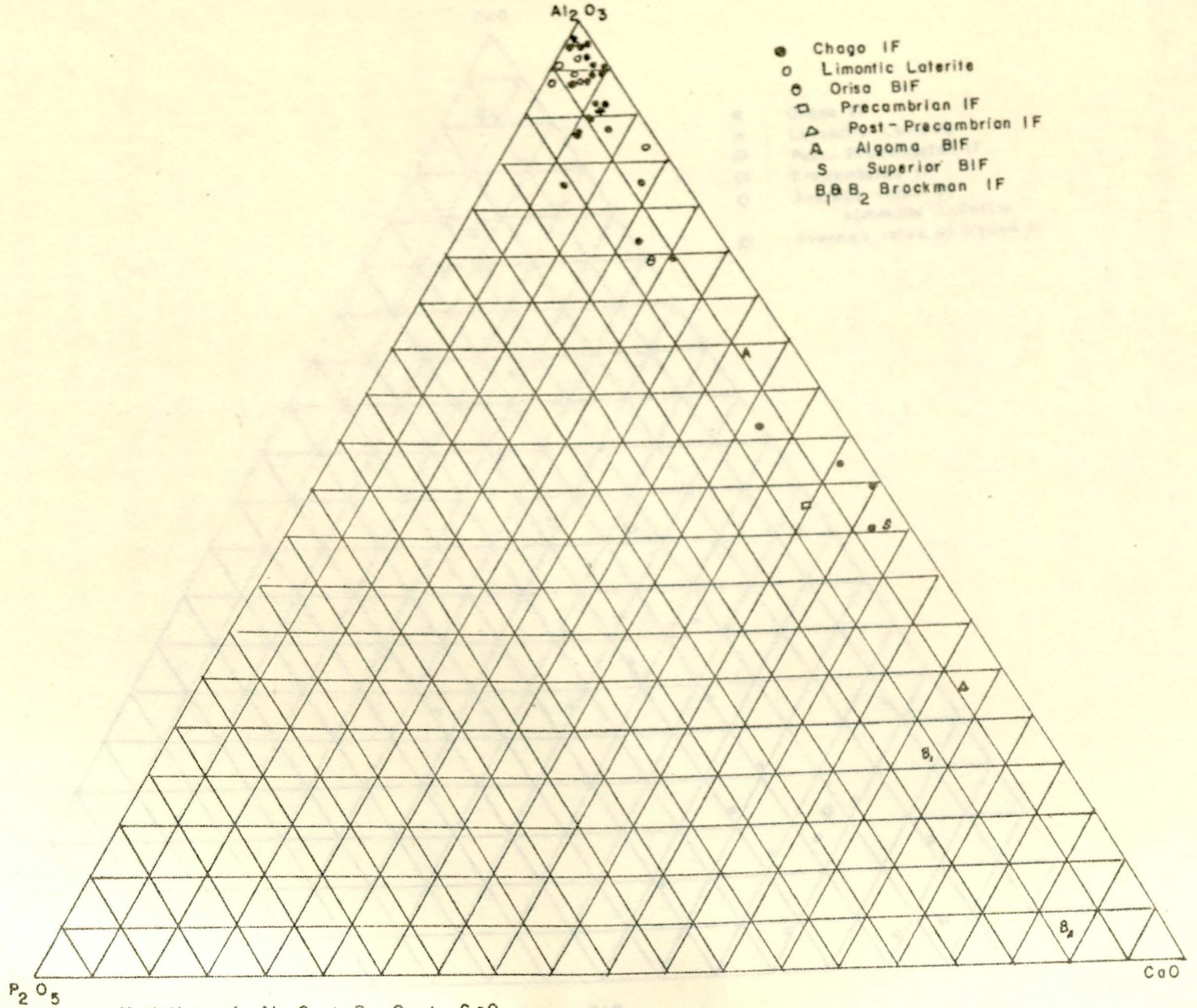

Variation of Al_2O_3 : P_2O_5 : CaO

Fig. 57

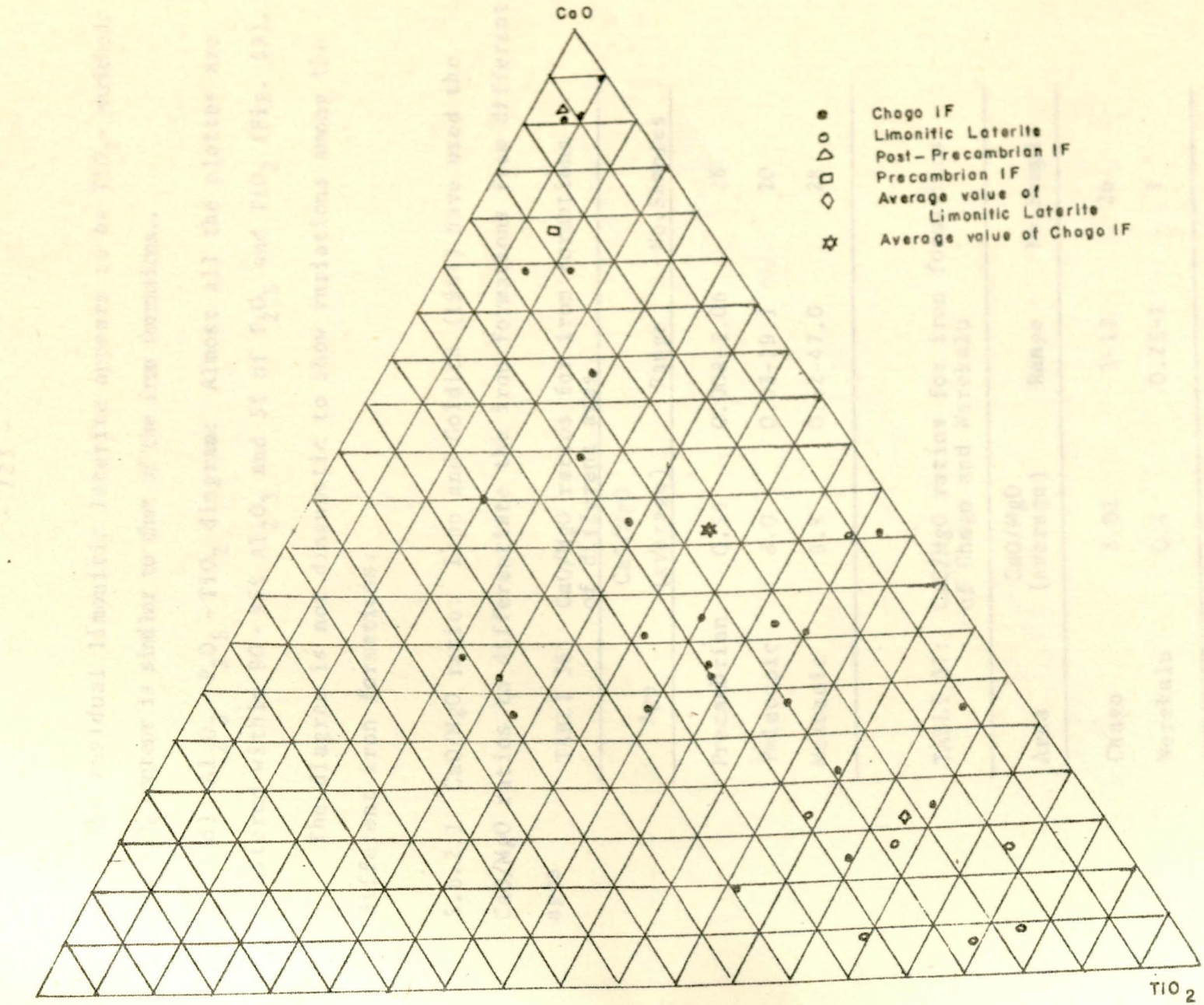

Variation of CaO P_2O_5 TiO_2

Fig. 58

The residual limonitic laterite appears to be TiO_2- enriched. Its P_2O_5 content is similar to that of the iron formations..

d) $Al_2O_3 - P_2O_5 - TiO_2$ diagram: Almost all the plottes are clustered within 90 - 95% Al_2O_3 and 5% of P_2O_5 and TiO_2 (Fig. 59).

The diagram is not diagnostic to show variations among the different iron formations.

5.6.2.1 CaO/MgO ratio: Lepp and Goldich (1964) have used the CaO/MgO ratios to differentiate the iron formations from different ages

TABLE 36: CaO/MgO ratios for iron formations of different ages

Age	CaO/MgO (average)	Range	No.Samples
Precambrian	0.59	0.008-2.06	26
Paleozoic	8.0	0.03-19.1	20
Mesozoic	8.8	0.62-47.0	28

TABLE 37: CaO/MgO ratios for iron formations of Chago and Werekalu

Area	CaO/MgO (average)	Range	No.Sample
Chago	3.02	1-12	26
Werekalu	0.4	0.25-1	2

From Tables 36 and 37, it is apparent that the average CaO/MgO ratios for Chago and Werekalu are more similar to that of Precambrian

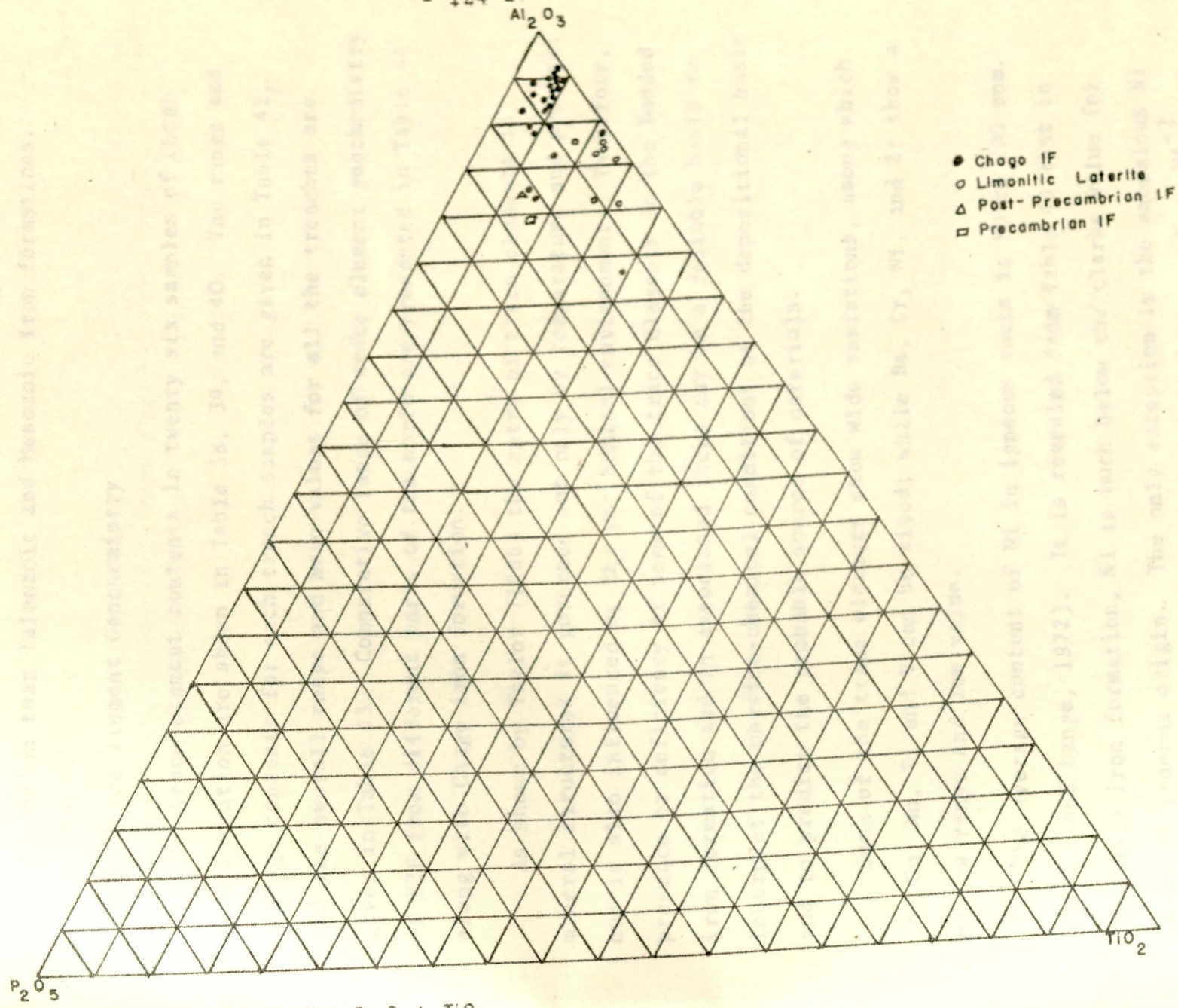

Variation of Al_2O_3 : P_2O_5 : TiO_2

Fig. 59

iron formation than Paleozoic and Mesozoic iron formations.

5.6.3 Trace Element Geochemistry

The trace element contents in twenty six samples of Chago iron formation are shown in Table 38, 39, and 40. The range and average contents for each trench samples are given in Table 42, and the overall range and mean values for all the trenches are given in Table 43. Comparative range of trace element geochemistry of BIF from different parts of the world are presented in Table 44 along with Chago iron formation.

As shown by Taylor (1965) the entry of trace elements in mineral structures is governed not only by temperature and presure; but is also influenced by the geochemical environment. Therefore, presence or deficiency of some of the trace elements in the Banded iron formation and in associated rocks may be a reliable basis to interpret the physico-chemical conditions of the depositional basin and to predict the probable source of materials.

Some of the trace elements show wide variations, among which Co, Cu, Mn, Ti and V can be sited; while Ba, Cr, Ni, and Zr show a narrow range and low value.

The average content of Ni in igneous rocks is 80 to 200 ppm. (Rosler and Lange, 1972). It is revealed from Table 43 that in the Chago iron formation, Ni is much below the clarke value for rocks of igneous origin. The only exception is the anomalous Ni content of some of the magnetite-hematite lenses, where Ni^{+2}

TABLE 38: Trace Element Contents in PPm of Magnetite Hematite Lenses from Trench - 2

Field No.	Co	Ni	Cu	Pb	Cr	Mn	Ti	V	Zr	Ba	Mo
T_2-1	120	40	220	30	-	2000	1000	30	30	-	2
2	70	50	240	20	-	700	700	50	5	-	0.5
3	85	45	220	20	-	n.d	n.d	n.d	5	-	n.d
4	40	50	90	20	-	200	200	200	-	-	0.5
5	55	100	190	30	-	n.d	n.d	n.d	-	-	n.d
6	55	80	185	20	-	n.d	n.d	n.d	5	-	n.d
7	60	75	140	20	-	100	20	20	-	-	-
8	185	70	1520	30	-	70	50	50	-	-	-
9	65	30	480	30	-	150	100	100	5	-	0.5

n.d = not determined.

TABLE 39 : Trace Element Contents in PPm of the Ferruginous Quartzites from Trench - 3

Field No.	Co	Ni	Cu	Pb	Cr	Mn	Ti	V	Zr	Ba	Mo
T_3-1	90	50	680	30	30	2000	1000	50	20	-	1
2	60	40	680	30	7	500	1000	30	5	-	1
3	95	40	1480	35	-	n.d	n.d	n.d	-	-	n.d
4	50	30	520	30	3	70	100	20	5	-	2
5	70	45	600	35	-	200	200	5	-	-	0.5
6	35	40	520	20	-	70	200	30	5	-	1
7	55	45	520	30	3	150	500	50	5	-	150
8	220	30	580	35	3	5000	700	30	20	-	1
9	65	30	400	40	-	1000	500	20	10	-	1
10	35	30	680	40	30	150	300	50	5	-	2
11	20	30	1320	30	20	500	200	30	10	-	1

n.d = not determined.

TABLE 40 : Trace Element Contents in PPm of Iron Bearing Horizon from Trench-4

Field No.	Co	Ni	Cu	Pb	Cr	Mn	Ti	V	Zr	Ba	Ma
T_4-1	70	40	600	30	-	700	70	20	30	-	1
2	65	30	365	25	-	n.d	n.d	n.d	5	-	n.d
3	120	30	720	30	-	2000	200	50	30	0.5	0.5
4	120	40	350	30	10	200	150	50	10	-	0.5
5	225	50	440	30	-	n.d	n.d	n.d	30	-	1
6	155	40	560	20	15	300	50	30	30	-	1

TABLE 41: Trace Element Contents in PPm of Magnetite-hematite Ore from Werekalu

52a	50	120	560	55	-	100	2000	10	10	-	0.5
52b	80	65	1000	40	-	500	500	10	-	-	1

n.d = not determined.

TABLE:42: Range and Average Values of Trace Elements Contents in PPm of the Iron Bearing Tranch Samples and Limonitic Laterites

Elements in PPm	T_2		T_3		T_4		Limonitic Laterite	
	1	2	1	2	1	2	1	2
Co	40-185	81.66	20-220	72.27	65-225	125.83	20-95	42.86
Ni	40-100	60.0	30-50	37.27	30-50	38.33	30-65	52.86
Cu	90-1520	365.0	520-1320	725.45	350-720	505.83	40-130	89.28
Pb	20-30	24.44	20-40	32.27	20-30	27.5	40-115	59.28
Cr	-	-	0-30	8.72	0-15	4.16	0-200	71.14
Mn	70-2000	536.66	7-5000	957	200-2000	800	100-5000	1271.43
Ti	20-1000	345	100-1000	470	50-200	117.5	700-5000	2385.71
V	20-200	75	5-50	31.5	20-50	37.5	7-30	26
Zr	5-30	5.55	0-20	10.5	5-30	22.5	10-200	75.71
Ba	-	-	-	-	0-0.5	0.12	-	-
Mo	0-2	0.58	0.5-150	16.05	0.5-1	0.8	0-2	1.14

1. Range of values
2. Average Values

TABLE 43: Range and average values of trace element contents in ppm of all the trench iron bearing samples

Element	Range	Average
Co	20-225	87.88
Ni	30-100	45.38
Cu	90-1520	500
Pb	20-40	28.46
Cr	0-30	4.65
Mn	20-5000	803
Ti	20-1000	362
V	5-200	45.75
Zr	0-30	10.38
Ba	0-0.5	0.03
Mo	0-150	8.4

TABLE 44 : Average Trace Element Content in PPm of Iron-formation of Chogo-Werekalu and Different Environments

	1	2	3	4	5	6	7	8
B	n.d	n.d	160	240	<5	10-100	-	-
Ba	0-0.5	0.025	170	180	10	-	<100	179
Co	20-225	87.88	38	27	<10	600	< 20	69
Cr	0-30	4.65	78	122	30	-	66	28.5
Cu	90-1520	500	96	10	10	30-50	< 20	22
Mn	20-5000	803	1400	4600	120	-	-	1785
Ni	30-100	45.38	83	32	15	10-20	< 20	20.5
Sr	n.d	n.d	98	42	15	1000	< 30	-
Ti	20-1000	362	860	160	40	-	-	216.6
V	5-200	45.75	97	30	30	3-5	-	35
Zr	0-30	10.38	84	56	<10	10	<30	17.3

< = less than..

1. range of trace element content in chago-werekalu iron formation.
2. average trace element content in chago-werekalu iron fromation.
3. algoma facies oxide iron-formation. (.Grossetal, 1980.
4. Lake Superior facies oxide iron-formation Table 3.)
5. Oxide facies BIF from Orissa.
6. BIF of volcano-sedimentary origin of USSR (Alexandrov, 1973).
7. Banded quartz-magnetite rock from Paakko iron-formation of Finland
8. (Laajoki and Saikkonen, 1977, Table 14, No. 1).
8. Itabarite from Minas Gerais, Brazil (Eichler, 1976, p. 186.)

TABLE 45: Trace Element Contents in PPm of Quartz-Chlorite-sericite Schist

Field No.	Co	Ni	Cu	Pb	Cr	Ma	Ti	V	Zr	Ba	Mo
A-2a	50	130	210	25	1000	500	3000	300	70	-	1
22	25	60	125	30	100	2000	5000	200	300	-	0.7
51b	20	80	95	20	300	1000	3000	200	500	700	0.5
18	15	45	200	20	200	100	1%	300	300	200	0.7
53	25	50	100	20	100	1000	3000	300	300	1000	0.7
81	30	50	125	20	10	7000	7000	30	700	7000	0.5

TABLE 46: Trace Element Contents in PPm of Lithic-Arenite

A-3	35	70	210	25	500	500	3000	300	200	300	1
20	35	75	35	20	150	3000	7000	300	200	200	0.7
73	20	40	155	20	200	2000	7000	50	500	300	0.7
26	15	70	40	20	200	500	1%	500	500	500	1
35	20	70	155	20	300	200	3000	300	200	2000	0.5

TABLE 47: Range and average values of trace element contents in ppm of the Quartz - Muscovite - Sericite Schist

Element	Range	Average
Co	15.50	27.5
Ni	45-130	69.17
Cu	95-210	142.5
Pb	20-30	22.5
Cr	10-1000	285
Mn	100-7000	1933-33
Ti	3000-1%	5166-66
V	30-300	221.66
Zr	70-700	361.66
Ba	0-7000	1483.33
Mo	0.5-1	0.56

TABLE 48: Range and average value of trace element contents in ppm of the Lithic-Arenite

Element	Range	Average
Co	15-35	25
Ni	40-75	65
Cu	35-210	119
Pb	20-25	21
Cr	150-500	270
Mn	500-3000	1600
Ti	3000-1%	7000
V	50-500	290
Mo	0.5-1	0.78
Ba	200-2000	660
Zr	200-500	320

having similar ionic radius with Fe^{+2} may be fixed in the structure of sedimentary magnetite (Goldschmidt, 1954).

The Co/Ni ratio as shown by Frietsch (1970) of magnetite and hematite can be used to differentiate between rocks of igneous and sedimentary origin. According to Frietsch, the Co/Ni ratio is below unity for iron oxides of low temperature and sedimentary origin, but higher values are obtained in the iron oxides of igneous origin. An attempt was made to check the above statement by means of the data given in Table 44. Except for the BIF of volcano-sedimentary origin of USSR and Itabrite from Minas Gerais, Brazil, all the others agree with Frietsch's proposal. Some of the analyzed samples of the associated metasediments from the studied area also gave Frietsch's result. But in the Chago iron formation the Co/Ni ratio was found to be below unity for some of the samples, while it is above unity for most of the samples. Furthermore, the average Co/Ni ratio of all the samples is above unity.

Landergren (1948) showed the low concentration of Cr below the clarke value of sediments (110 ppm), as indication to origin of such ores as oxidates. Frietsch (1970) reported that Cr is present below the lithospheric content (90 ppm) in the magnetites of the iron ores of N-Sweden, which are non magmatic in origin. Majumder, et. al., (1982) reported that in the Orissa BIF (India), Cr ranges from 20 to 50 ppm, while in the separated magnetites it dropes to 4-5 ppm. On the other hand they showed that the Cr

content in the inter-layered tuff to be as high as 300-2000 ppm, thus strongly suggesting an igneous origin. In Chago iron formation Cr ranges from 0 to 30 ppm, while in the magnetite-hematite lenses is below the detection limit. The over-all Cr average content is 4.65 ppm. Hence the low Cr content of the Chago iron formation substantiates the assumption of its sedimentary origin as oxidates.

Titanium has also been used as a temperature indicator by Fretsch (1970) to differentiate between magnetites formed by high temperature magmatic process and low temperature sedimentary process. The clark value of lithospheric titanium is given as 10,000 ppm (Shaw, 1964), Majumder, et.al. (1982) have used Frietsch's idea to determine the formation of temperature of the Orisa BIF and associated tuff by using the titanium content. They found the Ti content of the BIF to be in the range 30-80 PPM, while the tuff exceeded 1000 ppm. The Chago magnetite-hematite lenses contain low Ti compared with the ferruginous sediments. The overall mean Ti content at Chago is 362 PPM, which is still low when compared with the lithospheric value. This possibly lead to infer that the Chago iron formation was formed by low temperature sedimentary processes. Ti content for associated metasediments (quartz-sericite-chlorite schist and lithic-arenite, Table 47 and 48 is rather high, ranging from 3000 to 10,000 ppm. This probably reflects incorporation of igneous material in the clastic fractions.

Hirst (1962) showed the distribution of Zr to be related to provenance rather than to sorting of sediments, as zircon is ultrastable and rarely decomposes. Hence rocks showing high Zr content can probably be taken to indicate either direct igneous origin or incorporation of igneous materials. The Chago iron formation shows very low content of Zr which is relatively high in the associated metasediments. This result also strongly substantiate the sedimentary origin of the Chago iron formation.

In order to extract more information from the trace elements, two triangular variation diagrams were made by using Co, Cr, Ni and Cu as end members.

a) Ni-Co-Cr diagram: This diagram exhibits that most of the plot lie on the Ni-Co line, because of very low or lack of Cr. Most of the points fall below 50% Ni content (Fig. 60). The graph shows similar value for the Ni content of Chago and Orisa iron formations. The Ni content for all BIF plotted shows a variation not exceeding 20% with a notable exception for the volcano-sedimentary BIF of USSR, whose Ni content is highly depleted. The graph also points out that Chago iron formation differs from other BIF for its low Cr content. According to Landergreen (1948), such a low Cr content strongly suggests that Chago iron formation is originated by oxidate accumulations.

b) Co-Ni-Cu diagram: This ternary diagram discloses the high concentration of Cu with respect to Co and Ni (Fig. 61) for Chago. The other oxide facies BIF plotted are low in their Cu

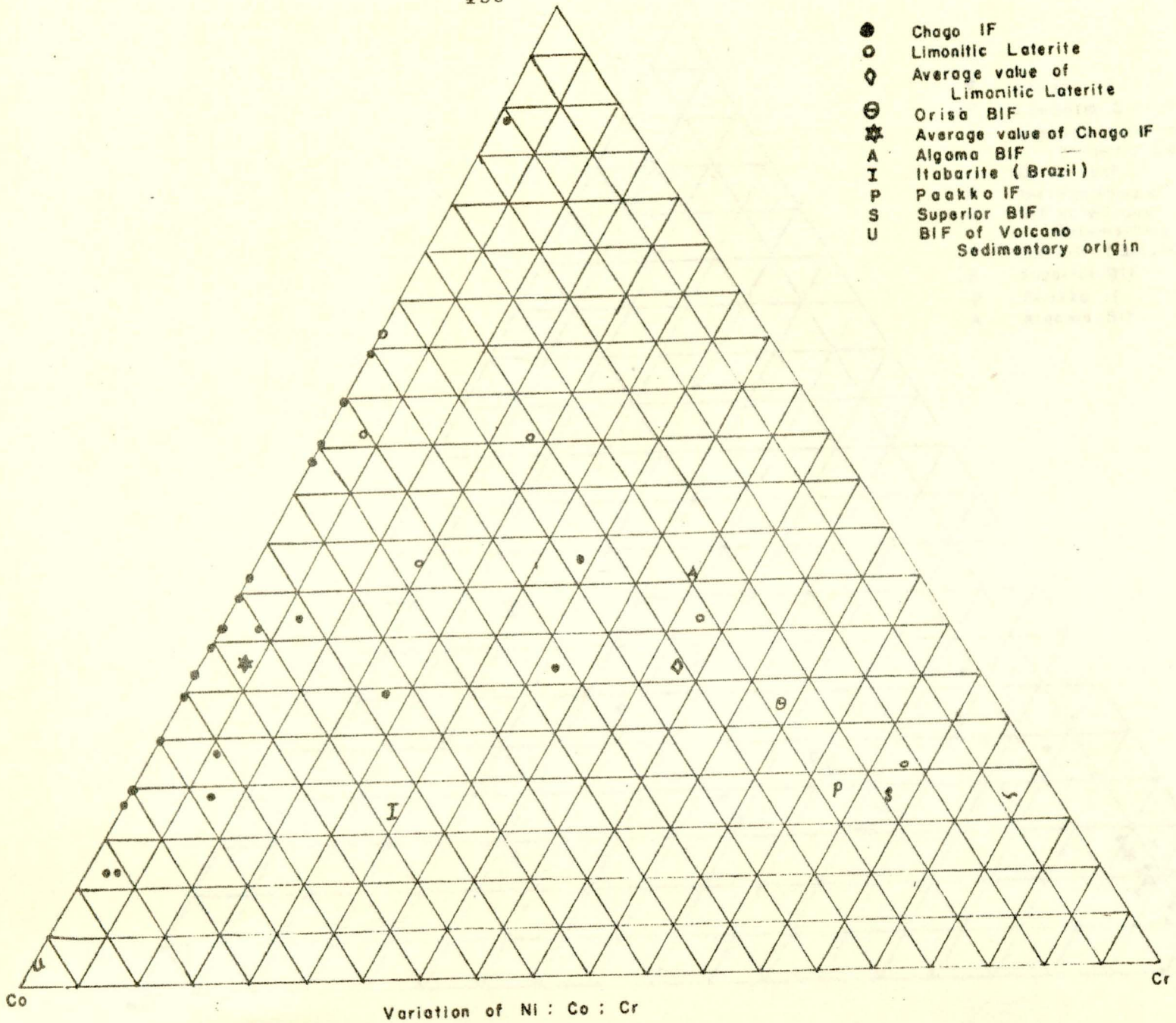
Chago IF
Limonitic Laterite
Average value of Limonitic Laterite
Orisa BIF
Average value of Chago IF
A Algoma BIF
I Itabarite (Brazil)
P Paakko IF
S Superior BIF
U BIF of Volcano Sedimentary origin
Co
Cr
Variation of Ni : Co : Cr

Fig. 6a

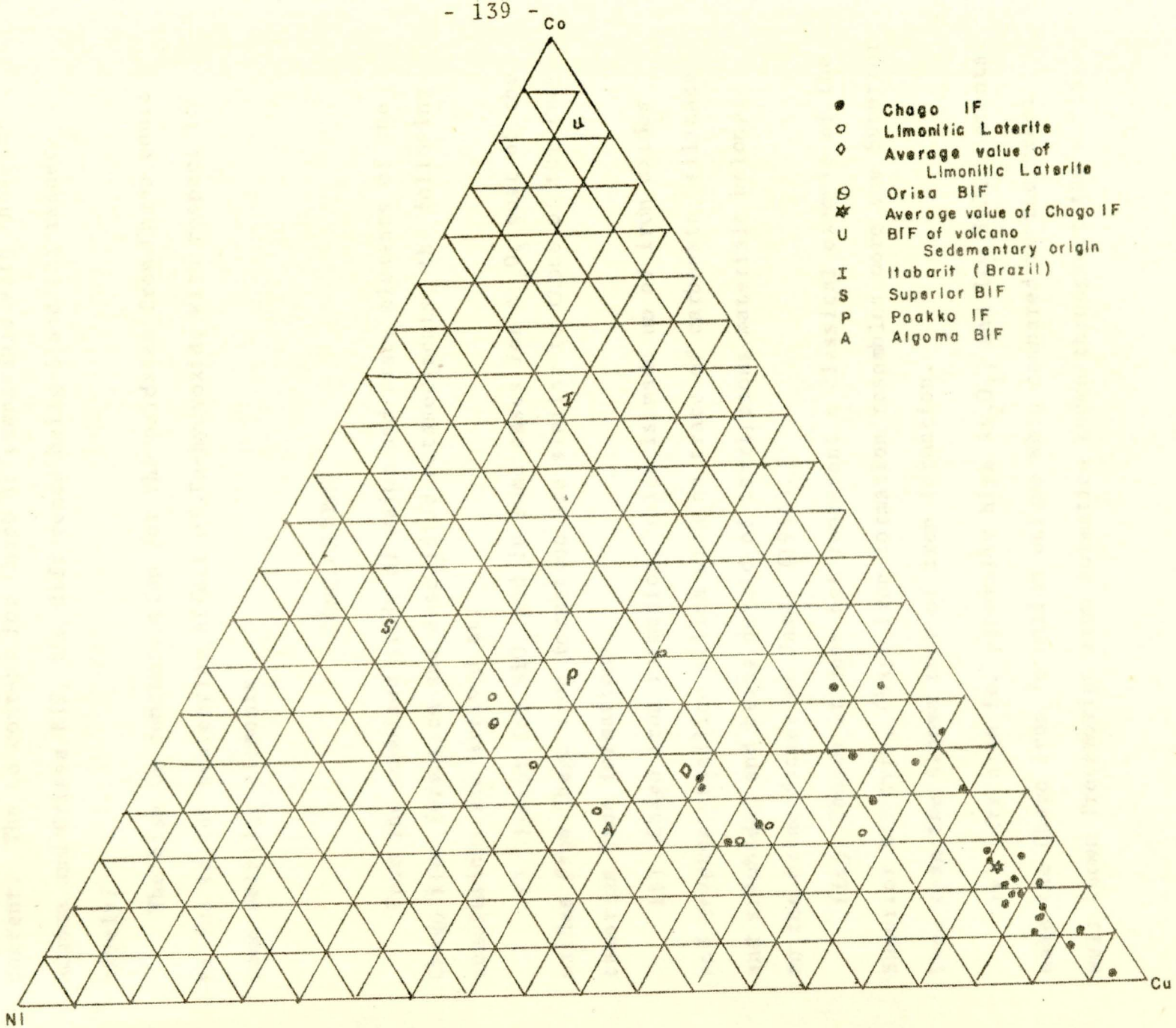

Variation of Co : Ni : Cu

Fig. 61

content. The Co content for Chago is comparable with those of Algoma and Orissa BIF, the difference being 5 and 15% respectively.

The high Cu concentration for the oxidates from Chago could be due to the scavenging effect of Fe-hydroxide with respect to some metallic elements.

CONCLUSIONS

From the combined study of major and trace elements of the Chago iron formation and associated metasediments, the following conclusions are arrived at:

i) Except for SiO_2 and in some cases for Al_2O_3 most of the oxides from Chago iron formation are similar to those of the Precambrian iron formations.

ii) Chago iron formation, which is made up of iron oxides and cryptocrystalline silica with no trace of carbonate, silicate and sulphides and being devoid of terrigenous materials belongs to the oxide facies of James (1954).

iii) Though it does not represent a classical example of the Superior BIF type, Chago iron formation resembles more the Superior Type than the Algoma type of iron formation.

iv) Its high Fe, generally high Al_2O_3, and low SiO_2 contents make the Chago iron formation unique when compared to the other well known Precambrian iron formation known throughout the world.

v) Depletion of trace element in the iron formation of Chago when compared to the associated metasediments, indicates the absence of clastic materials in the former.

vi) The low Ni, Cr, Ti and Zr contents shown by Chago iron formation indicates its low temperature sedimentary origin.

6. Mineralization

According to the works of Rudis (1964) the iron mineralization in the Gulliso-Chago-Yubdo area are divided into two genetic types:

1. Ferruginous quartzites with magnetite-hematite lenses, and
2. Silicified residual limonites.

The first type of iron ore deposits are represented by an iron bearing horizon interstratified in Precambrian metasedimentary units, while the second one is bound to the residual concentration of decomposed tertiary basalts.

The ironbearing horizon was deposited in a shallow water near shore environment as chemical pricipitate. But later all the sediments together with the surrounding plutonic rocks were subjected to a low grade regional metamorphism, belonging to the green schist facies. Mineralogy, texture, and structure, which generally have been the basis of iron formation studies, are mainly the result of depositional, diagenetic, and metamorphic conditions to which the particular rocks have been exposed. As a result of these the metamorphic effect could have remobilized and concentrated the iron ore, forming very thick bands and lenses as compared to the thin films of quartz and other gangue minerals. According to Rudis (1964) the occurrence of large magnetite hematite lenses within the ferruginous quartzites is probably the result of dehaydration of a primary limonitic ore bodies.

The tenor of the compact magnetite-hematite lenses ranges from 58.75 to 67.87 percent, while the ferruginous quartzites range from 31 to 56.3 percent. The overall average tenor of iron at Chago is 54 percent. The magnetite-hematite ores of the studied area represent a high grade iron, and unwanted impurities, like S and P, which harm the properties of pig iron and steel are below allowable limit. The content of silica is also extremely low even when compared with other well known iron formations of the world.

Rudis (1964) estimated the " geologic reserve" of the high grade ore to be 440,000 tons, taking 50 percent of the strike length (of 400 meters), 5 meters average width, 100 meters depth and 4.4 tons per cubic meter. Similarly the low grade ore ("33" percent of iron content) at Chago and the vicinity was estimated to be 12,000,000 tons based on 3.2 tons per cubic meter.

Belay, et. al. (1980) using the Rudis estimation method, calculated the maximum tonnage of the high grade ore to be 12,672 tons, concidering the strike length to be 120 meters and the width 2 meters. Similarly the Chago low grade material was estimated to be approximately 27,000 tons. According to the estimations of Belay, et.al. (1980) the total iron tonnage at Chago is approximately 40,000 tons. In all these estimates the maximum depth taken was 12 meters below the ccover.

According to its chemical composition and physical properties, the high grade ore of Chago is suitable for any kind of smelting process. But the amount of resource of the high grade ore is much below the world's exploitation limit. The estimated 27,000 tons of low grade iron ore was also proved by magnetometer survey to be much lower, due to the assumed uniform thickness of the magnetite-hematite layer was found to be lenticular and to attain only a limited size (Belay, 1980).

Despite the excellent quality of ore at Chago, it does not offer any chance for establishing a steel industry on a national scale. It is reckoned that for this purpose at least 15 million tons of high grade iron ore should be readily available.

Under the present conditions, local small-scale mining and smelting for manufacturing in situ products might be economically feasible.

7. Genesis of the Iron-formation

The lack of modern-day examples of iron formation deposition makes the subject of origin a fertile one for speculation. If the wide divergence of opinion in even the recent literature accurately reflects current geological thought, the sedimentary iron-bearing formations are still little understood.

Iron formation was defined by James (1954) as " a chemical sedimentary rock, typically thin bedded and/or finely laminated, containing at least 15% iron of sedimentary origin and commonly, but not necessarily, containing layers of chert." Iron formation and the genetically related chemical sediments included in this broadly defined lithological group are distinguished from the clay-iron stone ferruginous sediments by the presence of banded and layered chert and quartz, and siliceous matrix for iron minerals, by a lower alumina and titania content, and by characteristic primary sedimentary features (Gross, 1965, 1972).

Distinctive textures, primary sedimentary features, mineralogy, minor element content and the associated rocks indicate the wide range of environmental conditions in which iron formations were deposited.

A classification of the iron formation as Lake Superior and Algoma types was introduced (Gross, 1965) to emphasize differences in the kinds of associated rock in the depositional environments and geological settings for the various occurences of iron

formation. Sedimentary environments for the deposition of iron formation extends through a broad spectrum from neritic basins to the deeper parts of the continental shelves to tectonic-volcanic ridges offshore, and to deeper ocean basin (Fig. 62, Gross, 1980).

It has been suggested that extensive deposition of iron formation during the Precambrian was related to special factors in the development of the atmosphere and lithosphere involving the origin and evolution of organisms, and increase of oxygen in the atmosphere, the influence of carbon and oxygen in sedimentary environments, and the transportation and deposition of iron. Genetic models for iron formation which emphasize these factors have been proposed by several workers (MacGregor, 1972; Cloud, 1973; Holland, 1973; LaBerge, 1973; Garrels, et.al., 1973; Drever, 1974). However, Gross (1983) concluded that the deposition and distribution of iron formation has been controlled primarily by tectonic factors, and that biogenic factors and the composition of the atmospher had a lesser, and probably limited influence on the precipitation of those chemical sediments.

The Chago iron formation is associated with quartzites, different quartz rich schists, and graphitic phyllites. Their association clearly indicate the environment of deposition to be near shore or continental shelves. The barite which is interbeded with quartz and magnetite-hematite near Chago (St-29) signifies that the deposition had taken place in a very limited

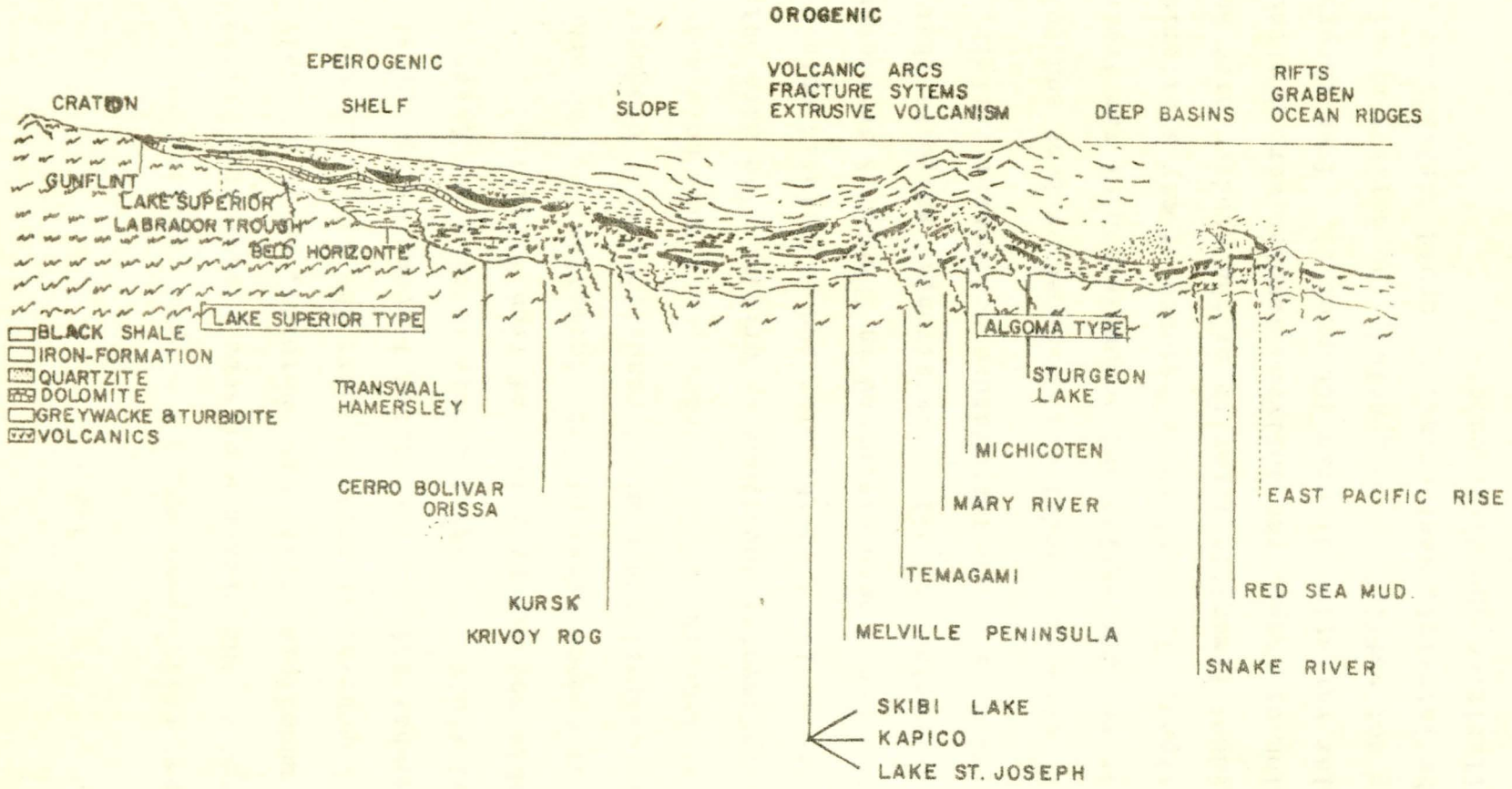

FIGURE 62 TECTONIC ENVIROMENTS FOR DEPOSITION OF IRON — FORMATION (FROM GROSS,1980)

basin of lagoonal environment which has been reducing for a short period (indicated by the presence of some disseminated sulphides). The associated undefferentiated biospheroids, which probably are blue-green algal genera, strongly support the idea that the Chago basin was a somewhat saline, restricted lagoon, and marginal to a true continental shelf. In its tectonic setting the Chago iron formation resemble the superior type of iron formation.

The chemical compositions of iron formation, on the other hand reflect the overall geochemical conditions that produced such concentrations of iron in the lithosphere, and they hold answers to some of the fundamental questions of origin. The data obtained from the chemical analyses of the ores and associated metasedimentary units, which has been discussed in Chapter 5 supplemented with the existing geological evidences strongly suggests that the Chago iron formation is a low temperature sedimentary origin.

A lateritic weathering model was designed by Lepp and Goldich (1964) to explain the derivation and accumulation of the Precambrian iron formations. To check the existence of any similarity between the residual limonitic laterite of the studied area and the iron formation of Chago, the analyzed samples were plotted in various triangular variation diagram (Chapter 5). Even though these graphs are not sufficient to conclude the derivation of the iron formation by lateritic weathering, it could derive some clue about their similarities and differences.

The source material that supplied the Chago basin with iron could probably be an iron rich and silica poor mafic rocks.

8. Iron Occurrences in Ethiopia

A primitive local smelting of iron ore for manufacturing of implements has been carried out in Ithiopia for centuries, and exists still nowadays. Small accumulations of iron ore have been exploited for this purpose throughout the country.

Series efforts to find iron ore in Ithiopia were made during the Italian occupation. No deposits of economic significance were discovered in that time (Hamrla, 1973). Later, following the stipulations of the second five years plan (1960-1965) to erect steel-mill industry in Ethiopia, the known iron ore occurrences were reassessed. Most of the work was performed by the Ministry of Mines during 1962-1964. Although high grade ore was discovered at places, the reserves are far too low to allow anything but a most modest local development. Most of the localities were iron ore has been found are shown in Fig. 63.

According to the map produced by Jelenc (1966) about seven of the administrative regions of Ethiopia are known with an indication of iron occurrences. Off all the occurrences the concentration known in Wollega and Eritrea are more important fllowed by Keffa, Tigre and Harrar Provinces.

Areas of larger deposits and of which has been investigated by various workers are given below:

Eritrea: Bodies of high grade magnetitic ore occur in the Sabub-Agametta area, about 40 km. east of Asmara (Hamrla, 1966;

Rudis, 1964). Mineralogically, the ores of Agmatta-Sabub area consists of granoblastic martitized magnetite in a quartz matrix with minor admistures of other minerals such as lamella hematite, chlorite, mica, epidote and calcite.

Different investigators have tried to estimate the ore of Agametta area. Krupp (1956) estimated it to be 2.5 million tons, whereas, according to Rudis (1964) there is only about 425,000 tons of ore. On the other hand Hamrla (1966) estimated the visible tonnage to be 132,000 tons with additional indicated and inferred ore in the order of 500,000 tons at maximum.

The accumulation of iron on Eritrea Plateau, south of Asmara as well as Northern Tigre is bound to pre-tertiary peneplanation and lateritization of Precambrian rocks. Iron oxides originated insitu in lateritic residue, forming ancient residual-lateritic deposits (Hamrla, 1973). The peneplain was buried under Tertiary Trap volcanics. Reddish layers of ferriferous rocks occur where the present erosion removed the basaltic capping, and can be observed everywhere, where the pre-trappean levelled surface is exposed. The largest exposures are between Asmara and Abarda, some 12 km. to the southwest of Asmara, whereas the other exposures are along the whole margin of the Trap capping (Hamrla, 1973).

The richest portions usually occur as reddish-brown spongy rock intermingled with iron hydroxides just at the top of the ferruginous layer. These bodies are said to have in average

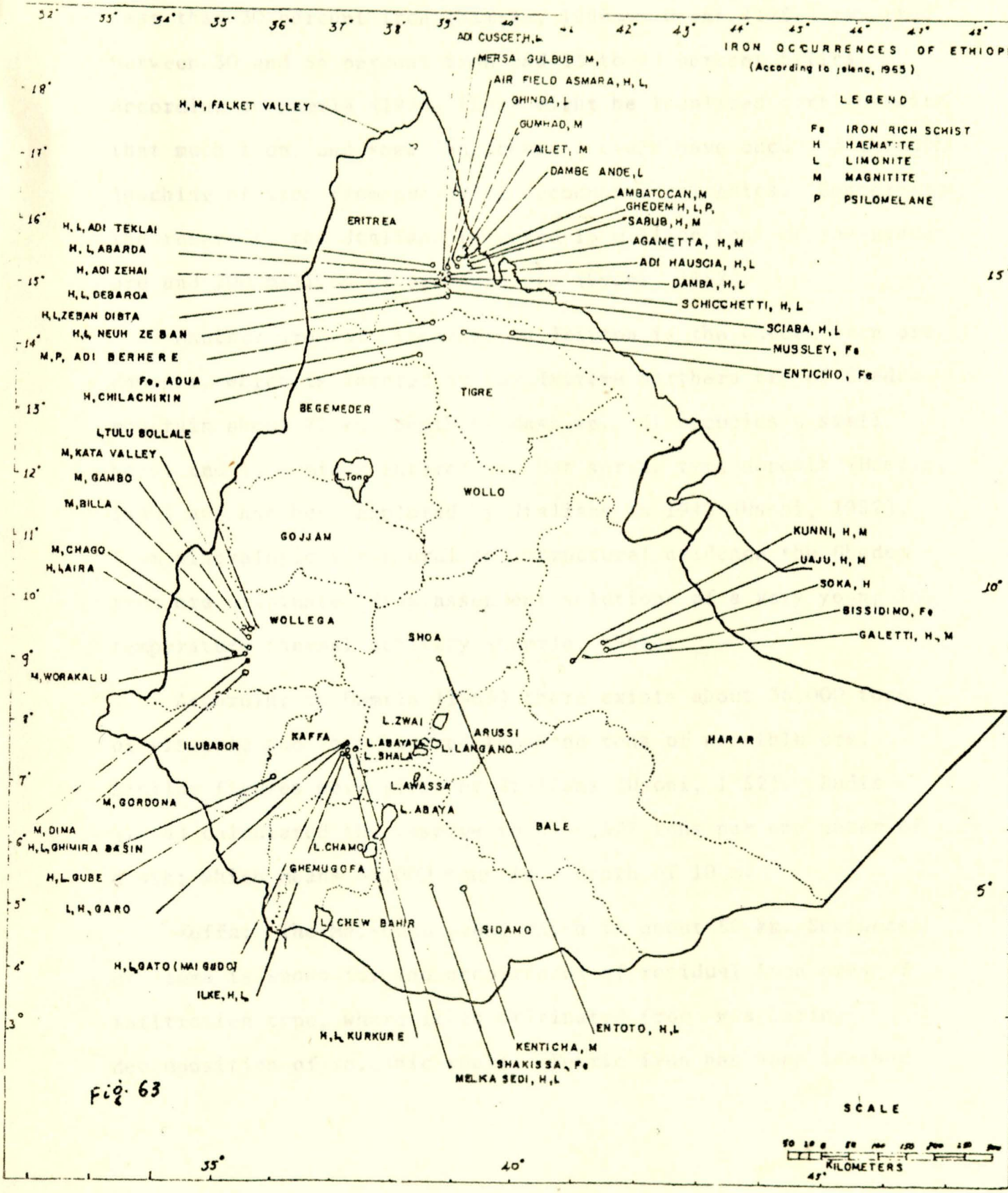
IRON OCCURRENCES OF ETHIOP
(According to Selenc, 1965)
LEGEND
Fe IRON RICH SCHIST
H HAEMATITE
L LIMONITE
M MAGNITITE
P PSILOMELANE
ADI CUSCETH, L
MERSA GULBUB M,
AIR FIELD ASMARA, H, L,
GHINDA, L
GUMHAD, M
AILET, M
DAMBE ANDE, L
AMBATOCAN, M
GHEDEM H, L, P,
SABUB, H, M
AGAMETTA, H, M
ADI HAUSCIA, H, L
DAMBA, H, L
SCHICCHETTI, H, L
SCIABA, H, L
MUSSLEY, Fe
ENTICHIO, Fe
H, M, FALKET VALLEY
H, L, ADI TEKLAI
H, L, ABARDA
H, ADI ZEHAI
H, L, DEBAROA
H, L, ZEBAN DISTA
H, L, NEUH ZE BAN
M, P, ADI BERHERE
Fe, ADUA
H, CHILACHIKIN
L, TULU BOLLALE
M, KATA VALLEY
M, GAMBO
M, BILLA
M, CHAGO
H, LAIRA
M, WORAKALU
M, GORDONA
M, DINA
H, L, GHIMIRA BASIN
H, L, GUBE
L, H, GARO
H, L, GATO (MAI GUDO)
ILKE, H, L
H, L, KURKURE
MELKA SEDI, H, L
SHAKISSA, Fe
KENTICHA, M
ENTOTO, H, L
KUNNI, H, M
UAJU, H, M
SOKA, H
BISSIDIMO, Fe
GALETTI, H, M
ERITREA
TIGRE
BEGEMEDER
WOLLO
GOJJAM
WOLLEGA
SHOA
ILUBABOR
KAFFA
ARUSSI
HARAR
BALE
SIDAMO
GHEMUGOFA
L. Tana
L. ZWAI
L. ABAYATA
L. SHALA
L. LANGANO
L. AWASSA
L. ABAYA
L. CHAMO
L. CHEW BAHIR
SCALE
KILOMETERS

Fig. 63

less than 30 percent iron (hamrla, 1966). Usoni (1952) reported between 30 and 56 percent iron and 13 to 28 percent Silica. According to Hamrla (1973) there might be localized portions with that much iron, and some 'enrichment' could have occurred through leaching of iron from overlying decomposed volcanics. Concerning the reserves, the Italians reported 15 million tons of low-grade ore and 200 million of probable ore (Usoni, 1952).

Another area of interest in Eritrea is the Ghedem iron ore deposit, which is located at the Extreme northern tip of Ghedem mountain about 71 km. South of Massawa. It occupies a small horst and is a minor interesting hot spring type deposit (Hamrla, 1960) and has been explored by Italians in 1940 (Usoni, 1952). From mineralogical textural and structural evidence the Ghedem iron ore originated from assendent solutions of a very young low temperature thermal activity (Hamrla, 1966).

According to Hamrla (1966) there exists about 36,000 tons of vissible and some hundred thousand tons of possible ore. Similar figures were given by Italians (Usoni, 1952). Rudis (1964) calculated the reserve to be 6,577 tons per one meter of depth; which means 65,000 tons to a depth of 10 m.

Keffa: The Mai-Gudo area, which is about 50 km. Southeast of Jimma is known for the occurrences of residual iron ores of infltration type, where it is originated from weathering decomposition of volcanic rocks. Ferric iron has been leached

transported and precipitated more or less in situ, partly in the soil residue, partly in weathered, cracked surficial portion of the country rocks. Because of abundant impurities an average grade would be lower and could not exceed 40 percent in the best case (Hamrla, 1973).

During the Italian occupation about 20,000 tons of ore was mined and the reserves were estimated to be 1.2 million tons (Usoni, 1952). Murdock (1960) calculated 120,000 tons of visible reserves and a probable 25,000 tons of ore.

Wollega: Various origin of variable grades of ore occure in different parts of Wollega among which the Chago, Werekalu, Dima, Gordana or Koree, Billa and Bikilal are at least investigated by different workers at different time. Mineralogically the iron ores of central Wollega consists of martitized magnetite-hematite which is massive at places Banded and usually coarse or crystalline aggregate.

Rudis (1964) surveyed the area geologically and by magnetometer. Representative samples were collected, tested, and put the reserves estimate at 800,000 tons of possible ore in central Wollega. On the contrary Hamrla (1966) estimated the visible ore reserves to be 160,000 tons for all known localities, with possible reserves ranging in the order of 300,000 tons.

Jelenc (1966) appeared with a positive idea by explaining the extension of the ferruginous schists in the area and expected

" many ten million tons of iron reserves" in this part of Wollega.

UN mineral survey (UN report, 1971) checked these iron ore occurrences by conducting geochemistry and magnetic survey and no conclusions were reached except that the deposits hold little promise of development as iron ore resources.

Iron occurrences has been also identified in Sidamo around Yabello and Arero: These are boulders and nodules of magnetite-hematite ore.

In Harrargie floats of iron has been reported in Precambrian rocks of Chercher Mountains and also around Jijiga and Dire-Dawa a ferruginous sandstone with 5-15% Fe has been reported.

Genetically the iron occurrences of Ethiopia belong to different types and the ores are mainly oxidic (Hamrla, 1966). The primary high grade ores are associated with the Precambrian environment while the secondary residual ores are wide spread throughout the country in different geological environments. Hydrothermal occurrences are subordinated. The following types are hither to recognized:

1. Deposits associated with Precambrian green-schist sequences. They are most probably sedimentary in origin, later affected by metamorphic processes.

2. Residual concentration deposits originated by weathering decomposition of ferruginous rocks and subsequent leaching and transportation of iron oxide by surface waters.

Secondary residual iron accumulation, a product of recent weathering and enrichment are widespread throughout the country, giving rise to local indigenous smelting at places, but in no case extensive enough to be of wider commercial value (Hamrla, 1973).

3. Known hydrothermal deposits are of hot-spring type.

4. Iron concentrations of magmatic type have been indicated.

CONCLUSIONS AND RECOMMENDATIONS

From geological, petrographical, and geochemical studies conducted on the rocks of the studied area, the following conclusions and recommendations are drawn:

1. The rocks of the studied area, except the tertiary volcanics have undergone through a regional metamorphism of green schist facies.

2. The plutonic rocks could have a probable comagmatic origin and derive from crystal fractionation.

3. Their similarities in most of the oxide composition of the younger tertiary basalts and of the protrozoic plutonic rocks of the area could indicate a probable resemblance of the original magmatic material of the plutonic rocks with the basalts and their generation in the same type of tectonic environment.

4. The Chago iron is considered to be a Precambrian Banded iron formation.

5. In most of its oxide contents, and environment of formation, the Chago Banded iron formation is similar to the Superior BIF.

6. Both major and trace element geochemistry testified that the Chago iron formation is formed by a low temperature sedimentary processes.

7. Further studies should be conducted to evaluate the nature and use of the microfosil ("undifferentiated biospheroids") as indicators of the environment of the depositional basin.

8. Except to its low quantity, the high content of iron make it to be a highgrade ore.

9. Despite the excellent quality of ore at Chago, the known reserve does not offer any chance for establishing a steel industry on a National scale.

10. Under the present conditions, local small-scale mining and smelting for manufacturing in situ products might be economically feasible.

REFERENCES

1. Alexandrov, E.A. (1973). The Precambrian of Banded Iron Formation in Cwnada. Canadian Mines, 181: 223-229

2. B. Desta, B. Tezera, T. Bekele (1980). A Short Review on the Geology and Iron Ore Occurrence at Chago

3. Cahen and N.J. Snelling (1966). The Geology of Equatorial Africa, Amsterdam.

4. Chater, A.M. (1971). The Geology of the Megado Region, Southern Ethiopia, Ph.D. Thesis, University of Leeds.

5. Clifford, T.N. (1970). The Structural Framework of Africa, in "African Magmatism & Tectonics", Oliver & Bold, Edinburgh.

6. Cloud, P. (1973). Paleoccological Significance of the Banded Iron Formation.

7. Drever, J.I. (1974). Geochemical Model for the Origin of Precambrian Banded Iron Formation Geol. Soc. Am. Buel; 85: 1099-1106.

8. Eichler J. (1976). Origin of Precambrian Banded Iron Formation. In: Wolf K N (ed). Handbook of Strataform & Stratiform Ore Deposit.

9. Frietsch, R. (1970). Trace Elements in Magnetic & Hematite. Sveriges Geol. Unders Arsbok 64: 1-136.

10. Frietsch, R. (1970). Trace Elements in Magnetite & Hematite Mainly from Northern Sweden.

11. Garrels, R.M. Perrg, E.A., Jr. and Meckenzie, F.T, 1973. Genesis of Precambrian Iron Formations and the Development of Atmospheric Oxggen. Econ. Geol. 68: 1173-1179.

12. Goldschmidt, VM (1954). Geochemistry-Claudon Press, Oxford pp., 1-730.

13. Gross, G.A., 1983. Tectonic Systems and the Deposition of Iron Formation. Precambrian Res., 20: 171-187.

14. Gross, G.A., 1965. Geology of Iron Deposits in Canada. I. General Geology and Evolution of Iron Deposits. Geol. Surv. Can. Econ. Geol. Rep., 22: 181.

15. Gross, G.A., 1968. Geology of Iron Deposits in Canada III. Iron Ranges of the Labrador Geosgncline. Geol. Surv. Can. Econ. Geol. Rep., 22: 179.

Gross, G.A., 1972. Primary Features in Cherty Iron Formation. Sed. Geol., 7: 241-261.

Gross, G.A., 1973. The Depositional Environment of Principal Types of Precambrian Iron Formation. Unesco Earth Sci., 9: 15-21.

Gross, G.A., 1980. A Classification of Iron Formation Based on Depositional Environments. Can. Mineral, 18: 215-222.

Gross, G.A., McLeod, C.R. (1980). A Preliminary Assessment of the Chemical Composition of Iron Formation in Canada. Canadian Mines, 181: 223-229.

Hamrla, M., 1966. The Iron and Manganese Ore Deposites of Ethiopia.

Hamrla, M., 1973. Iron Ore Deposit of Ethiopia (a Summary of the Present State of Knowledge), Addis Abeba.

Hirst, D.M. (1962). The Geochemistry of Modern Sediments from the Gulf of Paria. The Relationship Between the Mineralogy and Distribution of Major Elements: Geochimiet Cosmochimica Acta V. 26, p. 309-334.

Holland, H.D., 1973. The Ocean: as a Possible Source of Iron in Iron Formations. Econ. Geol; 68: 1169-1172.

Holmes, A., (1951). The Sequence of Precambrian Orogenic Belts in South & Central Africa. Cong. Geol. International XVIIIth: London, 1948 - Report 14.

James, H.L., (1954). Sedimentary Facies of Iron Formation: Econ. Geology, V. 49, No. 3 p., 235-293.

Jelenc, D., (1966). Mineral Occurrences of Ethiopia, Addis Ababa

Kazmin, V. (1971a). Geology of Ethiopia. Geological Survey, Ethiopia.

Kazmin, V. (1972c). Some Aspects of Precambrian Development in East Africa, Nature, Vol. 240.

Kazmin, V., A. Shiferaw & T. Balcha (1978). The Ethiopian Basement: Stratigraphy and Possible Manner of Evolution. Geological Rdsch. Vol. 67.

Kochemasov, G. (1970). Summary of Geology & Mineralization of Metti-Nedjo Mineralized Belt, Wollega.

31. Krupp, Col, 1956: Ethiopia Report. Arch. of the Ministry of Mines.

32. La Berge, G.L., 1973: Possible Biological Origin of Precambrian iron formation, Icon. Geol., 68: 1098-1100.

33. Landergren, S., (1948). On the Geochemistry of Swedish Iron-ore and Associated Rocks. Sveriges Geol. Unders Ser C., 42(5): 1-182.

34. Lepp, H. and Goldich, S.S., (1964). Origin of Precambrian Iron Formations. Econ. Geol., 59: 1049-1060.

35. MacGregor, A.M. (1927). Problems of Precambrian Atmosphere S. Afr. J. Sci., 24: 155-172.

36. Majumder, T. (1982). Geochemistry of Banded Iron Formation of Orisa, India, Mineralium Deposita, 17: 107-118.

37. Mohr, P. (1971). Geology of Ethiopia (2nd Edition), University College, Addis Ababa Press.

38. Murdock, T.C. (1960). Geology and Mineral Resources of Ethiopia (U.S. Dept. of Interior. Working Paper 10), Addis Ababa.

39. Rosler, H.H., Lange, H. (1972). Geochemical Tables. Elsevier Publication, Amsterdam, p. 1-468.

40. Rudis, Co. (1964). Iron Ore Deposits of Agmetta and on Ghedem Hill in Eritrea Province. Geological Survey Ljublijana. Yougoslavia. Arch. of the Mins. of Mines.

41. Rudis, Co. (1964). Iron Ore Deposits in Gulliso-Yubdo-Kore Area (Wollega Province) Arch. of the Mins. Mines.

42. S. Chewaka, & dewit (1980). Plate Tectonics & Mineral Occurrence in Ethiopia.

43. Shaw, D.M. (1964). Interpretation Geochimique des Elements en Frances dans les Roches Eristallines Mason, Paris.

44. Taylor, S.R. (1965). Application of Trace Element Data to Problems in Petrology. In Physics & Chemistry of the Earth, Vol. 6. Programon Press, Oxford, p. 133-273.

45. Tilahun Mammo, (1980). The Geology Geochemistry and Origin of Sulphide Mineralization in Katta Wollega Province.

46. Trendal, A.F., Blockley, J.G. (1970). The Iron Formation of the Precambrian Hamersley Group, Western Australia Geol. Surv. Bull., p. 119.

47. U.N. Mineral Survey of Ethiopia, 1971 - Report on the Mineral Survey in two selected areas of Ethiopia (UNDP, Addis Ababa).

49. Usoni, L. (1951). Resorse Minerie dell Africa Orientale. Roma.

50. Williams, H. and McBirney, A.R. (1979). Volcanology. Freeman, Cooper Co.

DECLARATION

I, the undersigned, declare that this thesis is my work and that all sources of material used for the thesis have been dully acknowledged.

Aberra Getahun,
Addis Ababa,
October, 1985.

STATION MAP

LEGEND

- STATIONS
- TRENCHES
- TOWNS & VILLAGES
- STREAMS
- MAJOR RIVER SYSTEMS
- MAIN ROAD
- MARSH AREA